NEW NIST PUBLICATION

October 1990

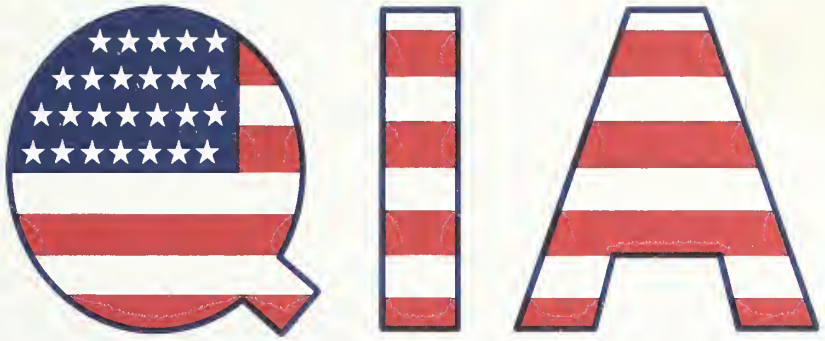

Q U A L I T Y ▪ I N ▪ A U T O M A T I O N

Progress Report of the Quality in Automation Project for FY89

Edited by:

T.V. Vorburger
B. Scace

U.S. DEPARTMENT OF COMMERCE

National Institute of Standards
and Technology
Gaithersburg, Maryland 20899

NISTIR 4322

May 1990

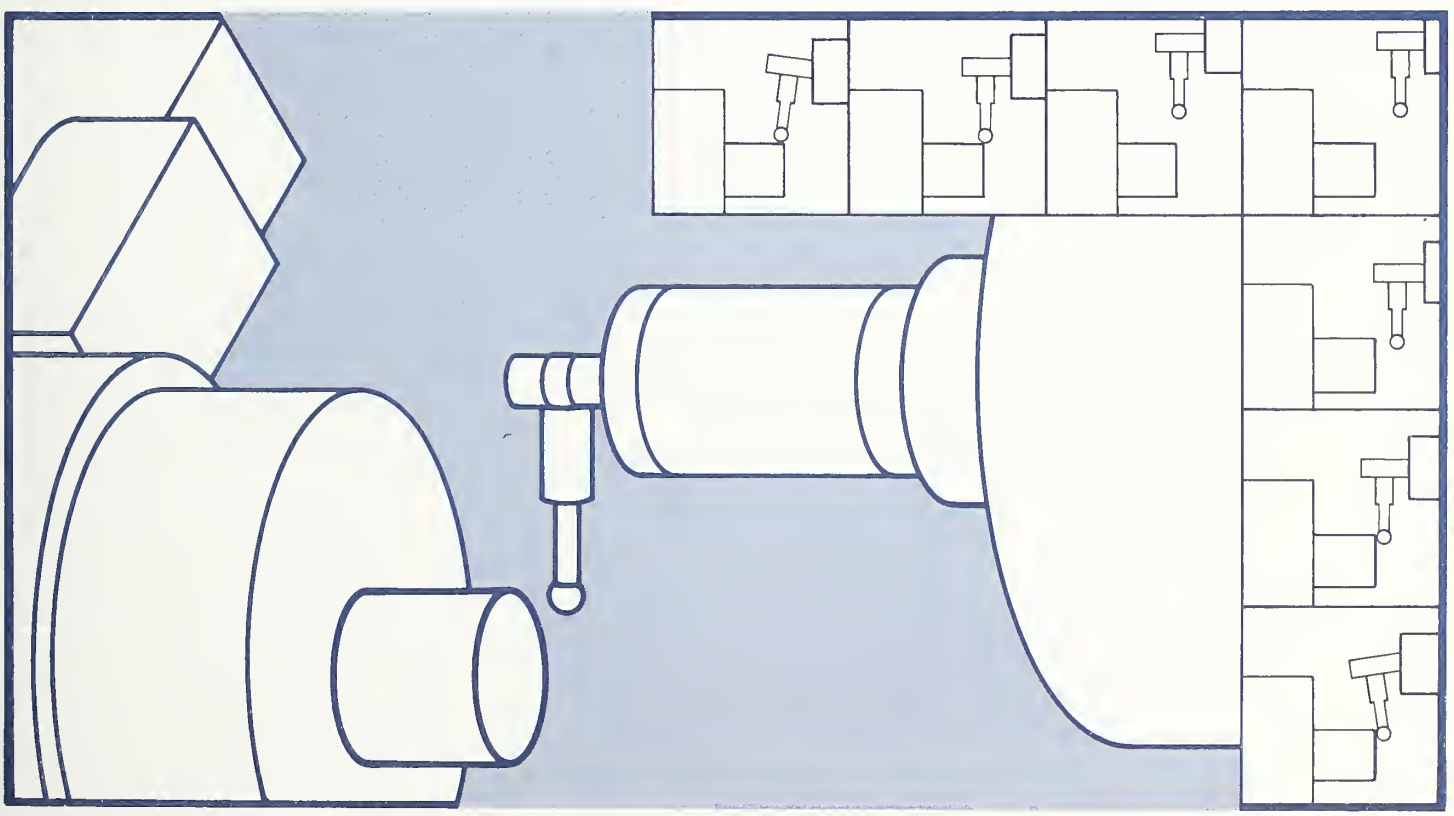

NISTIR 4322

PROGRESS REPORT OF THE QUALITY IN AUTOMATION PROJECT FOR FY89

Edited by
T. V. Vorburger
B. R. Scace

U.S. DEPARTMENT OF COMMERCE
National Institute of Standards
and Technology
Gaithersburg, MD 20899

May 1990

U.S. DEPARTMENT OF COMMERCE
Robert A. Mosbacher, Secretary
NATIONAL INSTITUTE OF STANDARDS
AND TECHNOLOGY
Dr. John W. Lyons, Director

DISCLAIMER

Commercial equipment, instruments, or materials are identified in this report in order to specify adequately certain experimental procedures. In no case, does such identification imply recommendation or endorsement by the National Institute of Standards and Technology, nor does it imply that the material or equipment identified is necessarily the best available for the purpose.

ACKNOWLEDGMENTS

We are grateful to the following industrial collaborators for their interest and technical contributions to the project:

Walter Augustyn	CMX Systems, Inc.
Livingston Davies	CADKEY, Inc.
Stephen L. Fix	Sheffield Measurement
Ernie Hollenbacher	Monarch Sidney
Richard Jennings	ICAMP, Inc.
Stephen Logee	Automation Software
Harry Mackie	Renishaw, Inc.
F. Daniel Myers	Monarch Cortland
David Pickle	Renishaw, Inc.
Ralph Prescott	Monarch Sidney

We also acknowledge technical contributions from D. Goodson, J. McMahon, and J. Riganati.

We are grateful to V. Gagne, C. Poffenbarger, D. Price, F. Sork, and M. Ugiansky for their assistance in the preparation of this document.

We would especially like to acknowledge the Navy's Manufacturing Technology Program, whose funding and support has made this project possible.

SUMMARY

This document describes the progress of the Quality in Automation (QIA) project during the fiscal year 1989, the second year of a continuing effort at the National Institute of Standards and Technology. The project's purpose is to develop a quality assurance program that demonstrates "deterministic metrology" in an automated manufacturing environment using commercially available and affordable equipment. Deterministic metrology is defined as a philosophy whereby quality assurance is based on verification of the manufacturing process itself during a production run rather than sole reliance on the more traditional post-process part inspection.

The project's initial year commenced with the creation of an overall strategy and control architecture that would combine traditional part inspection and statistical process control (SPC) methods with the tools of automation, such as on-machine sensing and gauging and network communications. Major equipment such as the two machine tools, the coordinate measuring machine, and computer hardware was procured. Design of the "real-time error corrector" unit began. Those activities were reported in detail in the progress report of the QIA project for FY88 [1-1].

During FY89 a very detailed characterization of the vertical machining center and CNC turning center has been initiated. A prototype of the real-time error correcting hardware has been built and is under test. High-speed on-machine probing with satisfactory repeatability at speed (100 in/min) has been demonstrated. A commercial coordinate measuring machine has undergone initial characterization and is operational. Several methods of real-time surface texture analysis are under consideration. Optical scattering analysis is one such method discussed in this year's report.

Once the initial experiments have been completed and the system subcomponents have been procured and tested, the entire system will be

tested using a modified BAS turning test part [1-2] and the NAS 979 milling test part [1-3]. Upon completion of these tests, the system will be considered for integration into the Automated Manufacturing Research Facility for further development.

Support for this project comes from the Navy as part of the quality efforts in the AMRF, from private industry, and from the National Institute of Standards and Technology.

TABLE OF CONTENTS

1. INTRODUCTION

Brian Scace

Traditional manufacturing techniques in this country have often been based on a one-person, one-process, one-machine system. It was not unknown for one operator to run a machine day in and day out for years creating the same part. The same operator not only generated this part but was also responsible for the control of the procedure. This included the required changes to the process as prompted by tool wear, machine condition, and material composition. The operator was also required to be responsive to changes in dimension and tolerance dictated by a design engineer equipped with a drawing board. These changes would be checked by the quality control people using micrometers and other types of single purpose gauges.

To remain competitive in today's world economy, these traditional procedures have changed. The operator is now in charge of several machines in a "cell" type operation. The design engineer uses a CAD system for design and modification. The inspector uses a coordinate measuring machine (CMM) to inspect a finished part. The machines themselves are controlled by computers using numerical code to dictate steps in the machining process.

All of these advances in manufacturing contribute to a new environment which generates a product faster and more efficiently than before; however, the operator is still responsible for the procedure. The operator must decide whether modifications in the tool path are necessary in response to changes in tool and machine conditions. The operator still has to modify the process in response to the information gathered by the CMM. How can one person keep up with several processes in a "cell" operation? What takes the place of that person in a totally automated environment?

In response to these questions, the National Institute of Standards and Technology has established the Quality in Automation project. First reported on in FY88 [1-1], the project's objective is to develop a quality

assurance system that demonstrates deterministic metrology in an automated environment utilizing commercially affordable and available equipment.

Deterministic metrology is a philosophy of quality control that relies on in-process measurements to characterize the machining process rather than post-process measurements on the finished product. This can be accomplished by combining the more traditional methods of quality control, such as statistical process control (SPC) and post-process gauging, with more recent developments in the field, such as network communications and automated sensing.

With the desire to shorten product cycle time and maintain product quality, the project's aim is to implement a complete machining system that can not only monitor significant parameters in the machining process but also can respond to changes in those parameters. A responsive, self-adjusting, "intelligent" machining system is both possible and desirable in today's manufacturing environment.

The foundation of the project is the control architecture proposed in FY88. This architecture consists of four loops: pre-process characterization, real-time sensing, process-intermittent gauging, and post-process gauging. Some of the activities in each loop are illustrated in Fig. 1.1, using terms defined below.

QC	Quality Controller. A unit that modifies and passes the NC part program to the machine tool controller and controls real-time adjustments to the tool path.
QM	Quality Monitor. A user-friendly computer that manages all of the quality data in the system and performs diagnoses of the machining processes.
CAD	Computer Aided Design
MT	Machine Tool
MTC	Machine Tool Controller
PI	Process-Intermittent
RT	Real-Time

The Pre-Process Characterization loop consists of two major activities: characterization of the thermal behavior of the machine tool and the determination of the geometric accuracy of the machine tool as a function of temperature variation.

The Real-Time Sensing loop refers to those measurements taken on the machine during the machining process. These measurements include the machine thermal state, tool forces, vibration levels, and surface roughness. These factors, when fed into the quality controller (QC), can result in an part program modification or, in radical circumstances, a controlled machine tool shutdown.

Process-Intermittent Gauging refers to those measurements taken on the machine tool but not during the machining process itself. The heart of this loop is "fast probing" using touch trigger probes driven at speeds of up to 100 in/min. The results here can be used to modify the part program for the next cutting pass.

Traditional quality control is performed in the Post-Process Gauging loop. Parts are measured for dimension and form using a coordinate measuring machine. These results can be used both to verify the part in question and the process under which it was manufactured. This information is accessible on the quality monitor terminal (QM).

This complete architecture is being applied to the following machine tools in the NIST Automated Manufacturing Research Facility (AMRF), the Automated Production Technology Division, and the Precision Engineering Division:

1. A Monarch VMC-75 Vertical Machining Center with a GE-2000 CNC Controller,
2. A Monarch Metalist Turning Center, also equipped with a GE-2000 CNC Controller,
3. A Sheffield Apollo Series Cordax Coordinate Measuring Machine.

In the FY88 Progress Report for the QIA project, we reported that a horizontal machining center was also included in the project. However, the project goals can be readily demonstrated with the vertical machining center and the turning center alone.

Each machining center has a PC-AT compatible computer called the quality controller (QC) interfaced with the machine controller. Each QC is equipped with an IEEE-488 communications board linked to a data acquisition system which controls a 40 thermocouple array. Elements of the array are located at key points of interest on the machine tool itself. The QC is linked to the machine controller via an RS-232 interface and will communicate with the QIA database and the post-process gauging loop via the communications network.

Each of the following sections describe the progress in one aspect of the project during FY89 as well as the direction that these tasks will take in the coming months. Once the initial experiments have been completed and the system subcomponents have been procured and tested, the entire system will be tested using the modified BAS turning test part [1-2] and the NAS 979 milling test part [1-3]. Upon completion of these tests, the integration of the system into the AMRF will be the next area explored.

During the fiscal year, progress has been made in several areas concurrently. In the process-intermittent gauging loop, work has proceeded on the application of probe systems to the machine tools, construction of an electronic unit known as the real-time error corrector (RTEC), and the interfacing of the system to the machine controllers. This system is currently under test with satisfactory repeatability at speeds up to 100 in/min. See Chapter 2.

Characterization of both the vertical machining center and the turning center has been a major task. This key element in the pre-process characterization loop is discussed in detail in Chapters 3 and 4.

Chapter 5 describes the Automated Manufacturing Programming Language Environment (AMPLE). This software system controlled the process-intermittent gauging tests completed last year and will be the controlling software for the quality controllers and quality monitor.

With the acquisition of a new coordinate measuring machine came a major effort to characterize its behavior and install the necessary accessories for its role in the project. Chapter 6 discusses this activity.

In the FY88 report, one approach to surface texture measurement, ultrasonic sensing, was discussed. This year another approach, optical scattering, is discussed in Chapter 7.

In the fiscal year 1990, there are several milestones identified for attention. They include, but are not limited to, the following:

1. Complete pre-process characterization of the vertical machining center and turning center.

2. Install an automated dimensional gauging package with a DMIS interface so that a CAD system and the CMM can communicate with each other fluently.

3. Survey and conceive alternative approaches to intelligent real-time control.

4. Demonstrate automated real-time and process-intermittent error compensation on the turning center.

5. Demonstrate fast probing and tool setting on the vertical machining center.

The demand for a shortened product cycle time, reduced waste, and a consistent high level of quality is a constant concern in the modern manufacturing environment. The implementation of a practical quality control system that monitors the entire fabrication process from conception to finished product in an automated environment will allow the manufacturer to better meet that demand.

This project is funded by the U.S. Navy in support of the quality effort in the Automated Manufacturing Research Facility, by support of equipment and software from private industry, and by direct funds from the National Institute of Standards and Technology.

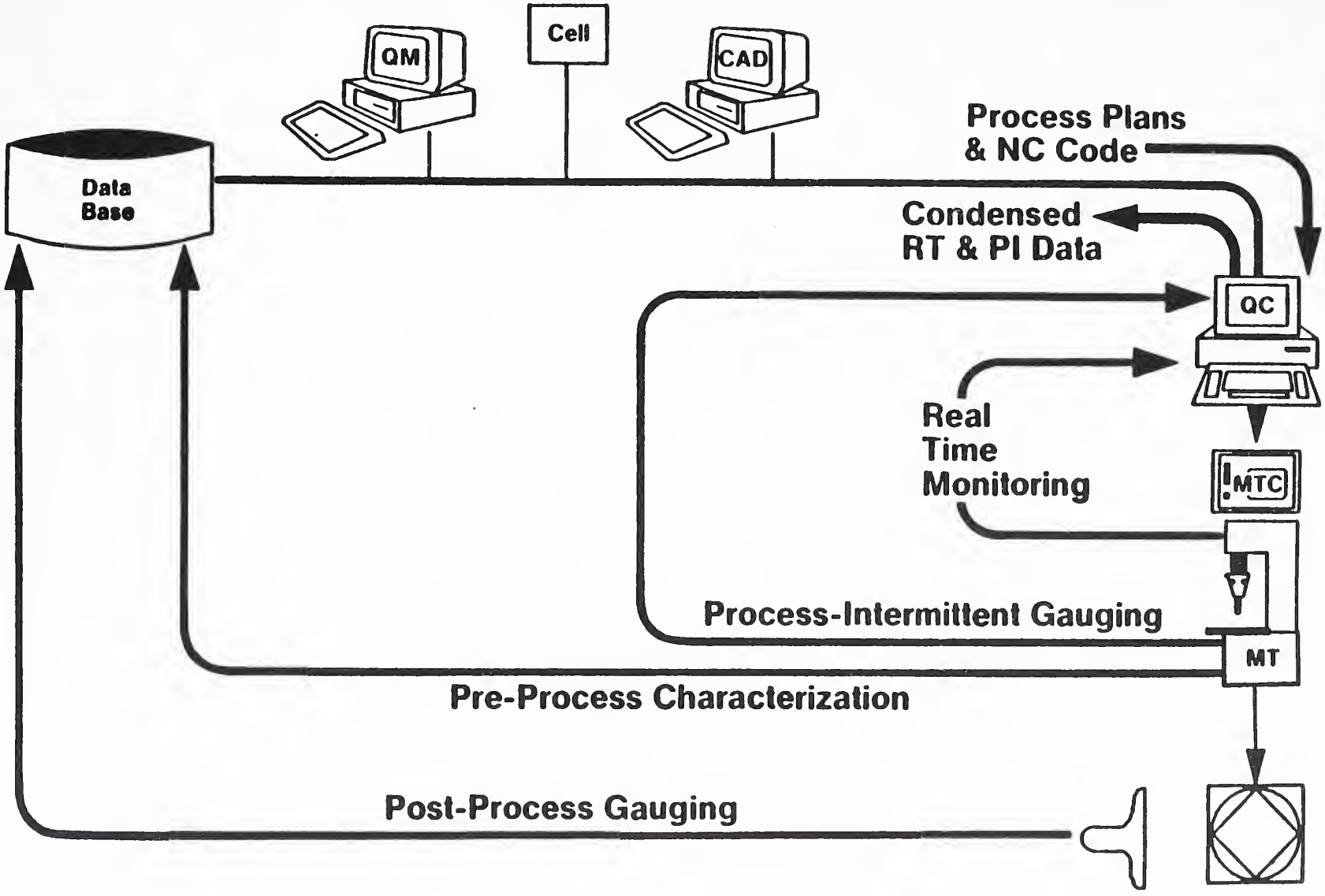
Cell
QM
CAD
Process Plans
& NC Code
Data
Base
Condensed
RT & PI Data
QC
Real
Time
Monitoring
MTC
Process-Intermittent Gauging
MT
Pre-Process Characterization
Post-Process Gauging

Fig. 1.1

2. REAL-TIME ERROR CORRECTOR AND PROCESS-INTERMITTENT PROBING

K. Yee

2.1 SUMMARY

The hardware design for the real-time error corrector (RTEC), shown in Fig. 2.1 in relation to the other components of the QIA system, has been completed and the first prototype hardware constructed. The RTEC implements the inner-most control loop using hardware to apply real-time error compensation for quasi-static geometric machine tool errors and thermally induced errors. It also operates in the next control loop by sending process-intermittent part probing data to the quality controller (QC), a PC/AT compatible computer. The RTEC also allows touch-trigger probing to be performed at more than an order-of-magnitude higher feed rate than is commonly used for on-machine part inspection in current installations. The prototype hardware, which will be described in detail below, has been connected to the turning center which has linear glass scales with encoder-type signals for position feedback.

Fast part probing has been demonstrated. Error compensation will be implemented when the laser measurements to determine the machine tool errors over the operating temperature range are completed.

2.2 DESIGN OF THE RTEC

2.2.1 Introduction

As a part of the Quality in Automation project, we are implementing real-time error compensation on a vertical machining center and turning center. The purpose of this project is to control the machining process in order to minimize errors in the finished part. In small-batch (one to ten parts) manufacturing, statistical quality-control techniques based on measurements of finished parts are not sufficient. The premise for this work is that many sources of errors in machine tools are repeatable and

predictable and that we can compensate for these systematic errors during the process, reducing the errors in the finished part. Such errors may be fixed geometric errors, such as lead-screw nonlinearity or straightness errors in the ways, or thermally induced errors such as spindle head growth [2-1]. It is not uncommon, now, to see general-purpose machine tools with advertised axis repeatabilities of one micrometer, but with systematic errors usually 2 to 5 times larger. Error compensation is intended to allow parts to be produced with errors approaching the repeatability limits even during much of the thermal transient periods.

This section will primarily discuss the plan for implementing the error compensation on a wide variety of machine tool controllers. The methodology for error compensation [2-2] and the mathematical model for the machine tool errors [2-3] have been previously described.

2.2.2 Objective

It is desired to build a "black box" that can be inserted between the position feedback elements (e.g., resolver, encoder, glass scale, Inductosyn, etc.) of the axes of a machine tool and the machine tool controller. This device will independently and simultaneously count the signals from the feedback element to produce the machine position. It will also include an interface to send this position data to the QC computer which will calculate the required error-compensation for each axis. The function of the proposed RTEC is to allow real-time corrections of positions of the machine tool axes. The objective is to perform this without intrusion into the machine tool controller and in a way that is invisible to the machine tool. This means that the signals from the position feedback elements are somehow modified to make the machine axes go to slightly different physical positions (as commanded by signals from the QC) than they would without the corrections applied.

The QC has the axes-position data available and can compute a real-time correction factor based on the positions and temperature-sensor data provided to it. The corrections are calculated for the current axis positions and temperatures from the empirically determined model [2-3] .

The coefficients for use in this model are determined from laser-interferometer and electronic-level measurements of each machine tool axis and their squareness with respect to each other over the range of machine operating temperatures. A small number of selected temperatures that correlate with the thermally induced errors for the axes are used by the model. Generally, errors caused by specific machining conditions, e.g., tool deflection and servo lag, cannot be compensated. The proposed unit would ideally work with a wide variety of computer controlled machine tools.

An additional function of the device is to allow high-speed part probing by latching the axes' positions in response to a measuring probe "trip" and outputting the positions to the PC. The device would produce the position data independently of the machine tool controller. The controller would be executing a part program to move the probe rapidly (at speeds of up to 100 in/min) past the expected position of the edge of the part (which would be well known since it would have just been machined). The part probing data would be analyzed off-line by the PC after probing is completed.

2.2.3 Background

The Center for Manufacturing Engineering has previously implemented error compensation on several machine tools. Two of them are a Brown and Sharpe 20 hp (15 kW) vertical machining center and a Hardinge Superslant 16.8 hp (12.5 kW) turning center.

The feedback elements for the Brown and Sharpe are linear glass scales, and the output signals are conditioned to appear as resolver signals (two sine wave signals that change in relative phase by 360° for one "rotation"). The position information was obtained by "piggy-backing" the counter-latches which contain the raw-count axis position of the machine tool controller. This technique was possible only because the manufacturer provided the physical location and logical address of the registers holding the position counts. The counts were simultaneously and

independently latched and sent by an 8051 family microcomputer to a Hewlett-Packard (HP) 1000 computer for off-line correction calculation.

In these calculations, machine tool geometric errors as well as thermal growth of the spindle head were taken into account. The spindle growth was measured in both the X and Y directions by two linear variable differential transformers (LVDT) mounted at the end of the machine tool table. Periodically, a reference "tool" was moved to these LVDTs where readings of displacement of the spindle head were taken. These displacement readings, along with the axis positions, were used by the HP to compute position corrections, which were sent back to digital-to-analog (D/A) converters. These D/A converters fed the reference inputs of analog comparators in the controller that convert the "resolver" output sine waves to square waves. Changing the reference voltage produced an apparent phase shift between the sine wave and the square wave which made the controller stop the axis at a slightly different position than without the correction. The amount of control available allowed for a range of about ±0.0035 inches (±0.1 mm) change in the axis positions, which was invisible to the controller.

The resolution of the correction was limited by the number of bits of the D/A, since the correction was analog. For example, an 8-bit D/A converter can resolve the correction signal down to 1 part in 256, or about 30 microinches (0.7 μm). Only the X and Y axes of this machine were compensated since the primary application requiring the compensation was drilling, which is not sensitive to Z-axis errors.

The Hardinge Superslant turning center has an Allen-Bradley 8200 controller which facilitated the error compensation without any hardware modifications [2-4]. The machine has resolver feedback, but since the position correction is done entirely in software, this is immaterial. An Intel 86/30 single-board microcomputer, using an 8086 microprocessor running at 8 MHz with a high-speed version of the 8087 math coprocessor, was used to calculate the corrections. Sixty-four bit digital Input/Output (I/O) interface boards in the 8200 provided axes positions to the 86/30.

The computed correction was fed back into the 8200 by modifying the contents of the "following error" register which held the difference between the programmed position and the position indicated from the processed resolver signals. The axis reached the desired position when the following error was zero, and the modification of this following error caused the machine to stop at a different position than it would without the correction. The resolution of the correction was the resolution of the machine tool controller. A new correction was calculated and inserted at every control cycle of 20 milliseconds. This correction rate approaches the computational speed of the 86/30 computer used for this application.

Both the X and Z axes of this machine had error compensation. The accuracy of part diameter and length over the cold-to-operating temperature range was improved on the order of 10 to 20 times when error compensation was implemented. Straightness was also improved by a factor of 4 to 5 over a 2.7-in (70-mm) length.

2.2.4 Present Approach

As previously suggested, a "black box" called the real-time error corrector (RTEC) will be inserted between the position feedback devices and the machine tool controller (MTC) as shown in Fig. 2.2. The RTEC will independently process the feedback signals and send the positions to the QC. This unit will compute the required axis position corrections and send them back to the RTEC, which will alter the position signals passed through to the MTC to implement the correction.

There are several types of position feedback devices in use today, including resolvers, encoders, linear glass scales, and the Inductosyn. All of them generate either "resolver-type" or "encoder-type" signals. The Inductosyn produces resolver-type signals while linear glass scales have signal conditioning available to produce either type of signal. Resolver-type and encoder-type signals are quite different and will

require different versions of the RTEC. The signals from both types of devices will now be discussed.

Resolver-type signals, obtained from either resolvers or glass scales, have two sinusoidal waveforms, as shown in Fig. 2.3. The electrical phase difference between the two waveforms is a function of angular position, changing 360° as the resolver turns one full revolution [2-5]. A third sinusoid is actually involved. The device may be excited by two signals with sine and cosine relationship. It then produces one output which changes in phase with respect to both excitation phases as the resolver is rotated. Alternatively, it may be excited with a single excitation and produce two outputs which change in phase relative to each other with rotation. In the first case either excitation can be selected as the "reference" signal in the figure. The other excitation is not illustrated. In the second case, one output is the "reference" signal, the other is the "output" signal, and the excitation is not illustrated. The frequency is fixed by the excitation, typically about 2 kHz. With no axis motion, the phase between the reference and output signals remain fixed such as shown in Fig. 2.3a. If the axis moves in the positive direction by an amount that rotates the resolver 1/8th turn, the output signal will appear as in Fig. 2.3b. Figure 2.3c illustrates the output signal when the axis moves an amount that rotates the resolver 3/8ths of a turn in the negative direction from Fig. 2.3b.

In order to handle resolver type signals, the RTEC must include circuitry to measure the relative phase between the reference and output signals and count the full cycles that pass by. A phase shifter will alter the phase of the output signal passed through to the MTC. The linear axis displacement for one rotation of the resolver is a function of the ball-screw pitch and the gear ratio between the resolver and the ball screw. The phase difference is generally measured with a resolution that corresponds to about 40 microinches (one micrometer) of axis movement. If the phase shifter increases the phase difference passed through to the MTC by this amount, the axis will stop 40 microinches sooner (less positive) than without the "correction."

Encoder-type signals, shown in Fig. 2.4, have two square-wave output signals (A and B) that are displaced in-phase by 90° (one-quarter cycle). These signals have the same period and a fifty-percent duty cycle. The signal which leads in-phase changes with the direction of axis motion. For rotary encoders, an additional signal, called the reference or index, produces one pulse per revolution. This signal, which is used when the axis is referenced, will not be modified by the RTEC and is not shown in the figure. The frequency of the square waves is a function of the number of lines per revolution in the encoder (perhaps 1000) and the rpm of the encoder. At rest, the two signals are static and either may be at high or low logic levels. Figure 2.4a shows the A and B signals with the axis moving in the positive direction (phase A leads phase B). Each cycle of the square waves corresponds to a unit of distance (δ) of axis movement which depends on the number of lines per revolution in the encoder, the gear ratio between the encoder and the ball screw, and the ball-screw pitch. The encoder-type version of the RTEC must contain circuitry to count the encoder cycles and determine which direction the axis is moving in order to know whether to add or subtract counts. This circuitry yields a position resolution of $\delta/4$. To make the machine axis stop sooner, by the distance corresponding to one square-wave cycle, the RTEC must insert extra pulses with the correct phase relationship as shown in Fig. 2.4b. Likewise, to make the axis go one cycle further, the RTEC must subtract one pair of pulses as in Fig. 2.4c. Note that the resolution of the correction is the displacement δ corresponding to one square wave cycle. This correction resolution is four times coarser than the axis position resolution.

2.2.5 Implementation

As stated earlier, and shown in Fig. 2.2, the real-time error corrector will be inserted between the machine tool axis position feedback device and the machine tool controller. The RTEC will be a microcomputer-based device, containing one microcomputer for each axis of the machine tool. Thus, there may typically be two, three, or more microcomputers in the RTEC used for the error correction of one machine tool, with each one communicating in turn with the QC computer shown in Fig. 2.2.

The RTEC implementation discussed here is to be used with a machine tool with encoder-type, axis-position feedback signals. The first machine tool will be a two-axis Monarch Metalist turning center with a General Electric Mark Century 2000 controller. For position feedback, this machine tool uses linear glass scales. After electronic conditioning, the machine tool controller receives the signals from the glass scale of the axis in motion as an encoder-type signal. Preliminary tests have been carried out, with a limited prototype of the RTEC, using this machine. Though this prototype did not contain a microcomputer, the physical locations of the axes could be modified without creating error conditions -- that is, without intrusion into the machine tool controller.

The following explanation of the RTEC and the correction process is somewhat simplified for clarity. It is assumed for this explanation that only one axis is being controlled by the RTEC. A more detailed explanation will follow later.

Basically, the implementation of the RTEC will appear as in Fig. 2.5. As previously discussed, quadrature position-feedback signals (square-waves A and B, displaced in phase by 90°) from the machine tool axis will pass through the RTEC. A microcomputer (for each axis) will control the operation of the RTEC. This device, an 8-bit microcontroller from the Intel 8051 family, will send similar quadrature signals on to the machine tool controller, and, depending upon the mode of operation, will communicate back and forth with the QC.

There are three possible modes of operation for the RTEC. The first is a "transparent" mode. In this mode the RTEC merely passes the quadrature position-feedback signals, unchanged, to the machine tool controller. The transparent mode is required for conventional, uncorrected operation of the machine tool, and will be necessary when the QC computer is disconnected from the RTEC. The second mode possible is the probing mode which will be described in Sec. 2.3.

The third mode is the correction mode, in which the RTEC actively changes the quadrature feedback signal before passing it on to the machine tool controller in response to the correction commands received from the QC computer. In this mode, the A and B quadrature signals from the axis encoder go to a quadrature decoder within the RTEC. Here, the direction of axis movement is determined from the phase relationship between A and B. The A and B quadrature signals are decoded into units, or counts, each count having one-quarter the resolution of the quadrature input. Depending upon the direction of axis movement, a counter adds or subtracts these units (or counts) and a continuously updated total is maintained. The number of counts, if multiplied by the resolution of one cycle, is the absolute position of that axis with respect to the axis reference position (or "home").

In the correction mode, the microcomputer does two things. It transfers the quadrature waveform received from the machine tool feedback device to the machine tool controller. It also continually reads the number of counts being accumulated in the quadrature decoder/counter unit described above. The axis position, expressed as counts, is periodically sent to the QC computer. The QC will calculate a position correction for each axis based upon the current axis position and temperature data and send this correction back to the RTEC.

The microcomputer in the RTEC interprets this correction as the number of pulses that must be added to (or withheld from) the original quadrature signal (A and B) before it is passed through to the MTC. The MTC has a quadrature decoder/counter also, and when additional pulses are inserted by the RTEC, it will count these and reach its own pre-determined destination count (and position) that much sooner. By the same reasoning, if some of the axis-encoder pulses are withheld from the MTC, the axis will be kept in motion for a longer distance - enough to compensate for the distance represented by the withheld cycles. For example, if one encoder cycle represents an axis-travel distance of 160 microinches, and an axis move is to be from the 1.000-inch position to the 2.000-inch position, then adding six pulses (approximately 0.001 inch) will cause the axis to stop at the 1.999-inch position. Withholding six pulses, however,

will cause the axis to continue to the 2.001-inch position. Note, however, that in either case the MTC will display 2.000 inch as the position. The correction implemented by withholding pulses will work whether the direction of axis movement is negative or positive. However, if a correction is desired which entails adding pulses, then the additional A and B pulses must have the correct phase relationship. For this reason, the microcomputer in the RTEC must always monitor the current direction in which the axis is moving.

We now discuss the RTEC correction process in more detail. In particular, we highlight the pulse-counting operation, the generation of additional pulses, communication with the PC/AT and potential problems.

First, it should be noted that the entire correction process must begin with all axes at the machine tool's home position, established when the machine tool is initially referenced during start-up. This is the position which the MTC has designated as reference for all axes. Once the machine tool is in this position, the QC signals the RTEC (for each axis) that it must reset its position counter to zero. This must be done whenever either the RTEC or the machine tool is turned off or reset to synchronize the RTEC position with the machine tool controller position.

As mentioned above, the jobs of decoding the incoming A and B signals, maintaining a total of the counts, and adding or subtracting depending on direction will be handled by a decoder/counter module. When the counter reaches its maximum count (4095), it goes back to zero ("rolls over") and begins again. The microcomputer will periodically read the output of this counter, and must do so often enough so that even during the most rapid axis movement the count remains unambiguous even though the counter has reset to zero and/or the direction of axis movement has changed. If, for example, the decoder is presented with one A and B cycle every 160 microinches (4 micrometers) of axis travel, then the counter (after decoding) will increment/decrement every 40 microinches (1 micrometer). If the counter is capable of counting up to 4095 and the maximum allowed axis speed is 300 in/min, then at maximum speed the counter will reset to zero every 33 milliseconds. The microcomputer must

be able to read the counter several times during this period to ensure unambiguity. The above feed rate is not used for cutting operations. The assumption is made that, while the RTEC must always track the axis position, corrections will only need to be made while actually machining when the feed rate may range up to 30 in/min. Otherwise, there would be little time left for the microcomputer to perform its other task of communication with the QC. The position count that the RTEC sends to the QC is the actual physical location of that axis, as seen by the feedback device (encoder, in this case). At a particular position, this actual (uncorrected) count will differ from the MTC internal count by the amount of the error correction.

Altering the A and B encoder signals to the MTC by adding or withholding pulses must be done in a way that does not cause the MTC to detect an interruption in the proper sequence of signals. Figures 2.4a and Fig. 2.4b illustrate the correct sequence of rising and falling edges for signals A and B in both the negative and positive directions of axis movement. If the additional pulses are not inserted properly, the MTC will detect this fault condition (meaningless encoder input) and shut down the machine. The most straightforward way to implement this correction is to pick a state, when both A and B are low for example, and only add pulses (or withhold them) during this time (Figs. 2.4b and 2.4c). This simplifies the task of the microcomputer during pulse addition. Similarly, it needs only to check for one sequence when withholding pulses. Another limitation pertaining to alteration of the encoder signals is the specification which determines the minimum pulse width which the MTC will accept. According to the specification the maximum frequency (for either the A or B signal) that the MTC can accept is 125 kHz; therefore, the minimum duration of any additional pulse should be 4 microseconds. On the other hand, there is no restriction that the width of the added pulse be comparable to the width of the pulses before or after it. In other words, it is allowable to add 4-microsecond wide A and B pulses whether the axis is travelling at 20 in/min or 200 in/min. Again, this simplifies the work of the microcomputer because it has to generate pulses of only one width.

The most important information communicated between the QC and the RTEC will be the present axis position (sent from the RTEC to the QC) and the axis correction required of the RTEC by the QC. The digital word which represents the present axis position (in counts) must be large enough to depict the number of counts in that axis. The longest axis in the turning center (Z-axis) is approximately 40 inches (1 meter), and if each count (i.e., after quadrature decoding) represents 40 microinches (1 micrometer), then the axis position word must go up to about 1,000,000. If 20 bits are used, the RTEC can keep track of up to 1,048,575 position counts. As for the required axis correction, it is expected that a ±20 milliinch (±0.51 millimeter) correction range will be adequate. Since the corrections will be made with respect to a cycle of A and B, not counts, and each cycle on the turning center represents approximately 160 microinches (4 micrometers), an 8-bit word (±127 correction counts) will suffice.

Communication between the RTEC and the QC will be controlled by the QC and take place at the minimum rate necessary to ensure adequate correction as determined by the operating conditions. Additional communication lines are also necessary for the RTEC to inform the QC how many correction units it has actually implemented (as opposed to how many were requested by the QC), and for mutual control ("handshaking") of the information between the two devices. As mentioned above, the RTEC will actually control the corrections for two or more axes. Each axis, with its dedicated microcomputer, will have its own set of the above communication lines, with each set going separately to the QC. In other words, the QC will sequentially read from and transfer information to each axis' microcomputer in the RTEC.

A limitation of the RTEC concerns the resolution of its corrections. A machine tool controller expects to receive encoder quadrature signals and to decode them internally into a resolution four times finer than the incoming cycles. Since the RTEC can only make corrections by adding or withholding whole cycles, the correction resolution is four times coarser than the measured position resolution. Corrections may be detectable in the workpiece if the resolution of each cycle is relatively coarse. If

this occurs, an appropriate time in the part manufacturing process may need to be selected for tool path modification to be implemented.

2.2.6 Summary

A device has been developed, initially for a two-axis turning center, which will facilitate the real-time compensation for systematic errors in machine tools. The device (the RTEC) will interface with the quality controller (PC/AT) and be inserted between the position feedback element and the machine tool controller so that the RTEC is nonintrusive to the MTC. The RTEC should not be specific to a particular machine tool controller or require significant hardware or software modifications. In practice, however, the type of position feedback needs to be known, as well as the encoder/machine tool controller interface circuitry.

Because the axis position correction is performed externally (i.e., the machine tool controller displays one position while the actual error-corrected position is another), there must be an external way of testing the RTEC operation. The final proof of the RTEC and the error compensation model is to test the results by cutting a series of test parts from a cold start, which assumes the "worst-case" thermal stability of the machine tool, then checking the accuracies of the parts. This will check the accuracy of both of the error-compensation components -- the thermal error compensation (as the machine tool warms up) and the geometric error compensation.

The proposed RTEC, as part of an error compensation system, will provide significant benefits. From previous experience on the Hardinge turning center [2-4], where dimensional accuracy improvements of up to 20 times were achieved in diameter and length, and a significant improvement was also realized in straightness, we believe an accuracy improvement of up to an order of magnitude can be achieved. We may not realize as large an accuracy improvement as in the past because ball screw errors do not directly contribute to the positioning inaccuracies in the present turning center due to the fact that linear transducers are used for position feedback, not rotary transducers. The accuracy of machined parts will be

improved over a wide temperature range for which the machine is presently being characterized by laser interferometry and electronic levels. The RTEC is also applicable to a wide range of machine tools, and it can be easily implemented because it is machine tool controller independent. The RTEC also has a fast probing mode for part inspection as discussed below.

2.3 FAST PART PROBING

An additional function of the real-time error corrector (RTEC) box, described above, is to facilitate fast part probing. Because the RTEC is inserted between the position-feedback elements and the machine tool controller (MTC) and is interfaced to a personal computer, it contains all the necessary components to allow fast part probing with touch-trigger probes in the process-intermittent gauging loop. In small-batch (one to ten parts) manufacturing, traditional statistical quality-control or process-control techniques are not sufficient. One method of improving the accuracy of parts is to use process-intermittent gauging (i.e., part probing on the machine tool). The probing data may be used to adjust the depth of cut on the finish pass, or correct tool offsets to improve the next part. Fast part probing using a touch-trigger probe, with about one probe trip per second, is desired to minimize the time consumed by the measurement, which reduces machining time and productivity. Probing cycles currently implemented by machine tool controllers use slow feed rates, about 5-8 inches per minute [2-6,2-7] (125 mm/min), and are slow in transferring the axes coordinates for the probed points to external computers usually through RS-232 interfaces for distributed numerical control (DNC). They waste time.

Over the last five years, touch-trigger probes have become common on machine tools. The initial applications were primarily to reduce set-up time. Recently, temperature control techniques and the use of glass scales have improved positioning of general-purpose machine tools. Advertised axis repeatabilities of one to three micrometers and accuracies about 3 to 5 times larger are the norm. On-machine inspection is now becoming more common. However, the desire to shave seconds from cycle times makes long inspection times unacceptable.

In typical MTC "canned" probing cycles, the probe is fed towards the part slowly. The axes are rapidly braked to a stop at probe trip (or a programmed distance after trip). The MTC then must determine how to retract to the starting point. Since the stopping point is variable, the retract procedure would involve several steps of calculations if the machine tool relies on relative, rather than absolute, sensing of its position coordinates. In our system the MTC will always be in control, moving the probe quickly to and away from the part between programmed points like any other tool, and will be unaware of the probing process itself.

The RTEC independently and simultaneously counts the signals from the feedback element to produce the machine position and also includes a parallel interface to send this position data to the QC which records the data at probe trip-points. The device allows fast part probing without intrusion into the MTC and in a way that is invisible to the machine tool. A minimum of hardware and software is MTC specific. For fast probing, the MTC merely executes a part program which moves the probe past the edge of the part with a feed rate of 100 in/min (2500 mm/min) and the device sends trip-point axes' positions to the QC. During inspection, the part location is known to within a few thousandths of an inch (about a tenth of a millimeter), since it has just been machined.

The probing data is analyzed off-line by the QC after probing is completed. Part dimension correction can be implemented by updating tool offsets or part program values before the finishing cut, or to correct the next part.

The initial fast probing installation is on the same two-axis turning center described in the previous section. The encoder-type position feedback signals are decoded and counted in the RTEC. In probing mode, the probe-trip signal "holds" the trip position at the decoder output until the microcomputer can read the position. The decoder is designed to continue to count the encoder signals to track the machine position. The microcomputer then outputs the trip position to the QC.

The part location is well known for fast probing in part inspection on a CNC machine tool. The part has just been cut and the location is known within the accuracy of machining. A program to move the probe can be written, in advance, from the same drawing or data used to generate the machining part program. The number of data points and the expected values are known within the machining error. The MTC is unaware of the probing taking place. The parallel data link from the RTEC to the QC bypasses the slow DNC data link to the MTC.

There are, however, many considerations to achieve successful fast probing. Probes are specified for relatively slow feed rates of 18 in/min (450 mm/min) and, up until now, used at even slower feed rates (about 5 in/min [127 mm/min]). At 100 in/min (2540 mm/min), the machine moves one micrometer (position resolution for the turning center) in 24 microseconds. Therefore, the required probing time variability must be an order of magnitude smaller. For precision probing, the effect of the delay, the probe tip diameter, and the effect of probe trip-force and pretravel must all be carefully calibrated at each velocity and direction of approach to be used.

For optimum repeatability in part inspection, the probe must trip during the constant velocity (programmed feed rate) part of each point-to-point move. For locating part blanks during set up before roughing cuts, this is not required. Usually, machines accelerate at approximately a constant rate until the programmed velocity is approached and maintain constant velocity until the end point approaches (see Fig. 2.6). The drive motors then brake to a stop. The acceleration and deceleration times (and the corresponding distances) are a function of the specific axis drive system. The starting point and end point of the programmed probe motion must be chosen to ensure tripping during the constant velocity part of the move. The probe pretravel and trip-force have a three-lobed characteristic in the radial direction, and probes have higher trip-forces in the axial direction, according to the manufacturer [2-8].

The actual machine position lags the MTC programmed position due to following error which is a function of servo loop gain. For this turning center, the following error is about 70 milliinches (1.78 mm) at 100 in/min (2540 mm/min) feed rate. To allow time for acceleration to 100 in/min (2540 mm/min) the probe must start about 0.2 in (5.1 mm) from the part. To allow time for deceleration, it must then move to 0.1 in (2.5 mm) beyond the part edge, and this distance must be within the probe overtravel limit. These considerations result in 0.12 in (3 mm) of constant velocity travel. A variation in part position (trip point) of ±0.04 in (±1 mm) could be tolerated. Since the probe trip signal holds the true position count from the feed-back device, the servo lag does not cause a dimensional error.

The concept of fast probing has been demonstrated. Repeated probing of the same point on the face of the chuck at 100 in/min shows a repeatability of one micrometer, which is the position feedback resolution and the probe repeatability specification. The probe retract is performed at machine traverse rate which is 275 in/min (6980 mm/min). The same point can be probed at the rate of two per second. In actual part probing, additional time is used to move to the next probing location. Fast probing of a demonstration part shows that a repeatability of ±1 μm can be achieved. A fast-probing program for six data points takes 11 seconds to run, but a significant portion of the time is used to move the probe from "home" position to the part and back again. The actual probing is at about one point per second. For the probe and stylus used, no false trips have been observed for rapid machine moves in the probe axial and radial directions. No delays (dwells) are needed between probings.

Machine Tool Quality Improvement Strategy

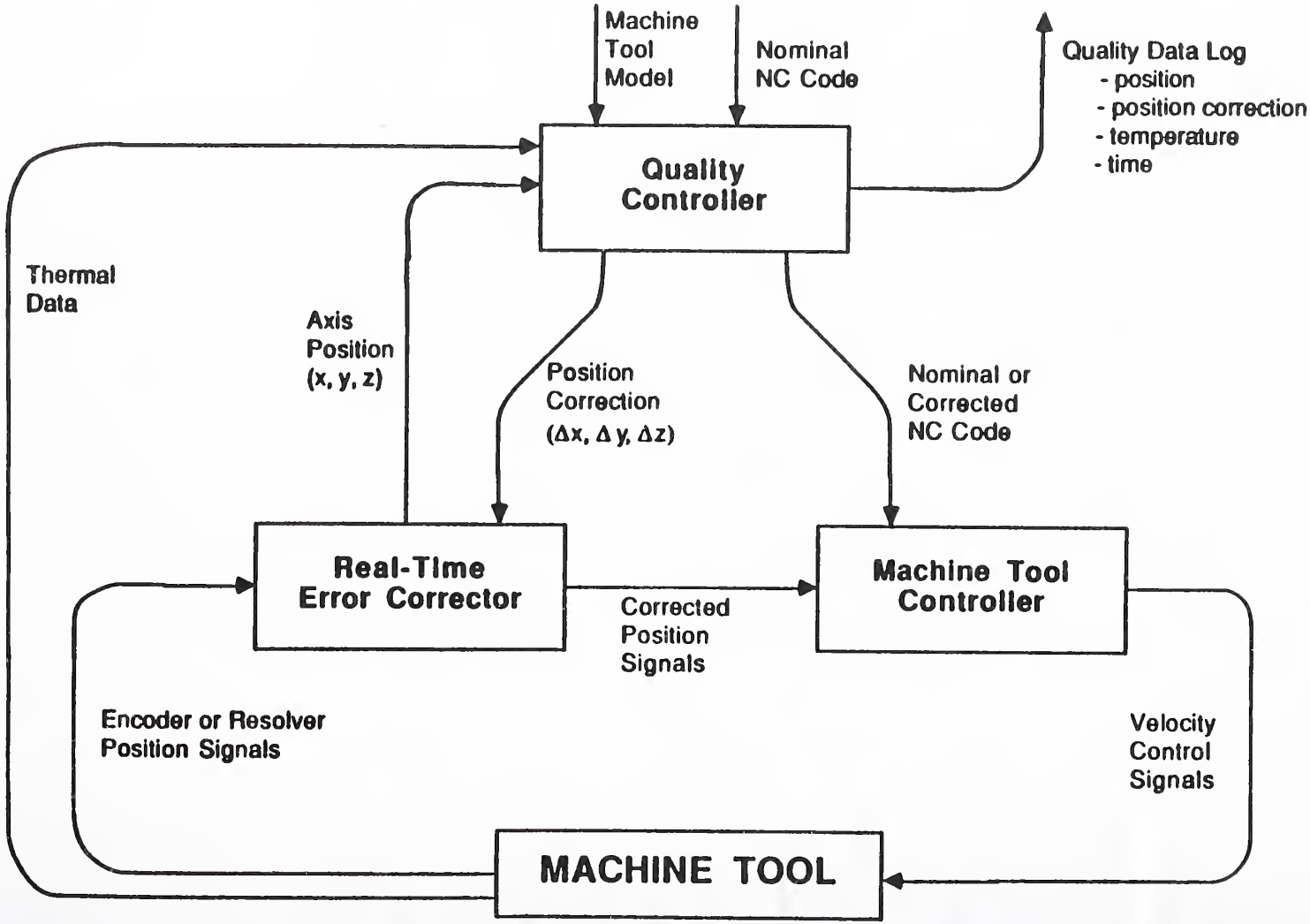

Fig. 2.1

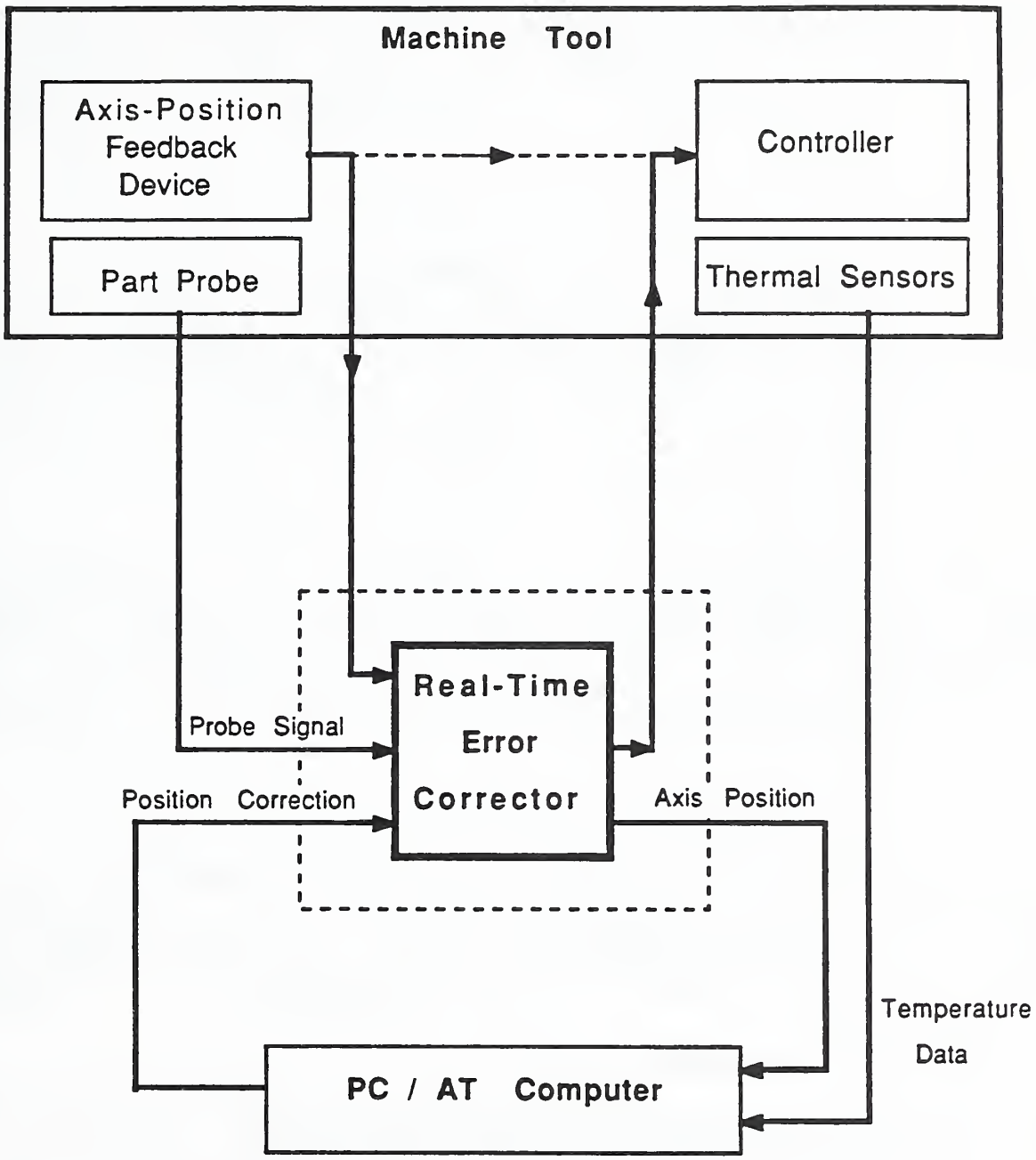

Real Time System Overview

Fig. 2.2

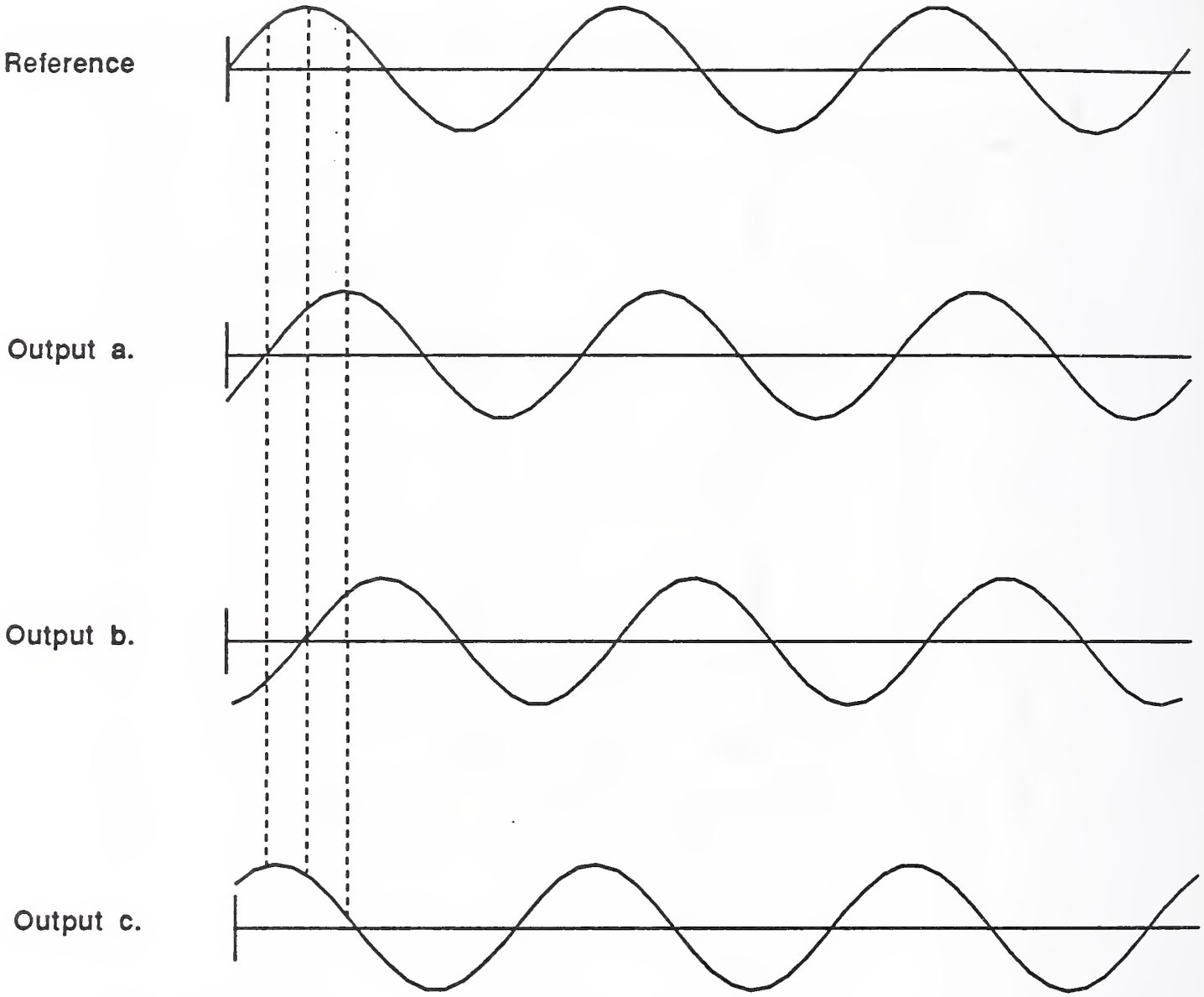

a. Output with axis stopped.

b. Output after axis has moved 1/8-resolver-rotation positive.

c. Output after axis has moved 3/8-resolver-rotation negative from (b) or 5/8-resolver-rotation more positive from (b).

Resolver Signals

Fig. 2.3

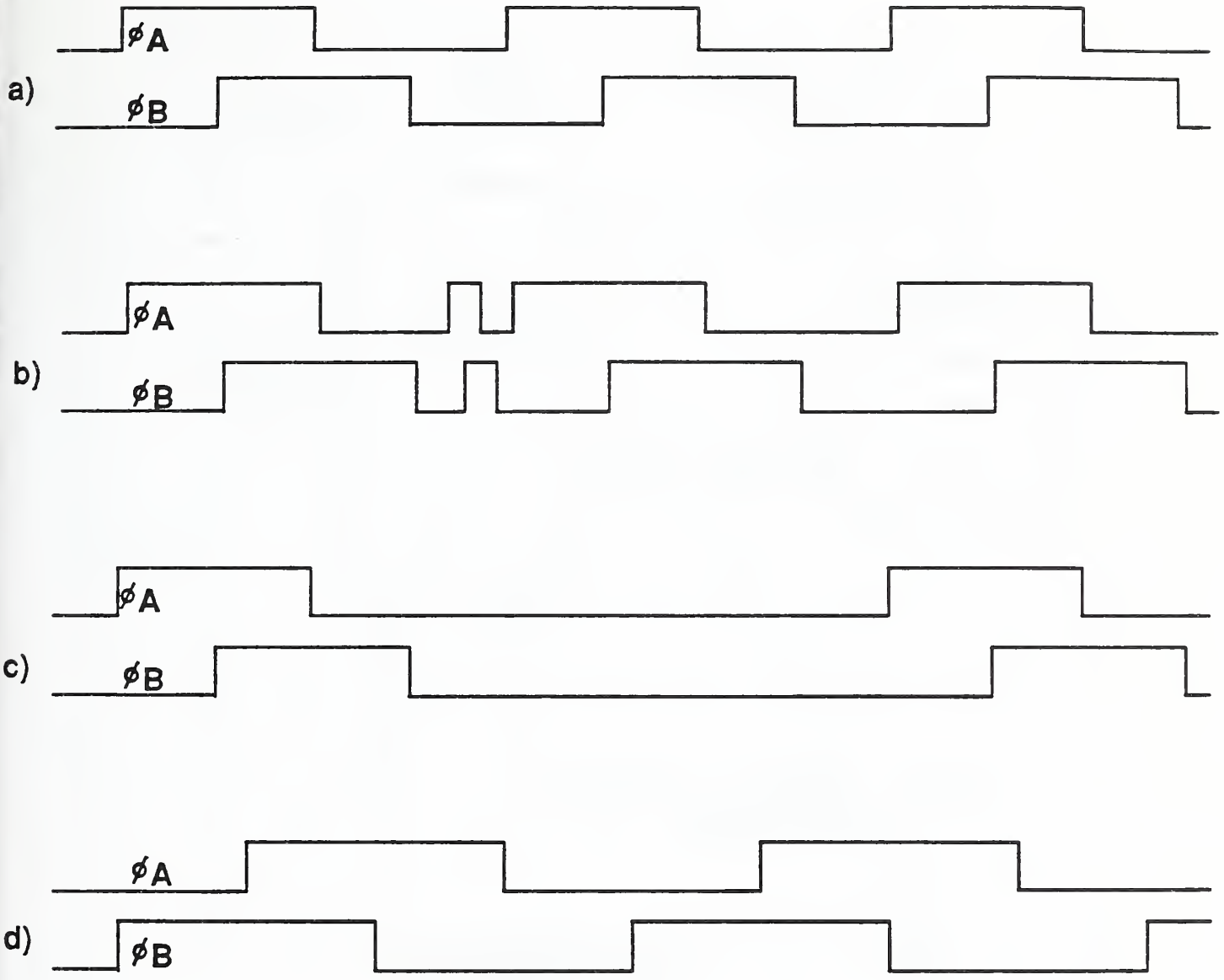

a.Axis moving in positive direction. **b.**One pulse added.

c.One pulse withheld. **d.**Axis moving in negative direction at a slower rate.

Encoder Signals

Fig. 2.4

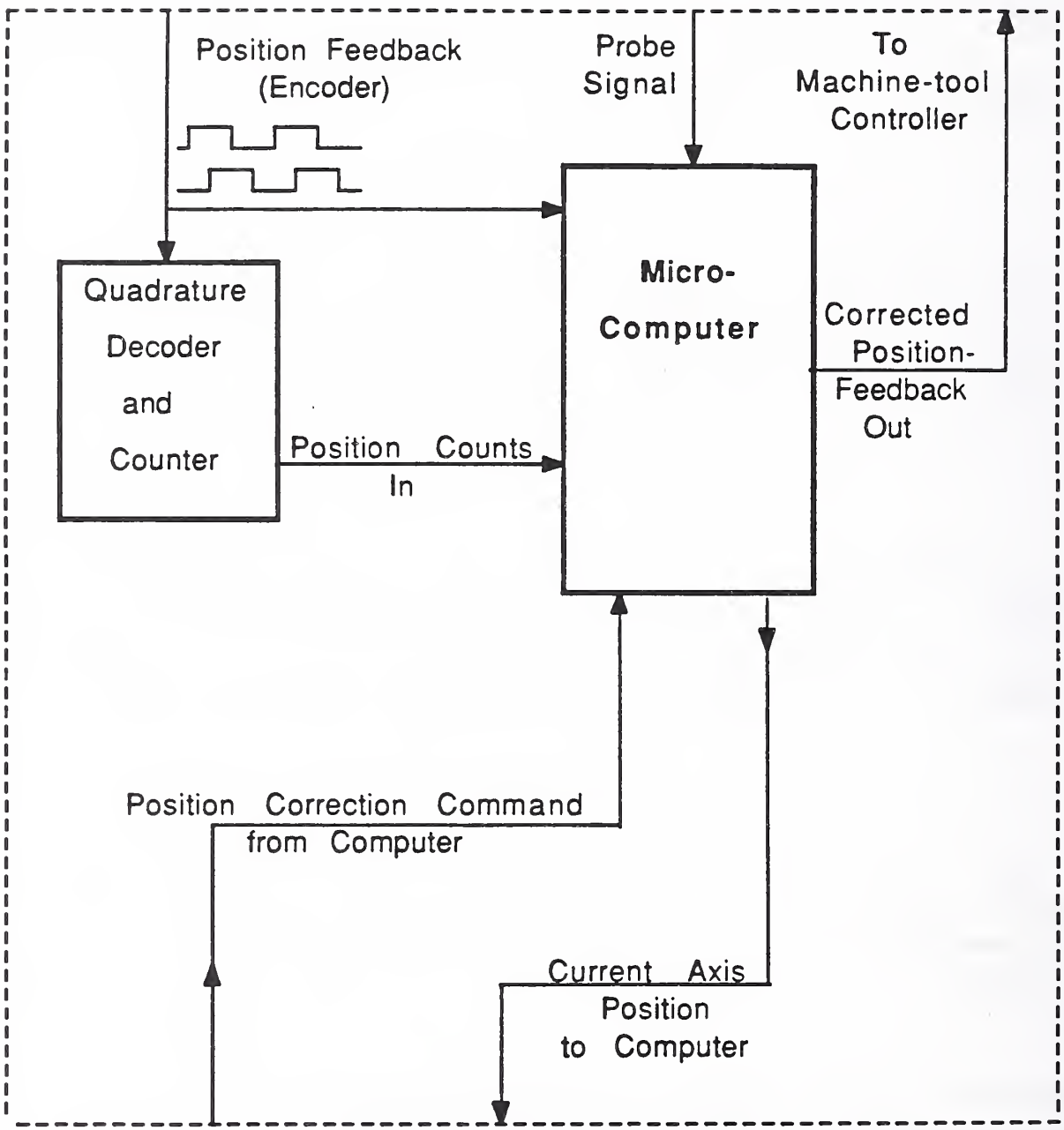

Real Time Error Corrector

Fig. 2.5

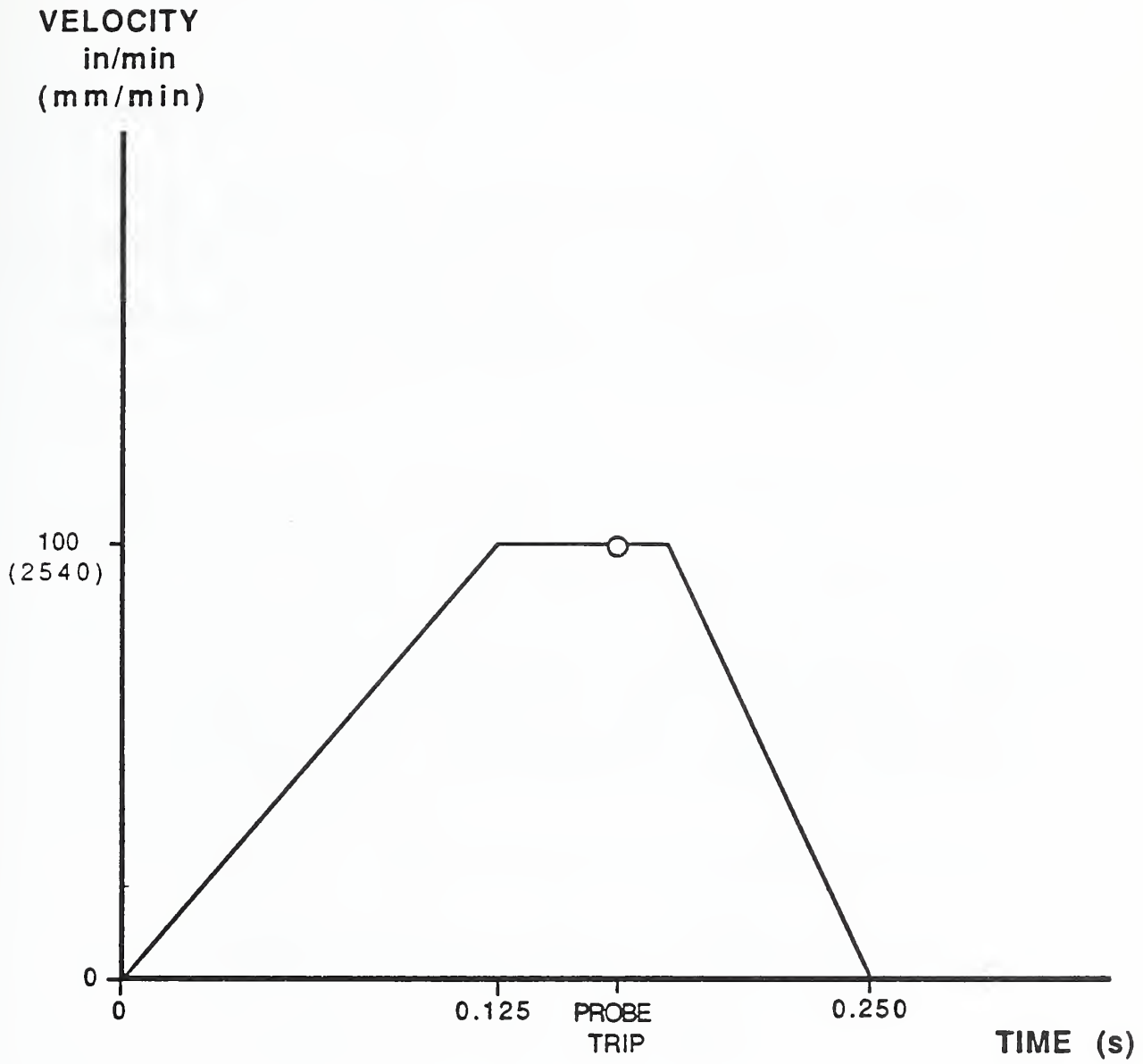

Velocity Profile for Fast Probing

Fig. 2.6

3. CHARACTERIZATION OF THE VERTICAL MACHINING CENTER

F. Rudder

3.1 OVERVIEW

During the past year we have progressed in the task of establishing the geometric and thermal characterization of a horizontal-axis and a vertical-axis CNC machining center. As reported in the last annual progress report, thermocouple installations were complete, PC-based data acquisition systems were in place and preliminary data had been acquired and presented.

During the present reporting period, the following technical accomplishments have been realized:

- thermal response characterization of each machining center;
- acquisition of geometric position error data as a function of machine tool temperature state for the vertical-axis machining center. (During the reporting period, changes in the AMRF program resulted in the deactivation of the horizontal-axis machining center. Thermal response data were obtained for this machine prior to its deactivation. Geometric position errors were not obtained).
- successful transfer of data files to the NIST Statistical Engineering Division for off-line analysis;
- preliminary statistical analysis of position error data to validate data acquisition and data logging procedures;
- formulation of axis-error surface models.

The following sections describe in more detail the specific technical accomplishments for this reporting period.

3.2 ERROR MODEL AND MACHINE TOOL KINEMATICS

The objective of our machine tool characterization is to establish an algorithm for introducing tool tip position compensation based upon active monitoring of the machine tool temperature distribution. The detailed form of this algorithm has not yet been established; however, the

measurements obtained and the preliminary analysis of these measurements are the basis for implementing compensation strategies that will be developed. Whatever form of compensation is selected will require knowledge of the error as related to both commanded position and temperature. As used here, "commanded position" is the axis position in the NC code.

Figure 3.1 represents a format for a compensation algorithm based upon measurement of the components of the machine tool position error. In Fig. 3.1, the independent variables are machine tool axis position (as programmed for machining a part) and temperature (as measured on the machine tool during machining). The dependent variable is the expected machine tool position error and represents the value or magnitude of compensation required. The "error surface" represents a visualization of the dependence between the independent variables and the magnitude of the error that must be compensated. This dependence must be determined statistically using experimentally measured values of the components of the machine tool position error. The following subsections decribe the procedures used and the raw data obtained for characterizing the components of the position error with temperature. Here, we discuss the statistical analysis of these data for the purpose of generating an error surface.

In Fig. 3.1 we present an inset illustrating a point on the error surface and we indicate an "estimation uncertainty" for this point. The utilization and analysis of our experimental data must minimize the estimation uncertainty. Further, the magnitude of the estimation uncertainty must not exceed the magnitude of the lower limit of desired compensation.

Our experimental data are measurements of the components of the machine tool position error for each machine tool axis and the squareness or orthogonality between the axes. These components are combined using the machine tool kinematics to predict the total position error of the axis. The total position error is the quantity we desire to compensate

and is the dependent variable indicated in Fig. 3.1, First, we consider what we mean by the term "temperature" as presented in Fig. 3.1.

The term "temperature" does not mean the value of a single measurement of a sensor during machining. Each component of the machine tool position error is measured (as described below) along with the temperature state represented by the 40 thermocouple measurements. Hence, the first step in analysis of our component data is to estimate the "best" temperature from a subset of thermocouples that correlates with that component's error. This estimate is characterized by its statistical uncertainty, and different error components will be characterized by different "best" temperatures. The second step in the analysis of our component data is to relate statistically the magnitude of the "best" temperature of a component to the magnitude of the error. This step introduces an additional statistical uncertainty that must be carried along with the characterization of the component error. Finally, we utilize the machine tool kinematics and our characterization of the component errors to predict the total position error of the machine tool axes. The expected prediction uncertainties associated with our prediction will be a sum of all of the errors associated with selecting the "best" temperature for each component and relating each component to its "best" temperature. This sum of all the uncertainties is the estimation uncertainty indicated in the inset of Fig. 3.1.

Now, considering the machine tool kinematics, the component errors combine such that the components may either increase or decrease the total position error of the machine tool. As described above, the statistical uncertainties for the components will be combined to establish the estimation uncertainty of the error surface illustrated in Fig. 3.1. Therefore, we will have to take careful account of the propagation of the uncertainties in the model and the correlations among the variables. We want to minimize this estimation uncertainty.

3.3 THERMAL RESPONSE MEASUREMENTS

For this project, thermal response measurements are simple temperature data logging tasks that may be classified according to the machine tool activity or motion. The resulting data are temperature-time histories for the machine tool. Four different machine tool motions have been utilized to characterize the machine tool thermal response for this project. These conditions are:

1) data logged during machining (i.e., metal cutting) operations
2) data logged during "air cutting" operations
3) data logged during long-term single-axis motion
4) data logged during position error measurements.

The QIA report for FY88 [1-1] presented typical results for machine tool thermal response during machining. That report also presented a detailed description of the location and the installation of thermocouples on the horizontal-axis milling machine, the vertical-axis milling machine, and the turning center. The results indicated that during typical machining operations, selected temperatures could vary over a 20°C range within a few minutes. In order to quantify the significance of the temperature variation and to establish a comparison for temperature data obtained with the position error measurements, the requirement for thermal response measurements during air cutting and long-term single-axis motion was established.

3.3.1 Air Cutting Response

These data comprise a continuous machine tool cycle wherein each axis undergoes independently a complete movement from limit to limit and return with the spindle speed fixed at a constant value. The cycle was repeated until the data logging indicated that all temperatures reached a steady value. This usually took several hours. (The axis feed rate was set at 50% maximum to prevent drive motor overheating.) Once the thermal equilibrium was achieved, the data logging continued to obtain steady

values for the machine tool temperature distribution. Finally, the machine tool motion was halted and the machine tool remained in a ready, but idle, state as data logging continued for several more hours. The idle period allowed data collection documenting the cool-down characteristics for the machine tool. Figures 3.2 and 3.3, respectively, represent typical thermal response of the horizontal-axis and the vertical-axis machining centers during an air cutting operation.

3.3.2 Long-Term Single-Axis Response

The air cutting response utilized spindle motion during data logging. Since a laser interferometer was to be utilized for position error measurements and since an optic must be spindle mounted with motion maintaining the continuity of the laser beam path, the need for a long-term single-axis response measurement was identified. This need raises the question of whether a temperature response under either metal cutting or air cutting operations can be simulated under conditions forced by the constraints of the laser measurements. Further, the acquisition of position error data was expected to result in atypical thermal input to the machine tool. Hence, the long-term single-axis temperature response measurements were conducted.

The response tests were conducted for each axis of each of the two milling machines and represent continuous limit-to-limit axis motion. As with the air cutting measurements, the axis feed rate was set at 50% of maximum feed rate to prevent drive motor overheating. The data logging continued over the transient period to reach steady conditions and a cool-down period.

Figures 3.4 and 3.5 present the thermal response measurements for the x-axis motion for the horizontal-axis and vertical-axis machining centers.

3.3.3 Position Error Measurements

Details of the position error measurements are presented in the following section. The discussion here focuses upon the machine tool temperature response during the position error measurements. First, it is appropriate to describe the temporal sequence utilized for obtaining the position error data and, hence, the technique utilized to warm-up the machine tool.

Position error data are obtained at discrete intervals along an axis. Motion between measurement locations is at a low feed rate to minimize any dynamic effects on the laser optics. Hence, it may take several minutes to obtain position error data for an axis. Since the machine tool drive motor is not in continuous operation and since other possible heat sources, such as friction, are expected to be minimal for these measurements, the anticipated effect was that the machine tool would cool-down during position error measurements. Hence, the temperature data logging was accomplished only at the beginning and at the end of each set of position error measurements. Following completion of a set of position error measurements, a machine tool warm-up cycle was conducted. This warm-up cycle was a repetitive limit-to-limit motion of the axis at approximately 65% maximum feed rate. Forty complete cycles of axis motion were utilized for each warm-up cycle which resulted in approximately 10 to 15 minutes of continuous operation. Warm-up cycles were alternated with axis position error measurements until the position error drift stabilized. As described in the following section, temperature and position error data were also obtained for the machine tool in a cool-down mode.

Figure 3.6 presents a composite plot of thermal response and position error (i.e., axis drift) of the vertical-axis machining center during x-axis position error measurements. The horizontal axis of Fig. 3.6 is time measured relative to the first element of the measurement set. The entire set of measurements spanned 8 hours. Figure 3.6 utilizes two vertical scales. The left hand scale is the measured x-axis position error component. The right hand vertical scale is the temperature of a

thermocouple at one end of the x-axis glass scale of the vertical machining center.

The data are classified by two time periods: warm-up and cool-down. Data for the warm-up period comprise the first 15 data sets (i.e., plotted points) or the first 320 minutes and data for the cool-down period comprise the period from 320 minutes to 480 minutes.

In Fig. 3.6, five curves are presented. Two curves are labeled "temperature". One curve is the temperature at the start of a measurement and the other curve is the temperature at the end of a measurement. For the temperature curves, the right hand vertical scale is used. Three curves are labeled "drift". These curves are plotted using the left hand vertical scale as the ordinate. As indicated in the figure legend, the upper curve (points indicated by an *-*) are data for the x-axis commanded position of 39.5 inches. One drift value is plotted for both the start time and the stop time of the individual measurement. This time difference is the time required to conduct a single measurement of the x-axis position error.

The two bottom curves labeled "drift" are for the x-axis commanded position x = 0. The curve plotted using "." corresponds to x = 0 before the axis move for increasing x values (denoted in the legend by →). These are the position data at the start of the individual measurement. The drift curve plotted using "x" corresponds to x = 0 after the returning axis move for decreasing x values (denoted in the legend by ←). The vertical distance between either "." and "*" or "x" and "*" corresponds to the total position error for the extreme values of x-axis commanded position. We call this error the relative error.

3.4 POSITION ERROR MEASUREMENTS

This section describes the effort conducted during the reporting period for obtaining position error data for the Monarch VMC-75 three-axis vertical machining center. In particular, we describe the machine tool

configuration, the measurement procedures developed and utilized, and a summary of the resulting position error data.

Since the objective of these measurements was to obtain data to relate tool tip position error to machine tool temperature distribution, the procedures utilized may not directly correspond to either actual machining conditions or to temperature distributions typical of machining operations. Rather, we were focusing upon obtaining data over a wide range of temperatures and machine positions recognizing that the thermal conditions may be more severe than conditions typical of machining operations. One should not assess the accuracy of this machine tool on the sole basis of position error data reported herein.

One may appreciate the significance of this statement by comparing Fig. 3.3 with either Figs. 3.5 or 3.6. Figure 3.3 is the air cutting thermal response measurement and from this it is seen that the x-axis scale temperature changes no more than 1°C during a 14 hour measurement period. From Fig. 3.5, one sees that a continuous x-axis warm-up cycle (in this case, 1350 extreme-to-extreme cycles) causes a change in x-axis scale temperature of over 10°C. From Fig. 3.6, the temperature change is over 6°C for the position error measurements. Hence, we see that the temperature range for the position error data covers the range encountered during normal machine operation. Further, position errors that we have measured as a function of temperature may be more extreme than the errors encountered during normal machine operation. This situation, however, is exactly our objective: obtain position error data utilizing a procedure that realizes machine temperature states encompassing a normal state.

3.4.1 Machine Tool Configuration

The data reported here are obtained on a Monarch Cortland VMC-75 vertical-axis machining center. The controller is a General Electric Mark Century 2000. The machine tool axes are identified in Fig. 3.7. For all measurements reported herein, the machine tool was operated with all axis compensation functions active and all mechanical systems performing their normal operations.

The specific machine tool is used solely for research in the AMRF. It has accumulated approximately 2000 hours of cycle-on time and has produced approximately 1000 parts.

3.4.2 Measurement Procedures

The data acquisition system used to log the position error data is described in the QIA report for FY88 [1-1]. This PC-based system was used to coordinate the measurement sequence among the execution of machine tool motion, temperature data acquisition, and position error measurements. One major effort of the project during the first half of the reporting period was to develop the necessary communication software linking the PC-controller and the VMC-75 controller.

The communications requirements are: 1) determination of active/idle status of the machine tool, 2) transfer of machine tool coordinate data from the machine tool to the PC, and 3) sequenced cycle-start activation of the machine tool. The present version of the data acquisition software performs these functions as well as executing the selection of user-defined part programs resident in the machine tool controller. The measurement procedure utilizes two types of part programs: 1) data acquisition programs and 2) warm-up programs.

For each position error measurement, a set of data is obtained. As indicated in Fig. 3.6, these data may be classified according to the temporal period of the measurement. Typically, a complete set of data requires a continuous elapsed time of at least 8 hours. This total time may be divided into two periods; warm-up and cool-down periods. For purpose of presentation, a specific set of data is called a cycle. Hence, each data set is identified either as a warm-up cycle or a cool-down cycle.

The practical significance of the term "cycle" is related to the structure of the NC program executed. Position error data are identified as a "warm-up cycle" if the data are immediately followed, in temporal

sequence, by the execution of the NC program used to warm-up the machine tool. The position error data are identified as a "cool-down cycle" if the machine tool remains idle, but in an active status, following the measurement. Hence, each data file is identified by the machine tool state following the measurement.

To determine the temperature dependence of the position error data, a typical data set may be comprised of over twenty individual data files (each "point" in Fig. 3.6 comprises a data file). The PC-based data acquisition system, as part of its bookkeeping function, creates an overview data file that logs start and stop times of each file, position data as measured at the axis limits, and the execution of a warm-up cycle following the measurement. Table 3.1 represents a listing of the overview data file or data chart for an axis distance measurement conducted on September 1989. This listing contains the following information:

- date of measurement: e.g., 0911 → month & day
- type of measurement: D → distance
  SS → short straightness
  A → angular (i.e., pitch or yaw)
  R → roll
- initial data file number: e.g., 01 → first data file
- machine tool: VS → vertical machining station
  HS → horizontal machining station
- measurement start and stop time: for example, file 0911D03.VSX, measurements started at 13:18:12 and ended at 13:27:41
- interferometer measurements logged at extreme axis positions: for example, for file 0911D03.VSX, the data began at machine position X = 0.0000 inch (-00.00052), continued to machine position X = 39.5000 inch (39.50111), and ended at machine position X = 0.0000 inch (-00.00041).
- warm-up cycle following measurement is denoted by * at the extreme right of the line

Hence, the data set comprises data file 0911D01.VSX through 0911D22.VSX (22 measurements) with fourteen warm-up cycles executed followed by eight cool-down cycles. These data are used for plotting the "drift" curves in Fig. 3.6.

Before execution of the first measurement, the machine tool was referenced and the laser initialized. Then, under manual control, the machine tool was slowly moved along the measurement axis from the initial position to the extreme position and returned to the initial position. This procedure was utilized for all measurements to establish, independently, the zero position of the measurement relative to the initial machine tool position.

The data in Table 3.1 allow one to overview the entire measurement or data set. A positive value for the measurement means that the laser optics have separated relative to the initialized location. A negative value means that the laser optics are closer to each other than the initialized value. Since the measurement procedures initialized the laser at the machine tool coordinate X = 0.0 inch, the data in the two columns headed X = 0 represent the position error drift of the machine tool for X = 0. The left hand X = 0 column is for X = 0 with subsequent motion for increasing X values. The right hand X = 0 column is for X = 0 with preceding motion for decreasing X values. The center data column, headed X = 39.5, is the laser measurement at the opposite extreme of the axis position and is recorded following a movement associated with increasing X values.

The next section presents a summary of the measurement data for the vertical axis milling machine. These data are "raw" data in the sense that detailed statistical analysis has yet to be conducted.

3.4.3 Raw Data Summaries

We present here summaries of the measurement data obtained so far. These summaries are concerned only with measurements for developing a compensation algorithm for the machine tool. Much more data has been obtained f the purpose of verifying measurement procedures, data repeatability, effect of measurement-axis location, and development of the data acquisition software. Details of these data and conclusions are appropriate for subsequent publication.

One salient aspect of this data acquisition project is that the primary variable, temperature, is not under direct experimental control, but is recorded as a parameter along with the position error data.

Table 3.2 is a listing of a single data file (0911D03.VSX) as logged during a measurement. All data are logged in an identical format. Each data file is comprised of four blocks of information:

- heading text and initial measurement
- initial temperature data
- measurement data
- final temperature data

The heading information is evident in Table 3.2. The initial measurement data consists of the data obtained from the laser (labeled "LASER-") and the data obtained from the machine tool controller (labeled "GE-"). This initial measurement can also be seen in Table 3.1 and is plotted as the third "." in Fig. 3.6.

The next block of data is temperature data. These data are identified by thermocouple number (data channel number), time of beginning the temperature data scan, and the temperature in degrees Celsius. Forty temperature values are logged (0-39). Each value corresponds to a specific location on the machine tool as reported in the QIA FY88 publication. The temperature for channel 3 (i.e., 24.47°C) is the third "+" point plotted in Fig. 3.6.

The measurement data comprise the next block of data. These data are pairs of values as obtained from the laser and from the machine tool control registers. The measurement sequence is evident. The difference between "LASER-" = 39.50111 and "GE-" = 39.5000 is the position error and the third "*-*" point plotted in Fig. 3.6. Special note should be made of the return measurement taken at X = 2.5000. The block following "GE-" is a result of a communication link failure between the PC-based data acquisition system and the machine tool controller. Such communication

failures are a common occurrence and represented the single most frustrating problem encountered. The PC-based software is capable of identifying such communication failures and automatically reestablishing proper communication with the machine tool controller. This protocol does not abort the data logging. As a result, a data file may contain either duplicate measurements or, as in this case, a blank measurement.

This problem is resolved by post-processing the data to create "clean" files to be used for data analysis. The software required to clean up the original data files was developed during the reporting period. All data are retained.

The final data block is a second temperature distribution of the machine tool identical in format to the temperature data block preceding the measurements. The difference between the initial and final temperature data blocks is the time of measurement and, of course, any temperature changes that may have occurred. The third "□" data point in Fig. 3.6 correspond to the channel 3 data (i.e., 24.62°C).

Figures 3.8 through 3.19 present a summary of raw position error data available at the time of publication. Figures 3.8 through 3.13 are for the x-axis and Figures 3.14 through 3.19 are for the y-axis. Each figure presents the axis position of the machine tool as the horizontal axis and the appropriate measure as the vertical axis. For each figure, four measurements are presented with each measurement corresponding to a data file such as listed in Table 3.2. Each measurement presents two sequences. One sequence corresponds to data for the table motion from the initial position to the extreme position and the other sequence is data for table motion from the extreme position to the initial position. For each figure a representative temperature is indicated for each measurement. These temperatures have been selected on the basis of their physical location rather than, at this time, any statistical significance.

3.4.4 Axis Drift

The data presented in the previous subsection (Figs. 3.8 - 3.19) are plots of measured data versus a commanded machine tool position. With the "axis drift" data in this subsection, we show the temperature dependence of the data for a fixed axis position. For these figures, temperature is considered as the independent variable and the error is the dependent variable. Since the data are acquired in a warm-up/cool-down sequence, the results show a form of hysteresis response for the axis position.

Time is an implicit parameter in these data. For either warm-up conditions or cool-down conditions, the machine tool is in a non-equilibrium thermal state. By considering error as a function of temperature at a fixed axis position, one must recognize that changes in both temperature and error occur over a time interval. For the data presented in this subsection the time interval between the temperature-error parts is on the order of several minutes. For practical error compensation, we must determine the compensation required within a time interval shorter than the time interval required for the machine tool to significantly change its thermal state. Hence, the format for data presentation used in this subsection is useful in quantifying important rates of change between error and temperature and provides a basis for establishing possible time constraints for implementing error compensation.

Figure 3.20 is a plot of x-axis position error versus x-scale temperature (channel #3 in Table 3.2) for x = 0.0 and x = 39.5. Three sets of curves are presented. The upper curve is the warm-up/cool-down response at x = 39.5. The lower four curves are for x = 0.0 with two curves corresponding to the x = 0.0 error at the start of the measurement and the other curves corresponding to the x = 0.0 error at the end of the measurement.

Figure 3.21 is a plot similar to Fig. 3.20. Figure 3.21 plots x-axis position error change or "relative error" versus x-scale temperature change for three different values of the x-axis commanded position. The

error change plotted in Fig. 3.21 is relative to the error for x = 0 at the start of each measurement. These data may be compared to those of Fig. 3.8 at the corresponding x-axis positions.

Figure 3.22 is a plot of y-axis relative position error at y = 19.5 inch versus the change in y-scale temperature. These data may be compared to those of Fig. 3.14 at y = 19.5 inch.

3.5 FUTURE EFFORT

The above discussion and the data presented summarize the results achieved during the reporting period. To complete the machine tool characterization, z-axis data acquisition must be completed as well as the squareness measurements. Data acquisition for the z-axis is currently in progress. Preliminary squareness data have been obtained for the x-y axis combination and we are evaluating both the data and alternative methods for measuring this parameter. In addition, the remaining issues of z-axis data acquisition and squareness measurements are currently being addressed.

As described above, the complete error data set will be analyzed along with the machine tool kinematics to obtain the predictive model for the total position error of the tool tip. The total position error is the basis for the error surface illustrated in Fig. 3.1. Hence, data reduction and the statistical analysis of the data will comprise a major effort during the next reporting period.

Finally, implementation of the error compensation algorithm based upon the machine tool characterization described above will complete the effort.

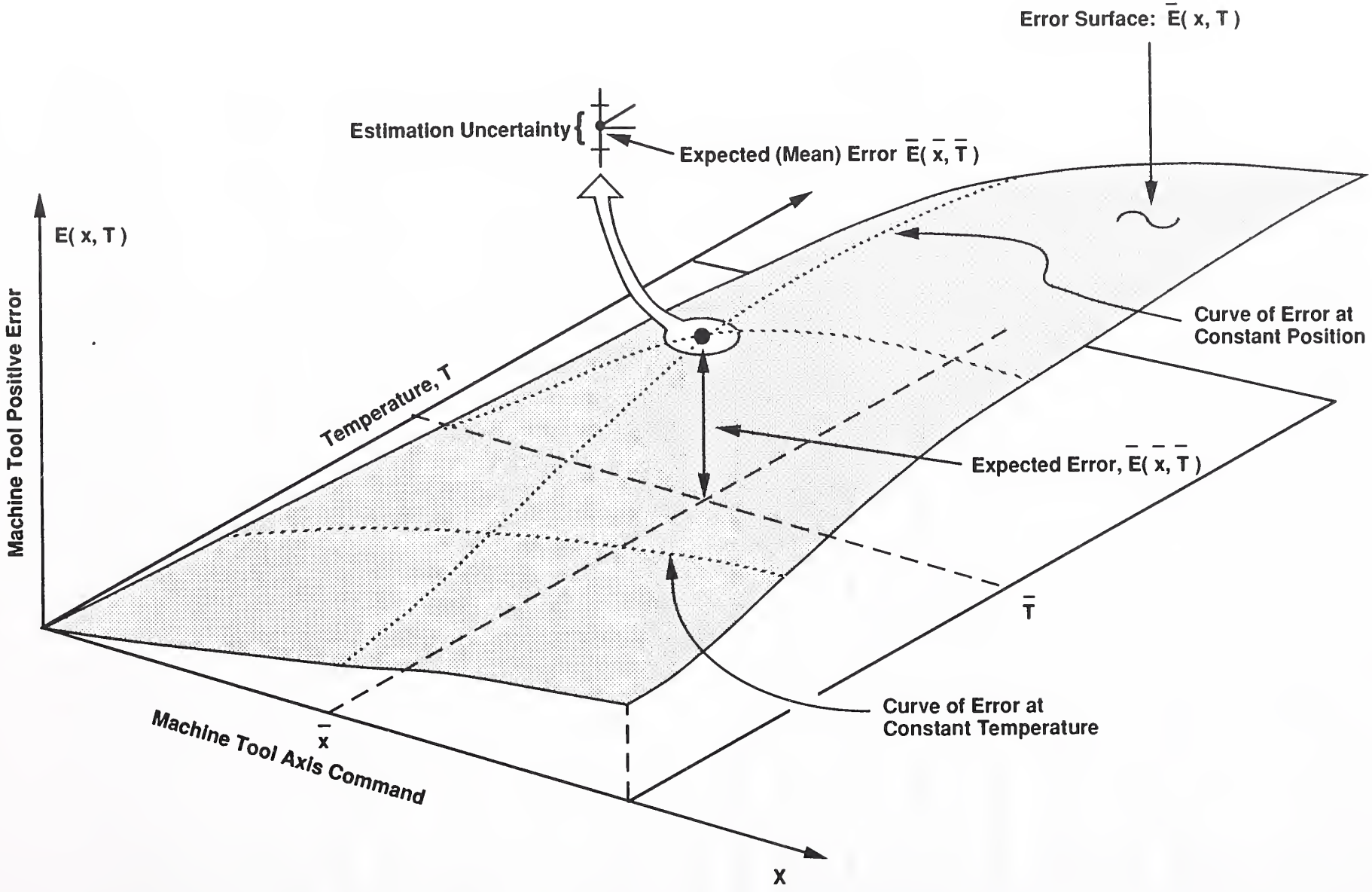

FIGURE 3.1
Error Surface for Axis Position and Temperature

Thermal Response - Horizontal Machining Center

Fig. 3.2a

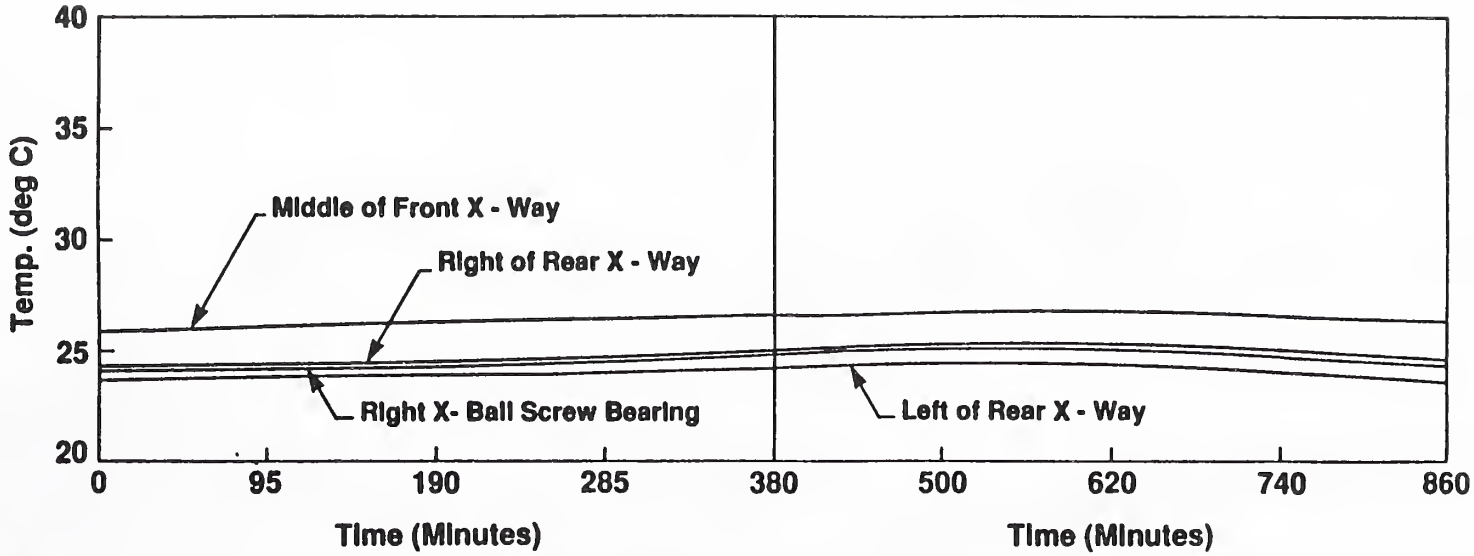
40
35
30
25
20
Temp. (deg C)
Middle of Front X - Way
Right of Rear X - Way
Right X- Ball Screw Bearing
Left of Rear X - Way
0
95
190
285
380
500
620
740
860
Time (Minutes)
Time (Minutes)

Fig. 3.2b

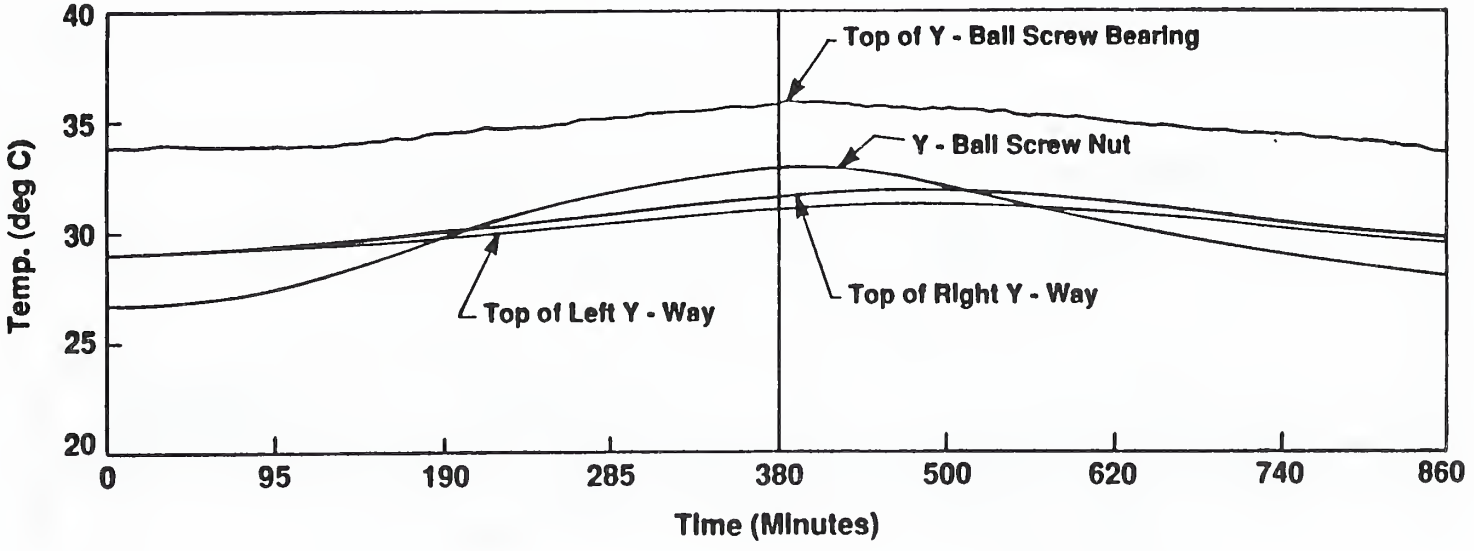
Top of Y - Ball Screw Bearing
Y - Ball Screw Nut
Top of Left Y - Way
Top of Right Y - Way
Temp. (deg C)
40
35
30
25
20
0
95
190
285
380
500
620
740
860
Time (Minutes)

Fig. 3.2c

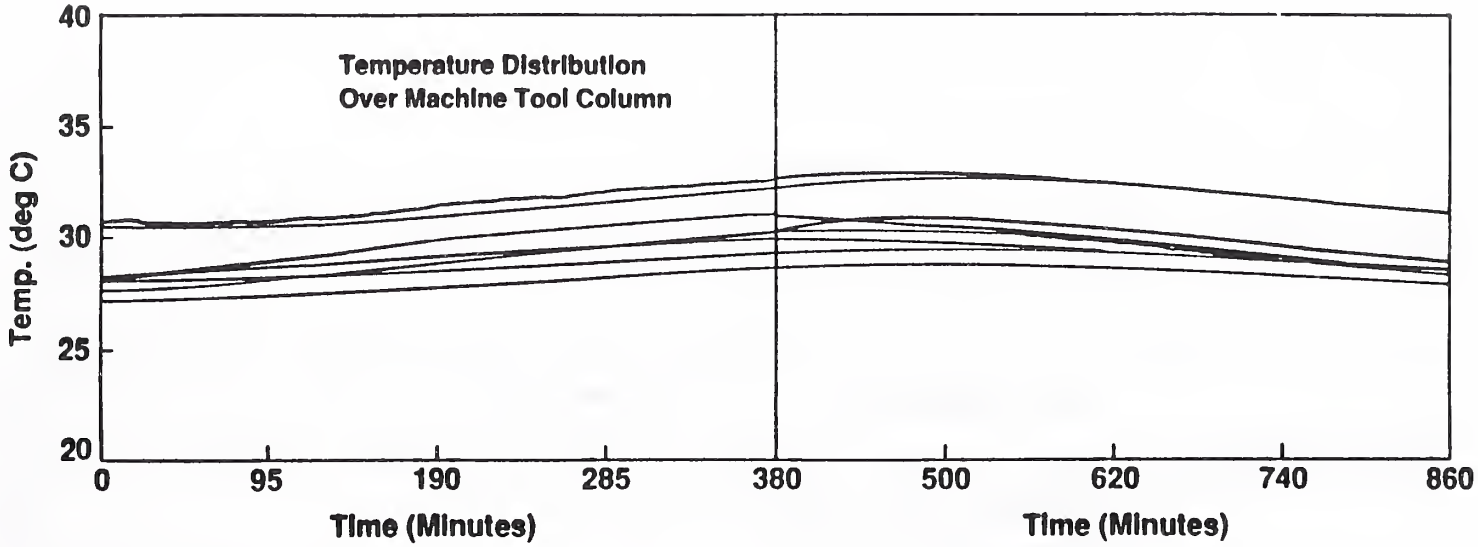
Temperature Distribution
Over Machine Tool Column
Temp. (deg C)
40
35
30
25
20
0
95
190
285
380
500
620
740
860
Time (Minutes)
Time (Minutes)

Fig. 3.2d

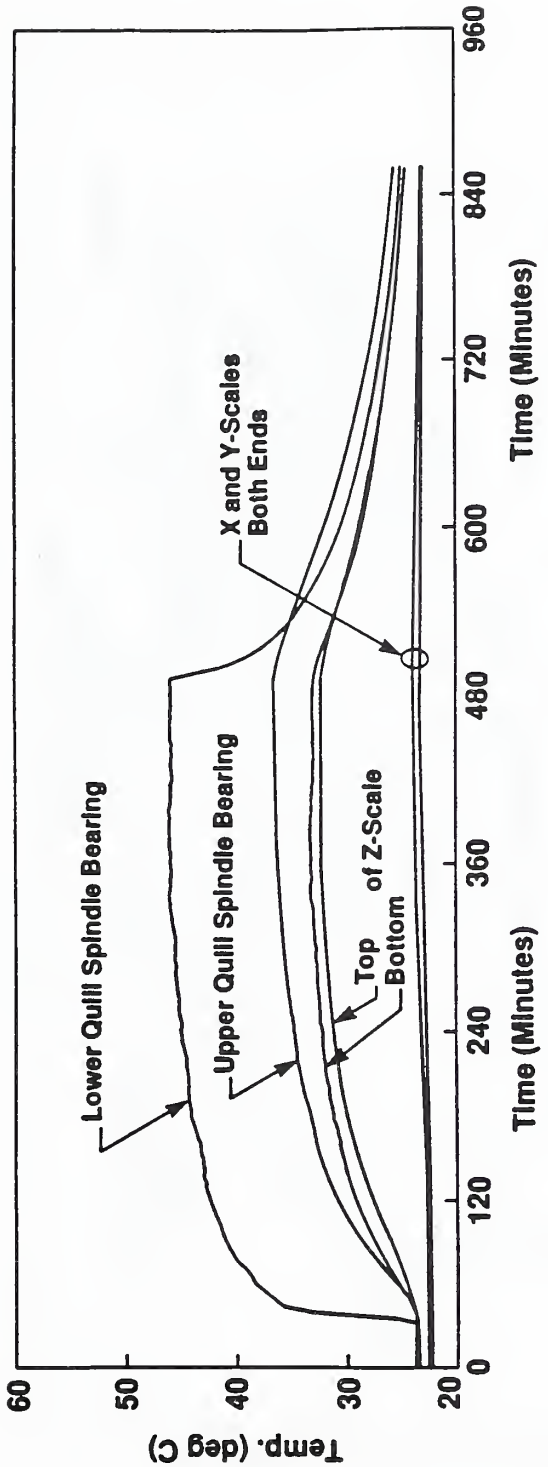

Thermal Response - Vertical Machining Center

Fig. 3.3

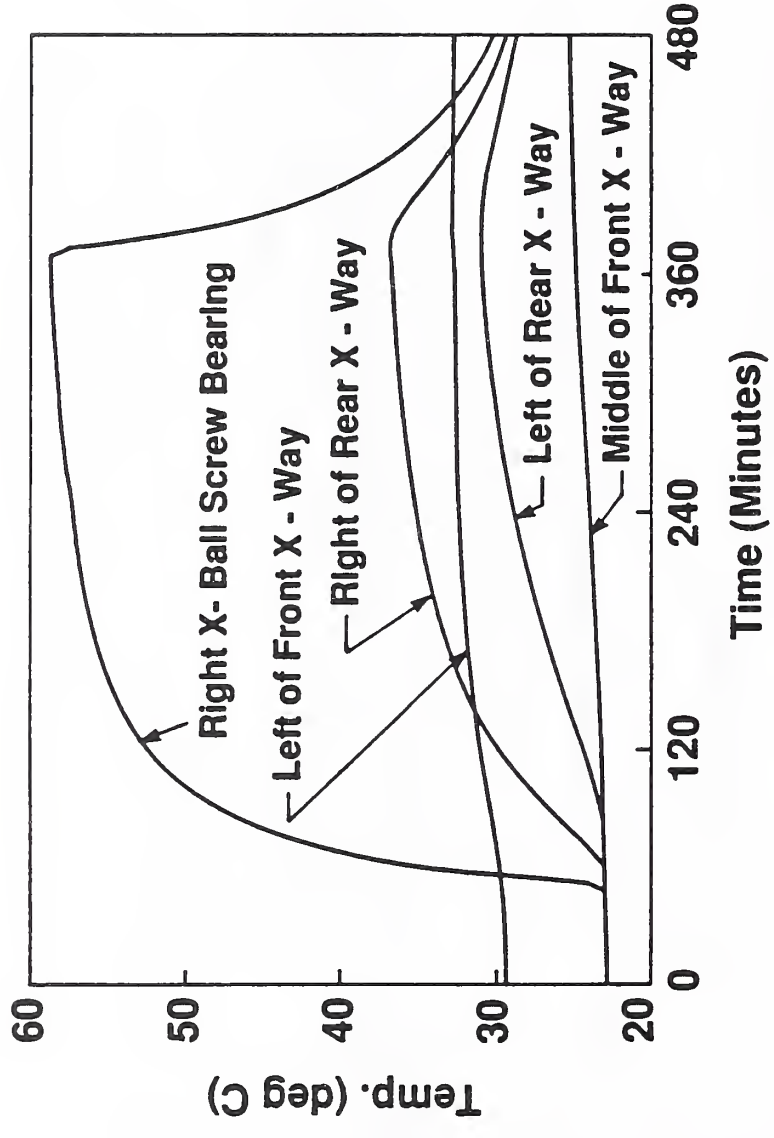

Thermal Response X-axis Motion
Horizontal Machining Center

Fig. 3.4

Thermal Response for X-axis
Vertical Machining Center

Fig. 3.5

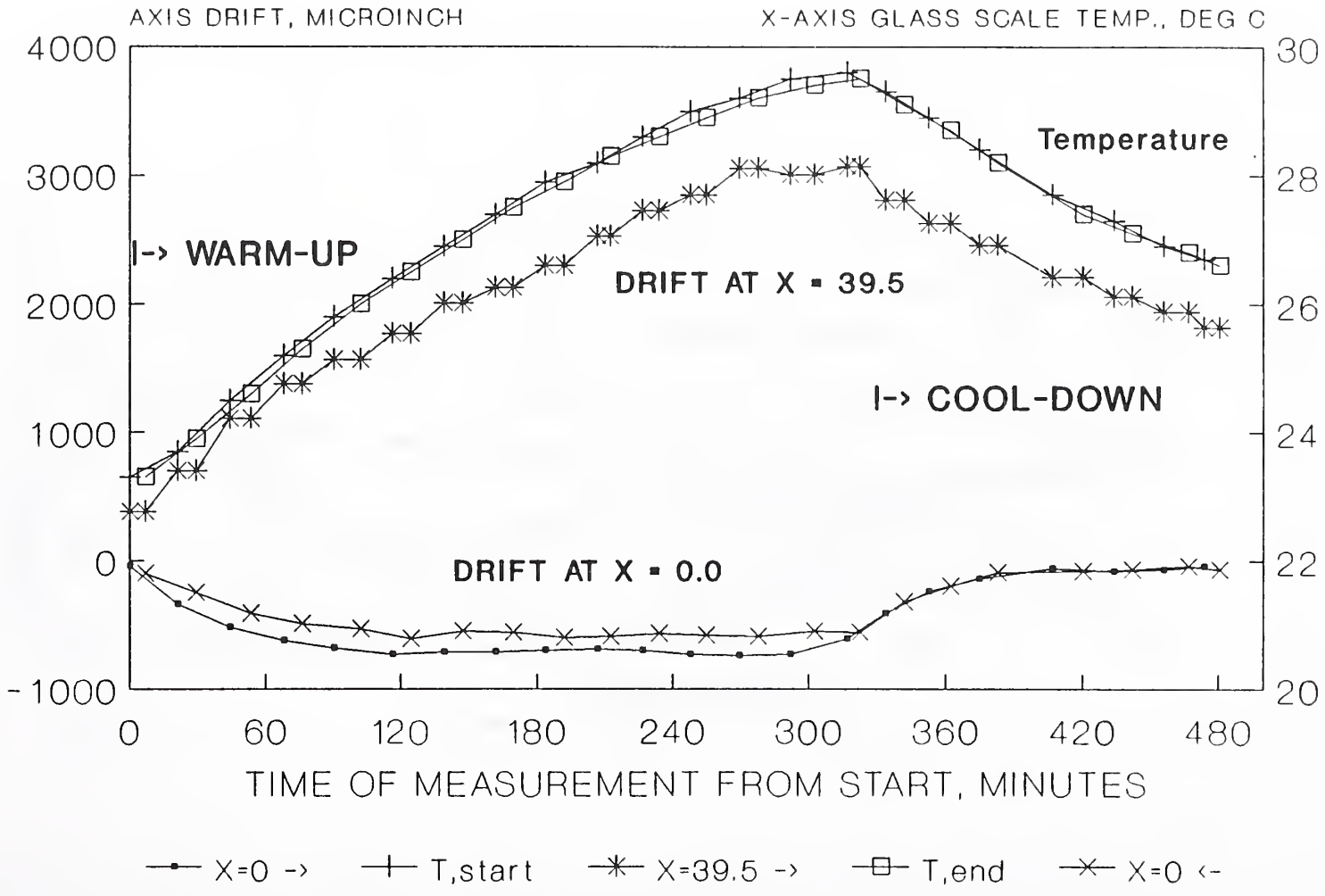
AXIS DRIFT, MICROINCH
X-AXIS GLASS SCALE TEMP., DEG C
4000
3000
2000
1000
0
-1000
30
28
26
24
22
20
Temperature
I-> WARM-UP
DRIFT AT X = 39.5
I-> COOL-DOWN
DRIFT AT X = 0.0
0
60
120
180
240
300
360
420
480
TIME OF MEASUREMENT FROM START, MINUTES
X=0 ->
T,start
X=39.5 ->
T,end
X=0 <-

Fig. 3.6

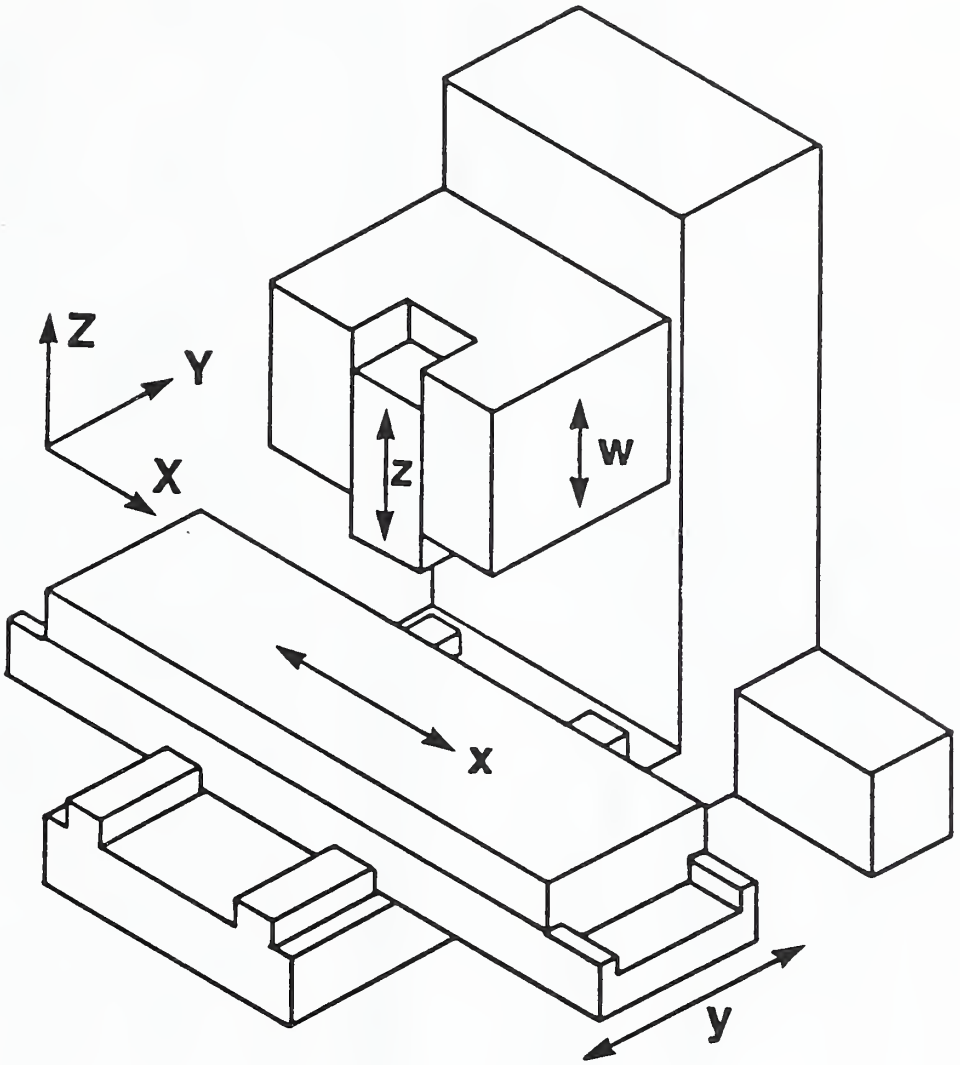

Fig. 3.7

Machine Tool Axes
Vertical Machining Center

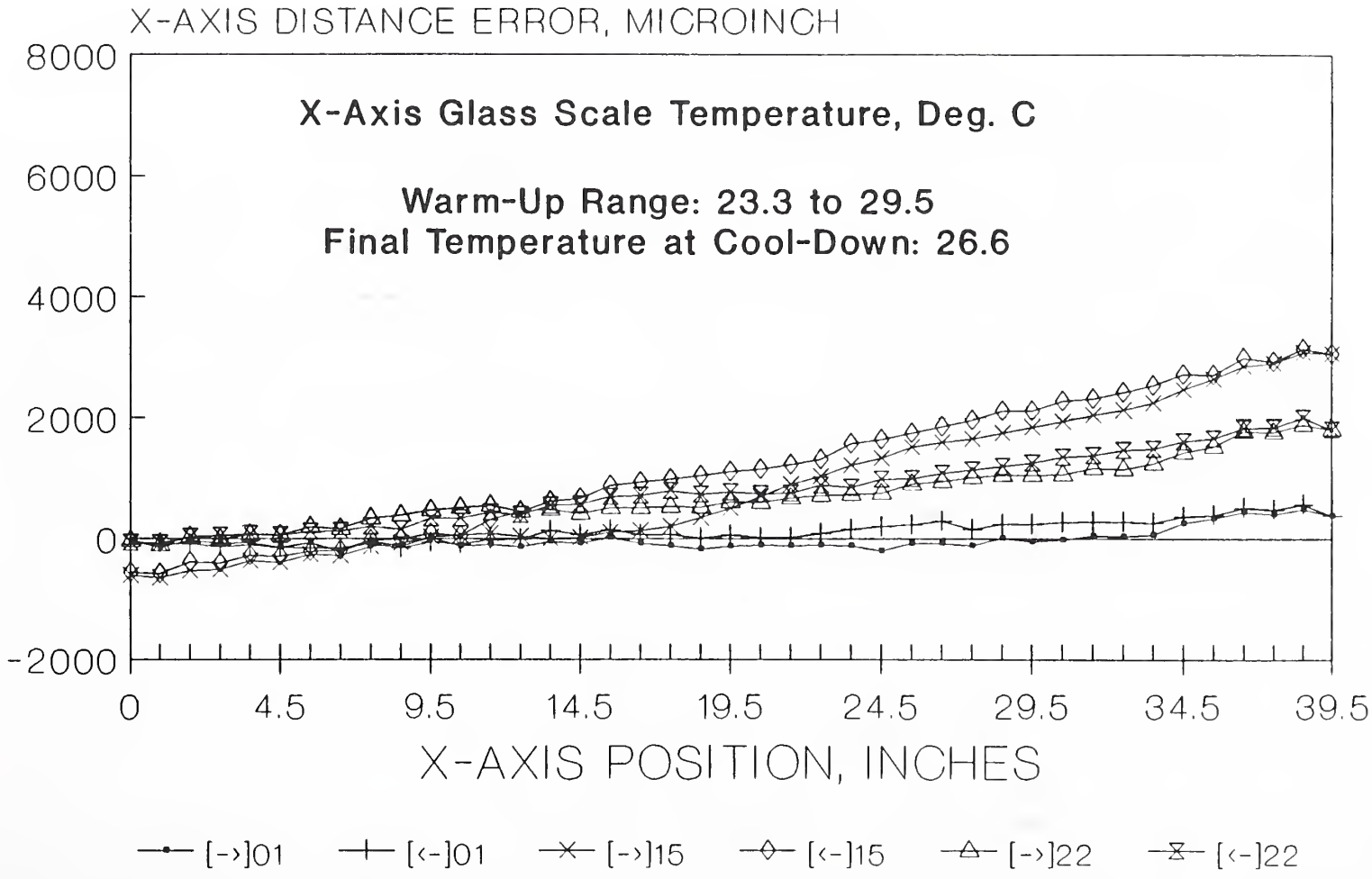
X-AXIS DISTANCE ERROR, MICROINCH
8000
6000
4000
2000
0
-2000
X-Axis Glass Scale Temperature, Deg. C
Warm-Up Range: 23.3 to 29.5
Final Temperature at Cool-Down: 26.6
0
4.5
9.5
14.5
19.5
24.5
29.5
34.5
39.5
X-AXIS POSITION, INCHES
[->]01
[<-]01
[->]15
[<-]15
[->]22
[<-]22

Fig. 3.8

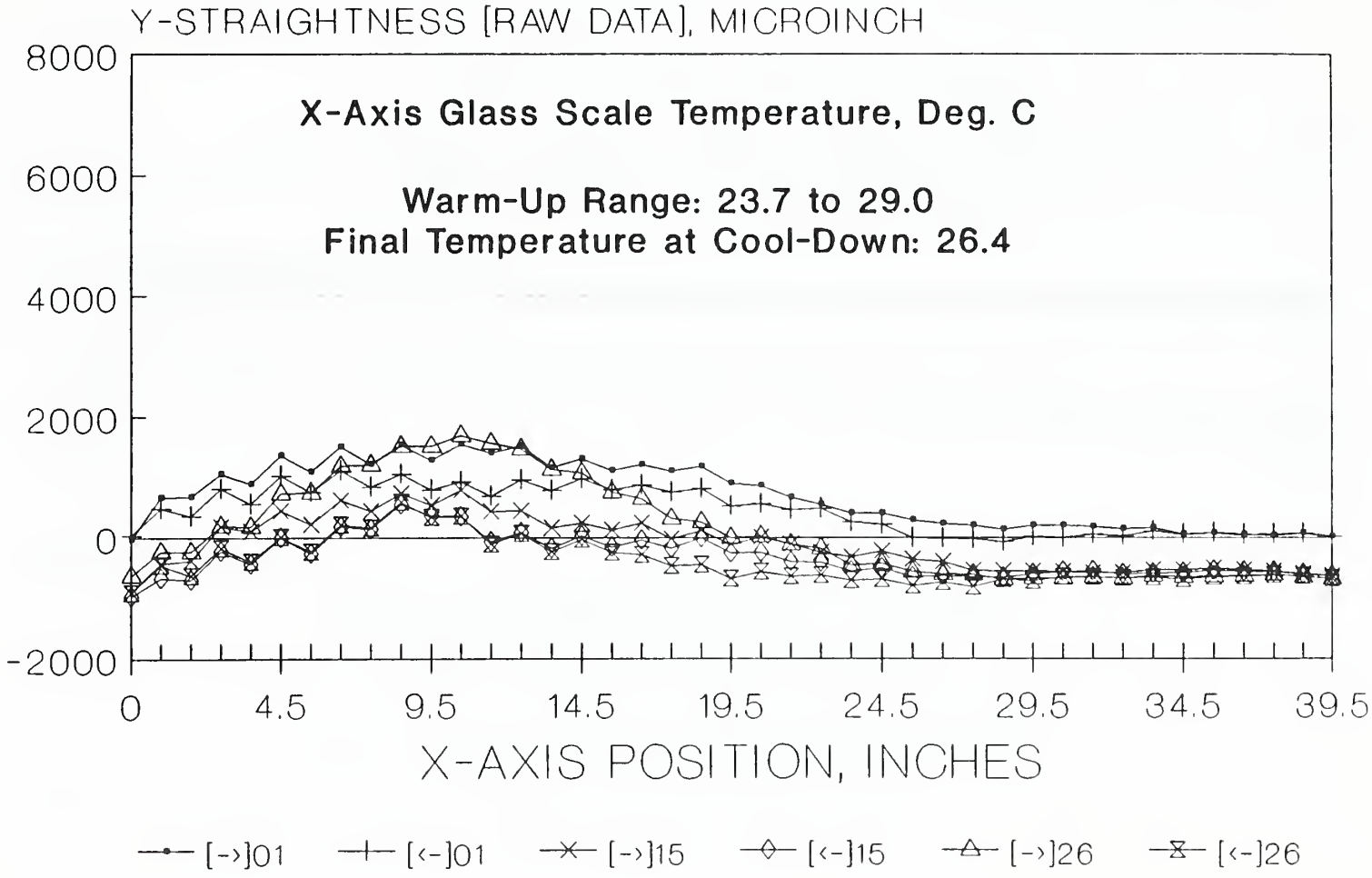
Y-STRAIGHTNESS [RAW DATA], MICROINCH
8000
6000
4000
2000
0
-2000
X-Axis Glass Scale Temperature, Deg. C
Warm-Up Range: 23.7 to 29.0
Final Temperature at Cool-Down: 26.4
0
4.5
9.5
14.5
19.5
24.5
29.5
34.5
39.5
X-AXIS POSITION, INCHES
[->]01
[<-]01
[->]15
[<-]15
[->]26
[<-]26

Fig. 3.9

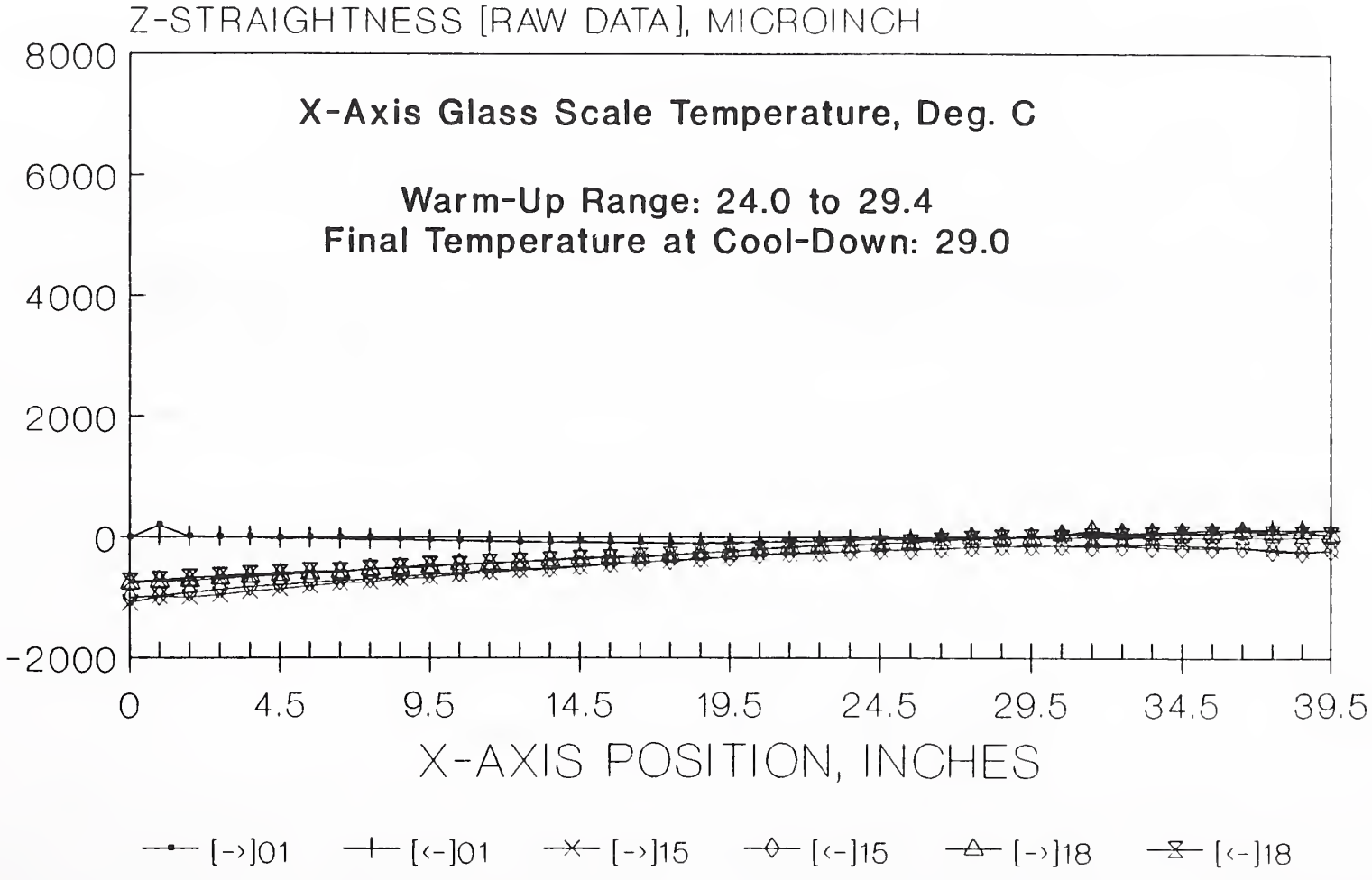
Z-STRAIGHTNESS [RAW DATA], MICROINCH
8000
6000
4000
2000
0
-2000
X-Axis Glass Scale Temperature, Deg. C
Warm-Up Range: 24.0 to 29.4
Final Temperature at Cool-Down: 29.0
0
4.5
9.5
14.5
19.5
24.5
29.5
34.5
39.5
X-AXIS POSITION, INCHES
[->]01
[<-]01
[->]15
[<-]15
[->]18
[<-]18

Fig. 3.10

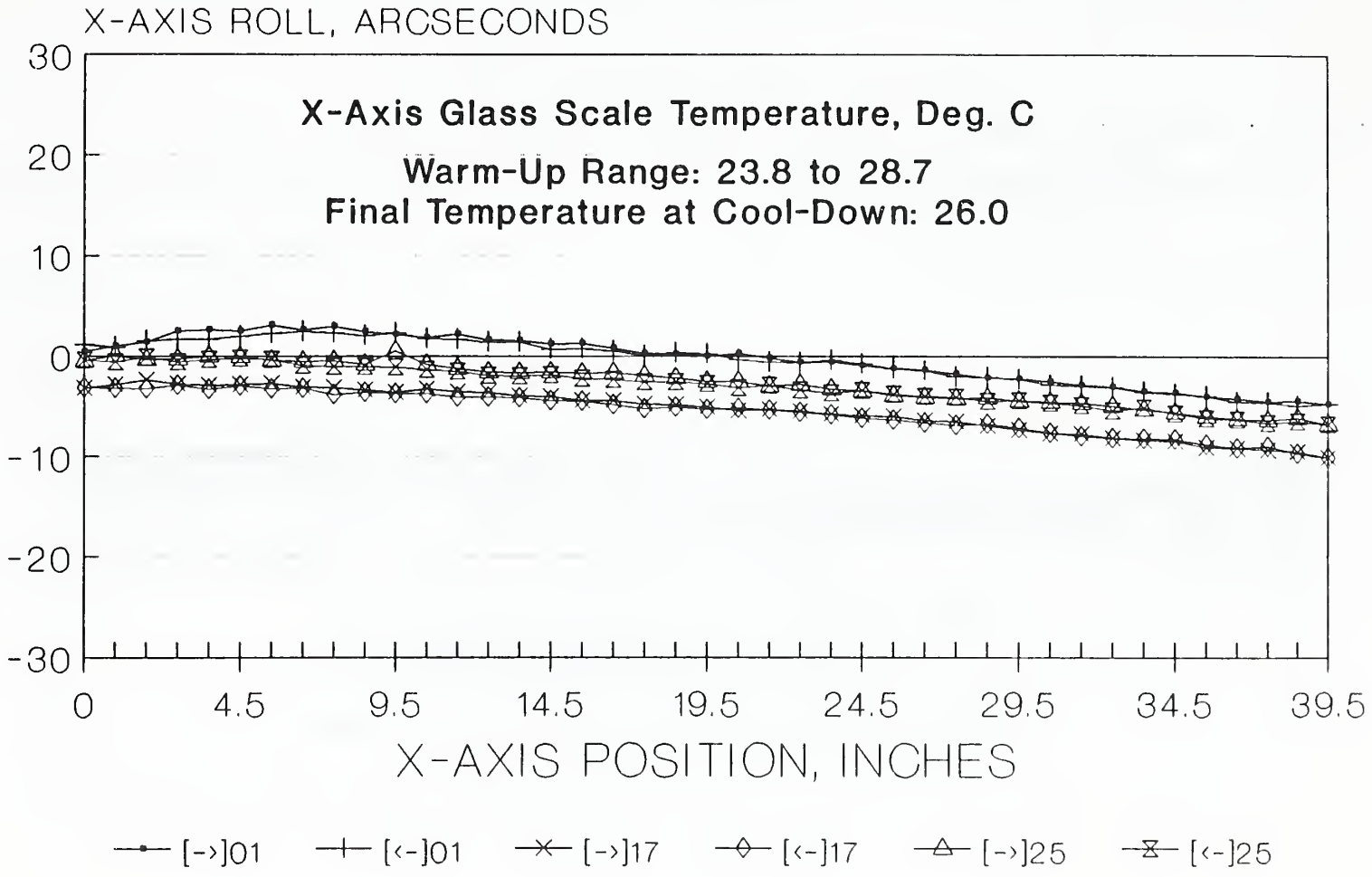
X-AXIS ROLL, ARCSECONDS
30
20
10
0
-10
-20
-30
X-Axis Glass Scale Temperature, Deg. C
Warm-Up Range: 23.8 to 28.7
Final Temperature at Cool-Down: 26.0
0
4.5
9.5
14.5
19.5
24.5
29.5
34.5
39.5
X-AXIS POSITION, INCHES
[->]01
[<-]01
[->]17
[<-]17
[->]25
[<-]25

Fig. 3.11

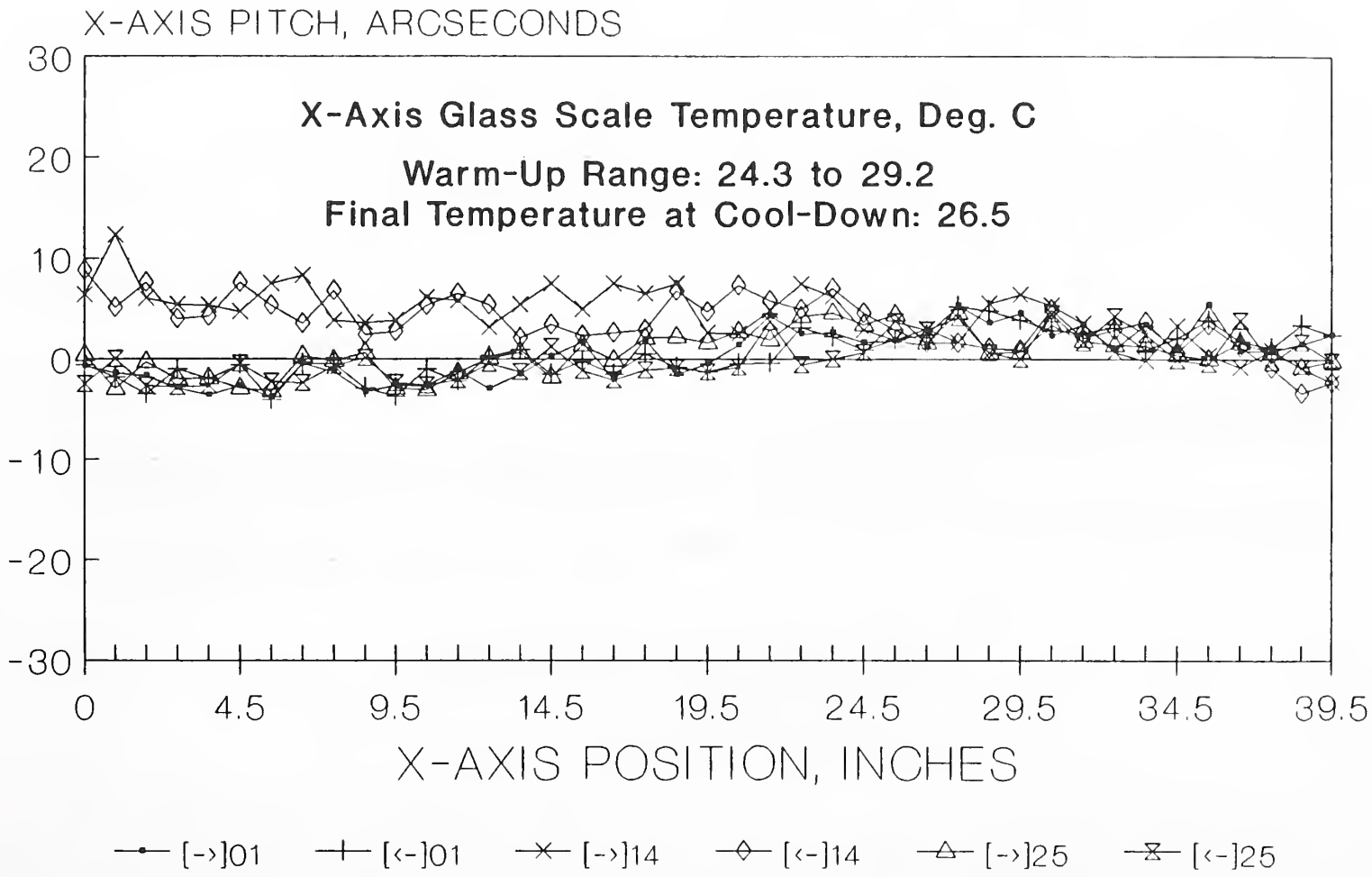
X-AXIS PITCH, ARCSECONDS
X-Axis Glass Scale Temperature, Deg. C
Warm-Up Range: 24.3 to 29.2
Final Temperature at Cool-Down: 26.5
30
20
10
0
-10
-20
-30
0
4.5
9.5
14.5
19.5
24.5
29.5
34.5
39.5
X-AXIS POSITION, INCHES
[->]01
[<-]01
[->]14
[<-]14
[->]25
[<-]25

Fig. 3.12

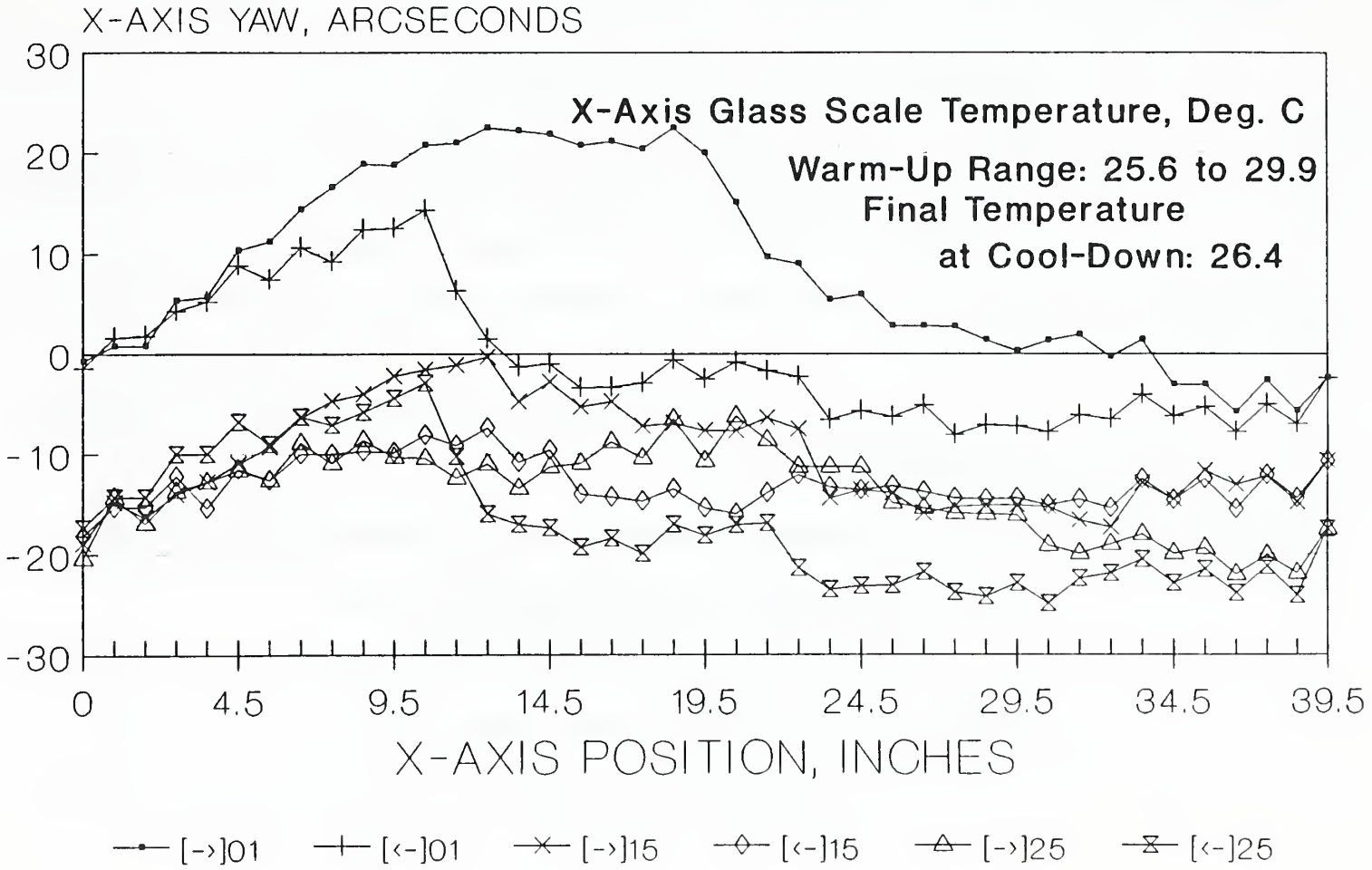
X-AXIS YAW, ARCSECONDS
30
20
10
0
-10
-20
-30
X-Axis Glass Scale Temperature, Deg. C
Warm-Up Range: 25.6 to 29.9
Final Temperature
at Cool-Down: 26.4
0
4.5
9.5
14.5
19.5
24.5
29.5
34.5
39.5
X-AXIS POSITION, INCHES
[->]01
[<-]01
[->]15
[<-]15
[->]25
[<-]25

Fig. 3.13

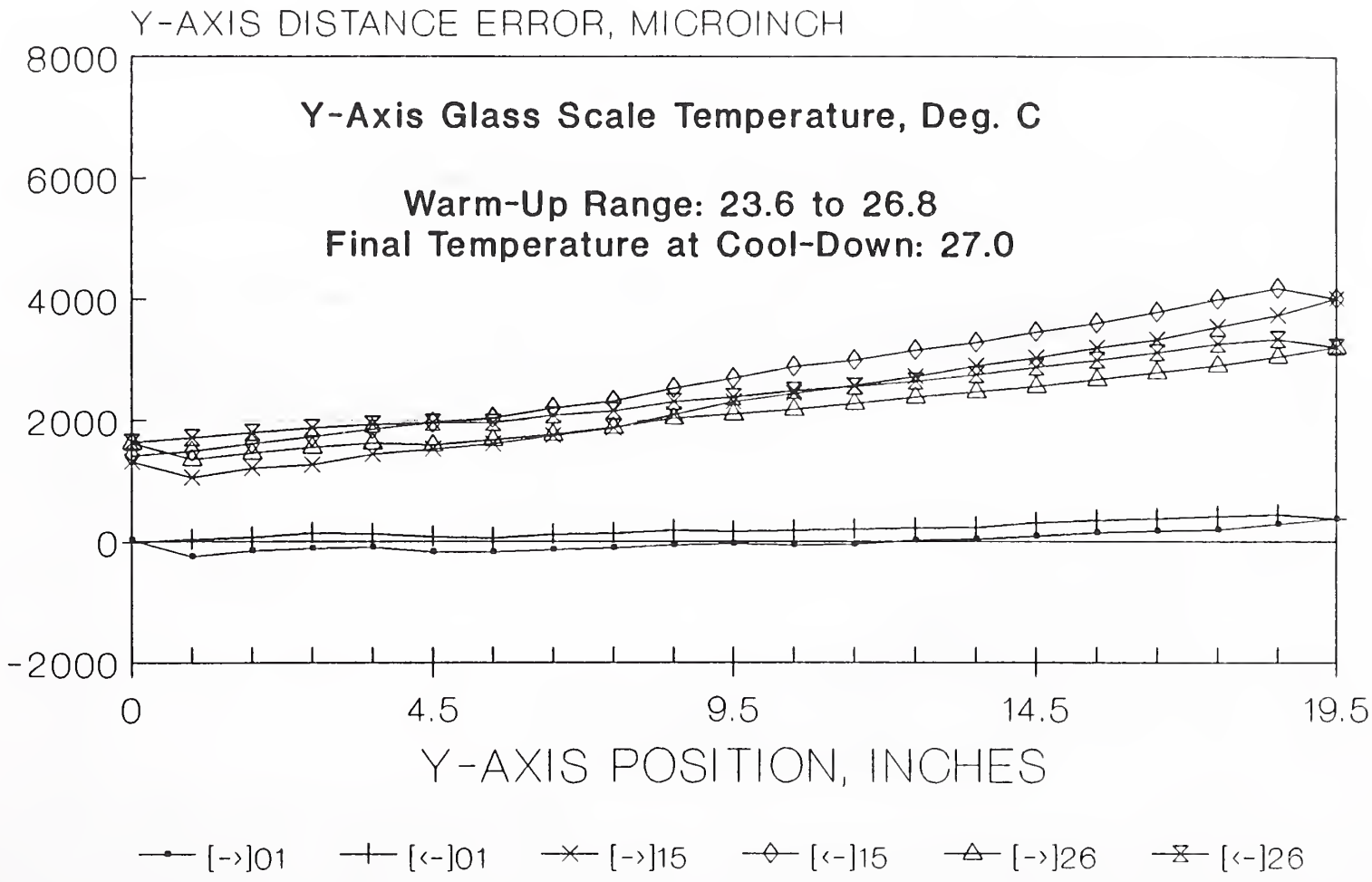
Y-AXIS DISTANCE ERROR, MICROINCH
8000
6000
4000
2000
0
-2000
Y-Axis Glass Scale Temperature, Deg. C
Warm-Up Range: 23.6 to 26.8
Final Temperature at Cool-Down: 27.0
0
4.5
9.5
14.5
19.5
Y-AXIS POSITION, INCHES
[->]01
[<-]01
[->]15
[<-]15
[->]26
[<-]26

Fig. 3.14

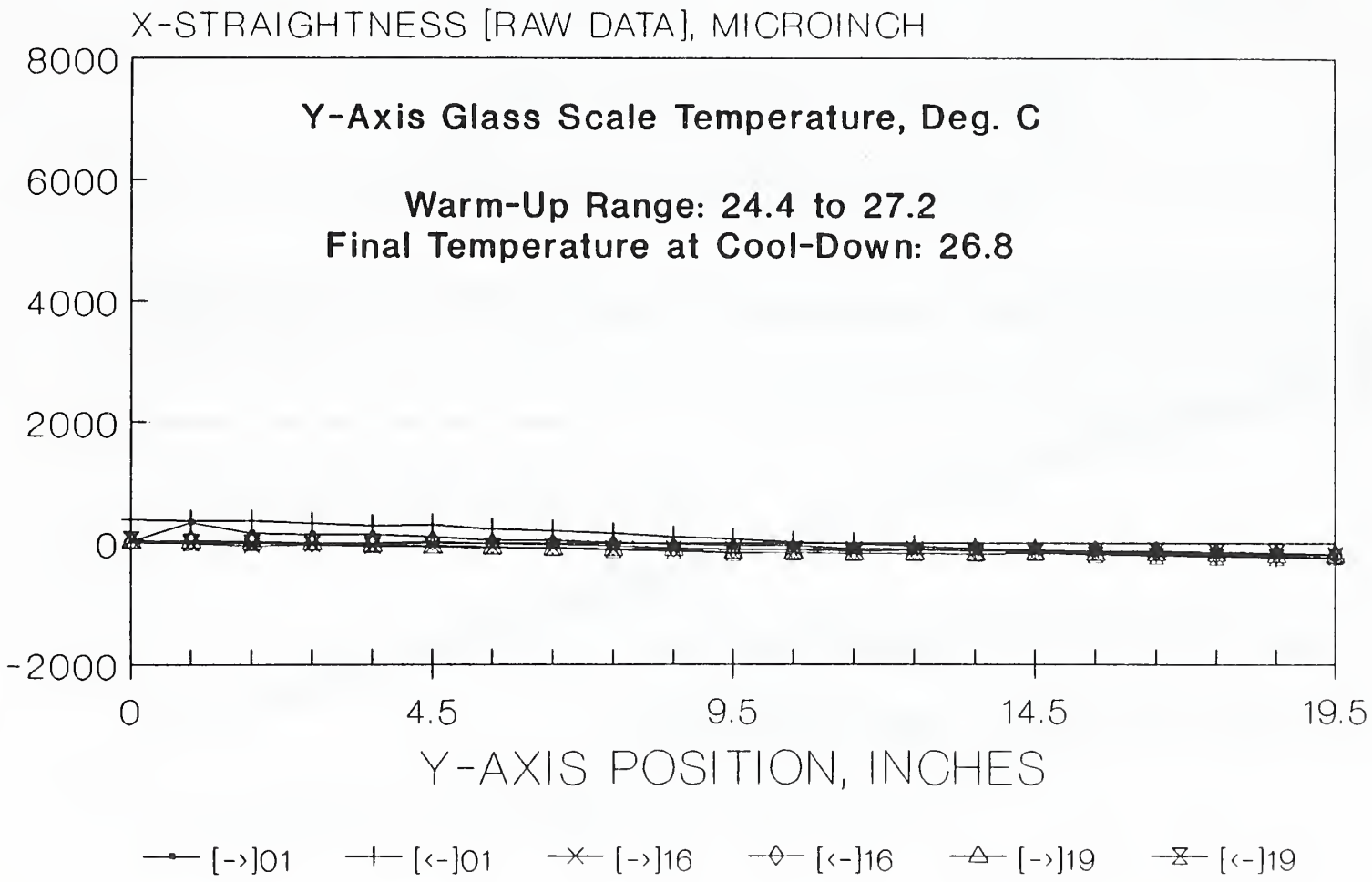
X-STRAIGHTNESS [RAW DATA], MICROINCH
8000
6000
4000
2000
0
-2000
Y-Axis Glass Scale Temperature, Deg. C
Warm-Up Range: 24.4 to 27.2
Final Temperature at Cool-Down: 26.8
0
4.5
9.5
14.5
19.5
Y-AXIS POSITION, INCHES
[->]01
[<-]01
[->]16
[<-]16
[->]19
[<-]19

Fig. 3.15

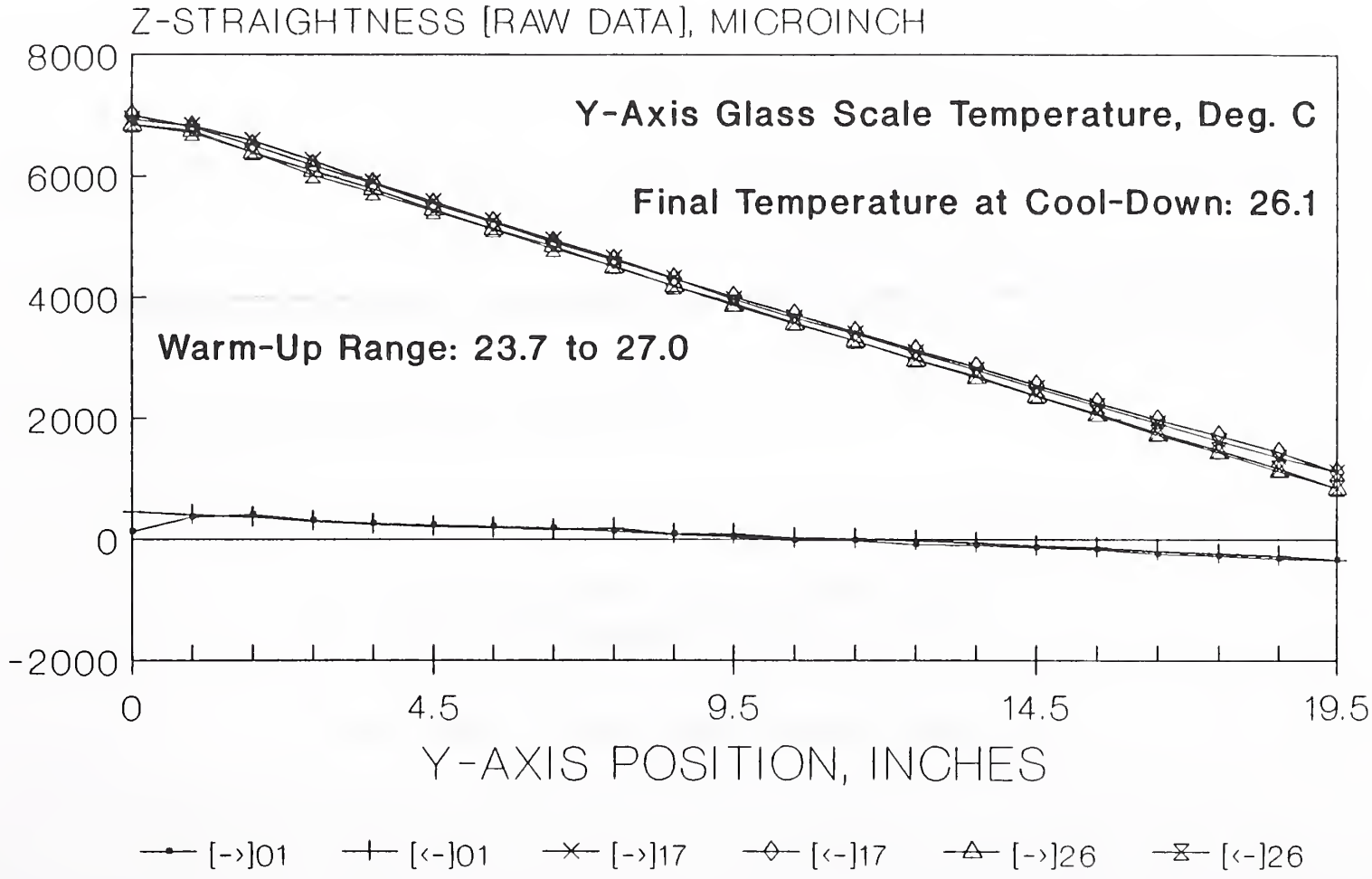
Z-STRAIGHTNESS [RAW DATA], MICROINCH
8000
6000
4000
2000
0
-2000
Y-Axis Glass Scale Temperature, Deg. C
Final Temperature at Cool-Down: 26.1
Warm-Up Range: 23.7 to 27.0
0
4.5
9.5
14.5
19.5
Y-AXIS POSITION, INCHES
[->]01
[<-]01
[->]17
[<-]17
[->]26
[<-]26

Fig. 3.16

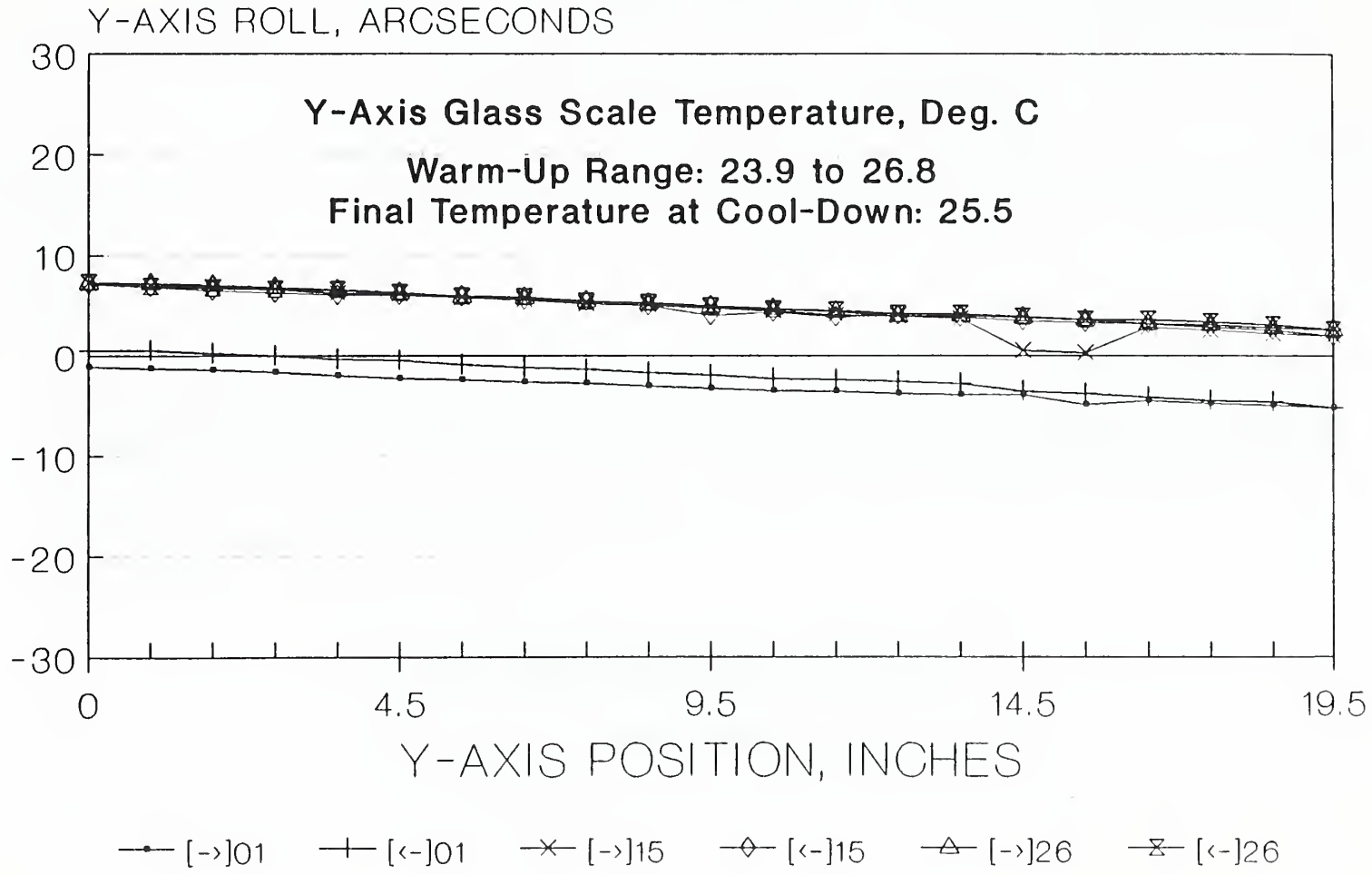
Y-AXIS ROLL, ARCSECONDS
30
20
10
0
-10
-20
-30
Y-Axis Glass Scale Temperature, Deg. C
Warm-Up Range: 23.9 to 26.8
Final Temperature at Cool-Down: 25.5
0
4.5
9.5
14.5
19.5
Y-AXIS POSITION, INCHES
[->]01
[<-]01
[->]15
[<-]15
[->]26
[<-]26

Fig. 3.17

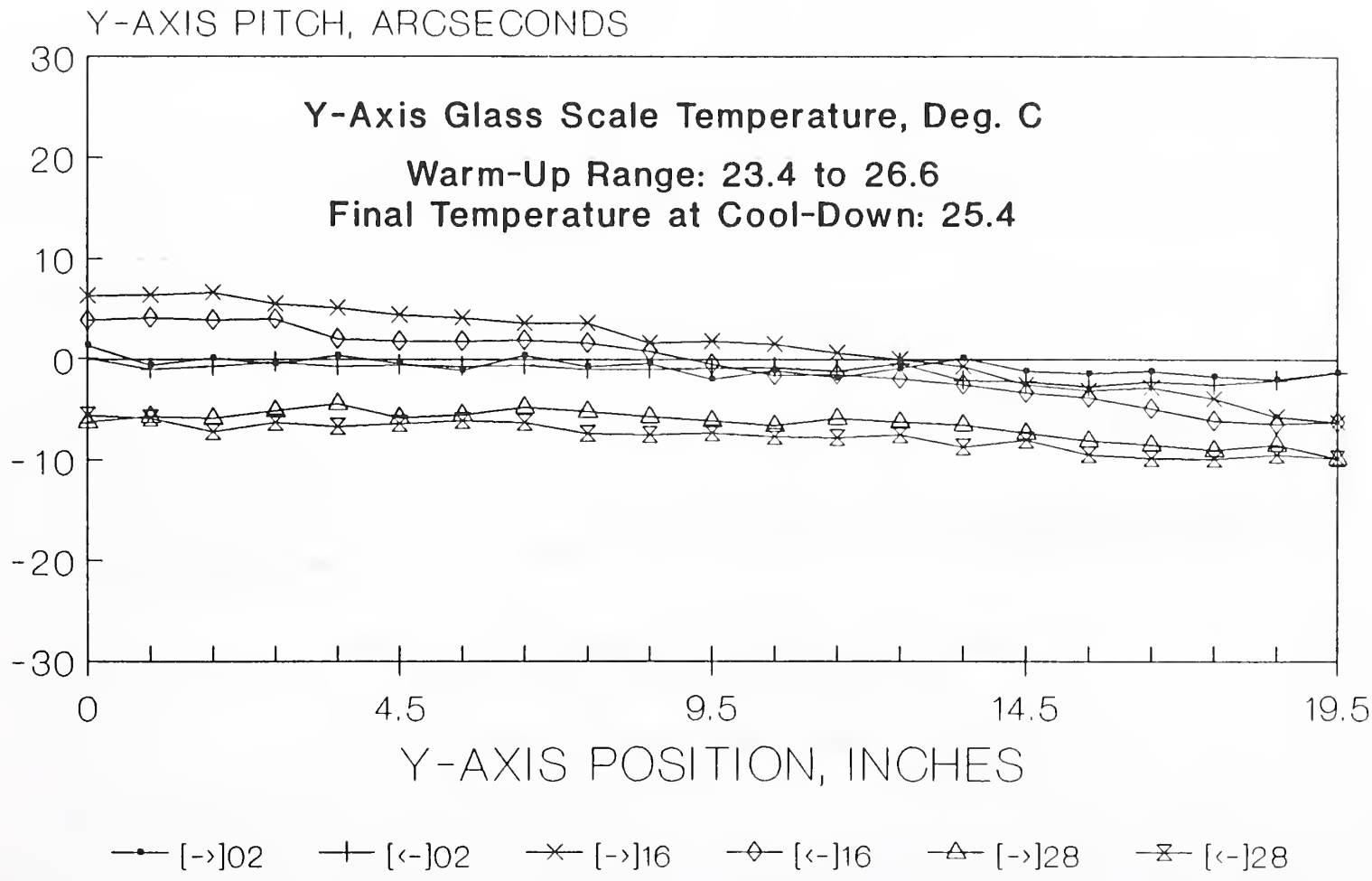
Y-AXIS PITCH, ARCSECONDS
30
20
10
0
-10
-20
-30
Y-Axis Glass Scale Temperature, Deg. C
Warm-Up Range: 23.4 to 26.6
Final Temperature at Cool-Down: 25.4
0
4.5
9.5
14.5
19.5
Y-AXIS POSITION, INCHES
[->]02
[<-]02
[->]16
[<-]16
[->]28
[<-]28

Fig. 3.18

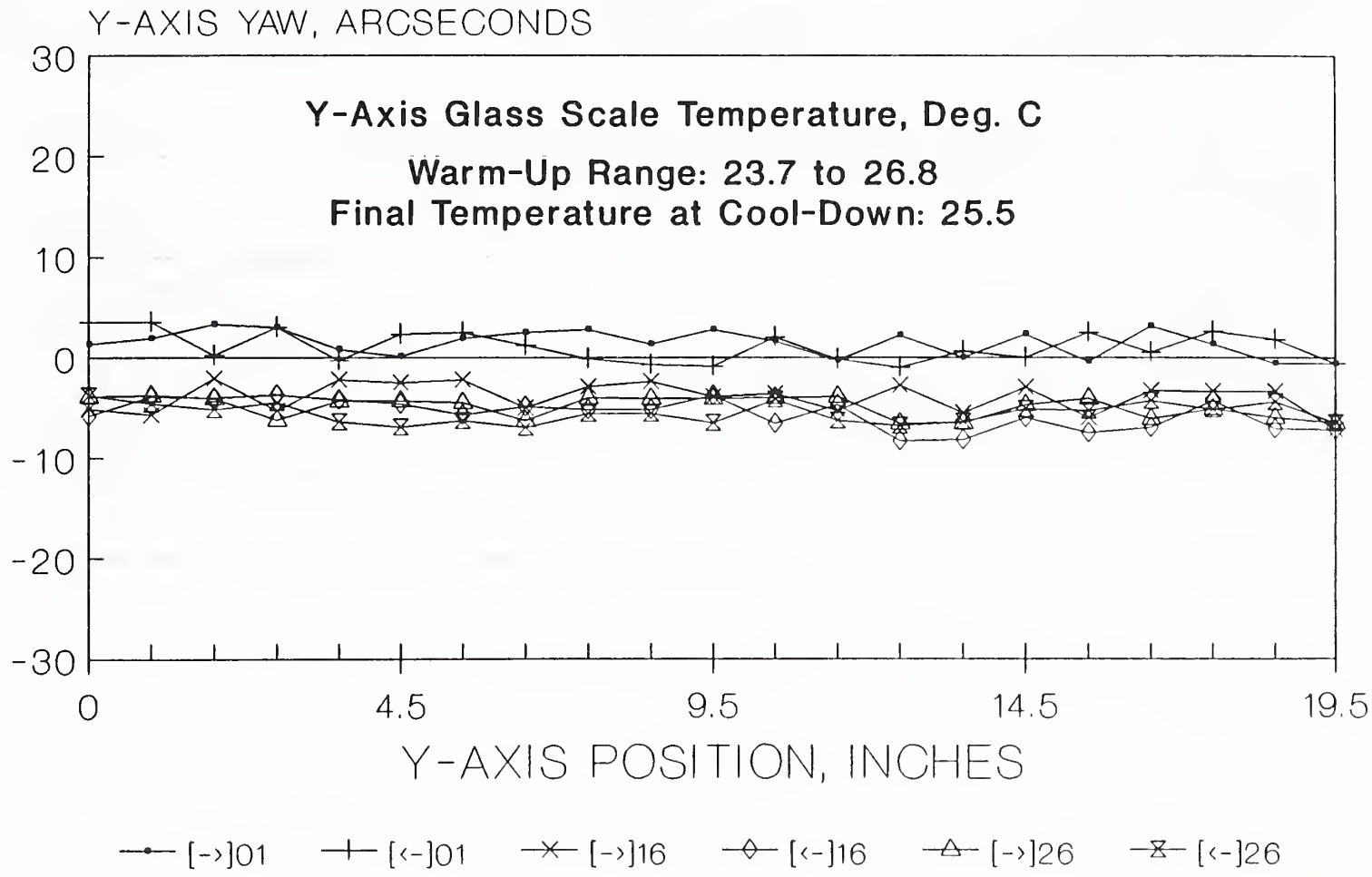
Y-AXIS YAW, ARCSECONDS
30
20
10
0
-10
-20
-30
Y-Axis Glass Scale Temperature, Deg. C
Warm-Up Range: 23.7 to 26.8
Final Temperature at Cool-Down: 25.5
0
4.5
9.5
14.5
19.5
Y-AXIS POSITION, INCHES
[->]01
[<-]01
[->]16
[<-]16
[->]26
[<-]26

Fig. 3.19

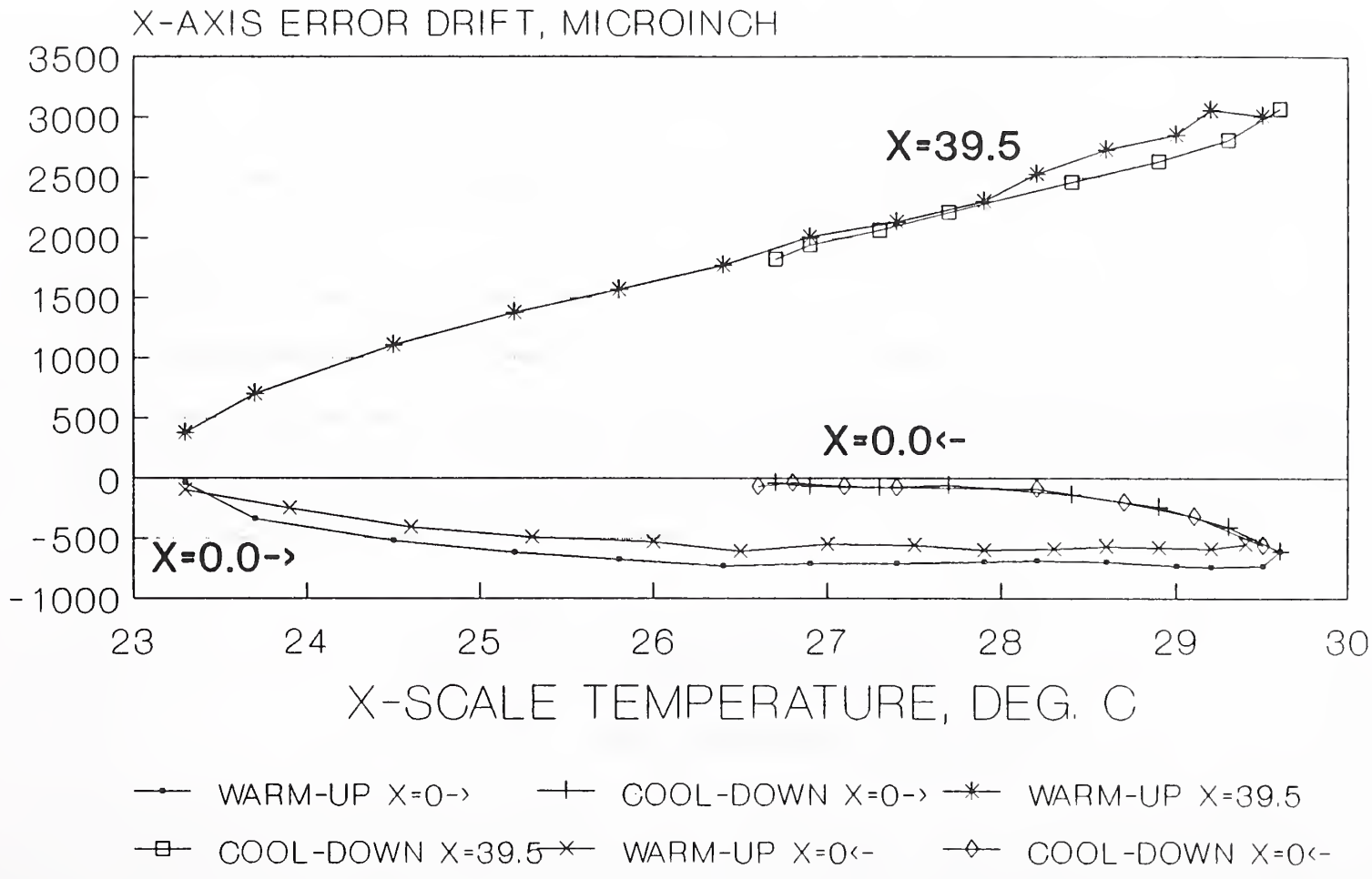
X-AXIS ERROR DRIFT, MICROINCH
3500
3000
2500
2000
1500
1000
500
0
-500
-1000
X=39.5
X=0.0<-
X=0.0->
23
24
25
26
27
28
29
30
X-SCALE TEMPERATURE, DEG. C
WARM-UP X=0->
COOL-DOWN X=0->
WARM-UP X=39.5
COOL-DOWN X=39.5
WARM-UP X=0<-
COOL-DOWN X=0<-

Fig. 3.20

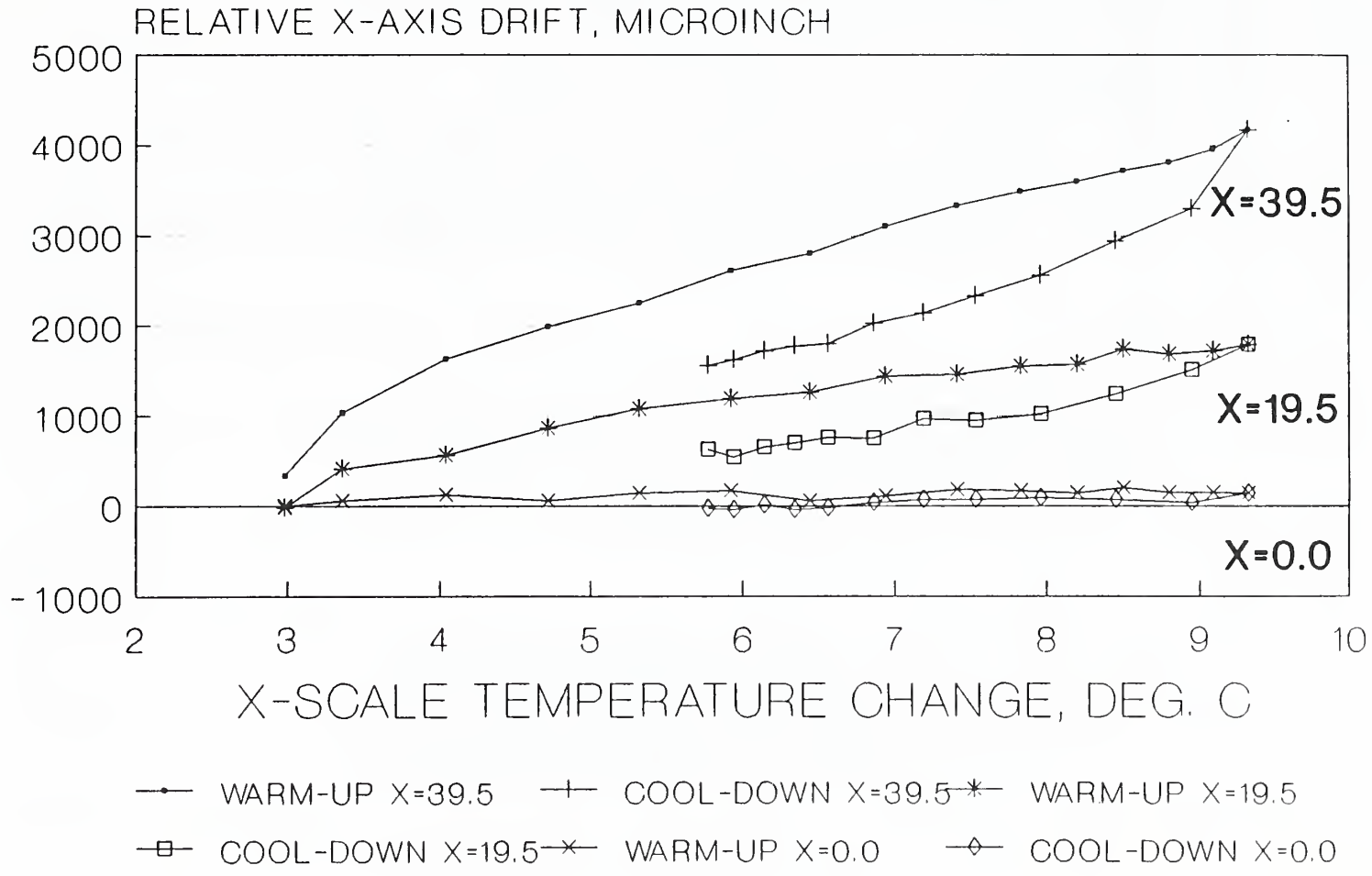
RELATIVE X-AXIS DRIFT, MICROINCH
5000
4000
3000
2000
1000
0
-1000
2
3
4
5
6
7
8
9
10
X=39.5
X=19.5
X=0.0
X-SCALE TEMPERATURE CHANGE, DEG. C
WARM-UP X=39.5
COOL-DOWN X=39.5
WARM-UP X=19.5
COOL-DOWN X=19.5
WARM-UP X=0.0
COOL-DOWN X=0.0

Fig. 3.21

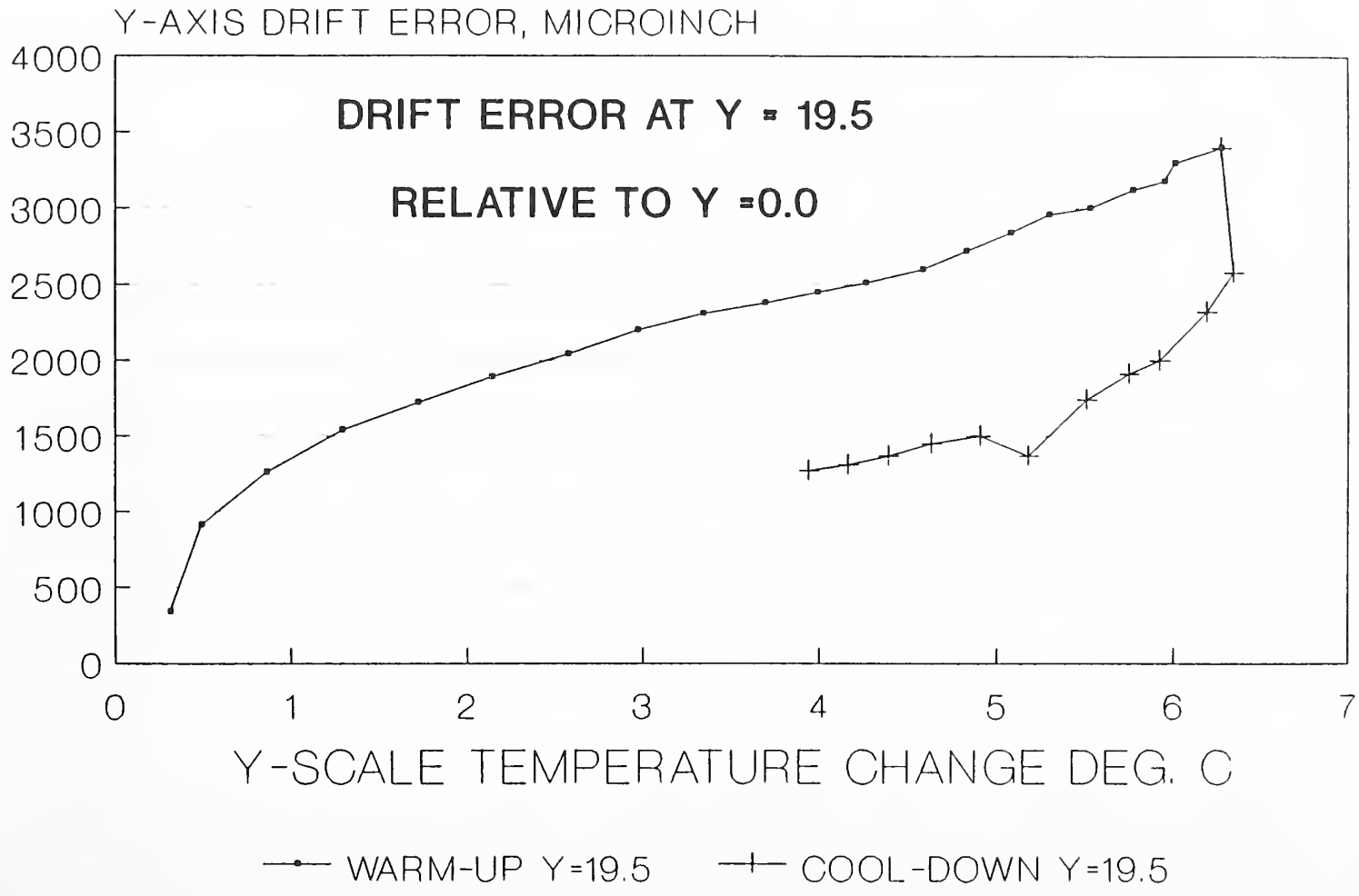
Y-AXIS DRIFT ERROR, MICROINCH
DRIFT ERROR AT Y = 19.5
RELATIVE TO Y =0.0
4000
3500
3000
2500
2000
1500
1000
500
0
0
1
2
3
4
5
6
7
Y-SCALE TEMPERATURE CHANGE DEG. C
WARM-UP Y=19.5
COOL-DOWN Y=19.5

Fig. 3.22

TABLE 3.1

DATA CHART FOR 0911D01.VSX

TEST OF VOL COMP WITHOUT LASER RESET

MEASUREMENT	X=0	X=39.5	X=0	END
12:34:06	-00.00004	+39.50038	-00.00010	12:40:58*
12:55:18	-00.00034	+39.50070	-00.00025	13:03:19*
13:18:12	-00.00052	+39.50111	-00.00041	13:27:41*
13:42:04	-00.00062	+39.50138	-00.00049	13:50:19*
14:04:33	-00.00068	+39.50157	-00.00053	14:16:15*
14:30:30	-00.00073	+39.50177	-00.00061	14:38:38*
14:53:08	-00.00071	+39.50201	-00.00055	15:01:17*
15:15:34	-00.00071	+39.50213	-00.00056	15:23:30*
15:37:40	-00.00070	+39.50230	-00.00060	15:46:00*
16:00:36	-00.00069	+39.50253	-00.00059	16:06:22*
16:20:36	-00.00070	+39.50273	-00.00057	16:27:53*
16:41:55	-00.00073	+39.50285	-00.00058	16:49:02*
17:03:40	-00.00074	+39.50306	-00.00059	17:11:50*
17:26:00	-00.00073	+39.50301	-00.00055	17:36:35*
17:51:03	-00.00061	+39.50307	-00.00056	17:56:39
18:07:39	-00.00041	+39.50281	-00.00032	18:15:54
18:26:35	-00.00024	+39.50263	-00.00020	18:36:15
18:49:04	-00.00014	+39.50246	-00.00009	18:57:01
19:21:04	-00.00006	+39.50221	-00.00008	19:34:24
19:48:16	-00.00008	+39.50206	-00.00007	19:56:16
20:10:24	-00.00007	+39.50194	-00.00004	20:21:01
20:27:50	-00.00004	+39.50182	-00.00007	20:34:30

TABLE 3.2a

DATA FOR VERTICAL MILLING STATION
STORED IN FILE 0911D03.VSX
09-11-1989 13:17:29   THE OPERATOR WAS RUDDER

NANCNC WAS USED TO MOVE THE MACHINE
LIN3NC WAS USED TO WARM UP THE MACHINE
DISTANCE MEASUREMENTS WERE TAKEN ON THE X AXIS
MEASUREMENTS TAKEN IN THE XY-PLANE

LASER-,-00.00052, GE-,+00.000000

0	09:11:13:18:23	24.27
1	09:11:13:18:23	24.59
2	09:11:13:18:23	24.27
3	09:11:13:18:23	24.47
4	09:11:13:18:23	23.31
5	09:11:13:18:23	23.41
6	09:11:13:18:23	23.39
7	09:11:13:18:23	24.54
8	09:11:13:18:23	24.59
9	09:11:13:18:23	24.79
10	09:11:13:18:23	25.64
11	09:11:13:18:23	24.09
12	09:11:13:18:23	23.76
13	09:11:13:18:23	23.46
14	09:11:13:18:23	23.69
15	09:11:13:18:23	23.41
16	09:11:13:18:23	23.66
17	09:11:13:18:23	24.54
18	09:11:13:18:23	25.54
19	09:11:13:18:23	24.44
20	09:11:13:18:23	24.52
21	09:11:13:18:23	24.24
22	09:11:13:18:23	25.37
23	09:11:13:18:23	24.67
24	09:11:13:18:23	26.19
25	09:11:13:18:23	25.49
26	09:11:13:18:23	24.67
27	09:11:13:18:23	25.07
28	09:11:13:18:23	25.39
29	09:11:13:18:23	25.64
30	09:11:13:18:23	26.04
31	09:11:13:18:23	25.72
32	09:11:13:18:23	24.32
33	09:11:13:18:23	24.54
34	09:11:13:18:23	24.74
35	09:11:13:18:23	25.04
36	09:11:13:18:23	25.59
37	09:11:13:18:23	25.47
38	09:11:13:18:23	23.69
39	09:11:13:18:23	25.09

LASER-,+00.49942, GE-,+00.500000
LASER-,+01.49955, GE-,+01.500000
LASER-,+02.49945, GE-,+02.500000
LASER-,+03.49956, GE-,+03.500000
LASER-,+04.49948, GE-,+04.500000
LASER-,+05.49954, GE-,+05.500000

TABLE 3.2b

LASER-,+06.49954,	GE-,+06.500000
LASER-,+07.49963,	GE-,+07.500000
LASER-,+08.49963,	GE-,+08.500000
LASER-,+09.49972,	GE-,+09.500000
LASER-,+10.49972,	GE-,+10.500000
LASER-,+11.49972,	GE-,+11.500000
LASER-,+12.49973,	GE-,+12.500000
LASER-,+13.49978,	GE-,+13.500000
LASER-,+14.49980,	GE-,+14.500000
LASER-,+15.49973,	GE-,+15.500000
LASER-,+16.49967,	GE-,+16.500000
LASER-,+17.49967,	GE-,+17.500000
LASER-,+18.49958,	GE-,+18.500000
LASER-,+19.49971,	GE-,+19.500000
LASER-,+20.49971,	GE-,+20.500000
LASER-,+21.49977,	GE-,+21.500000
LASER-,+22.49991,	GE-,+22.500000
LASER-,+23.49999,	GE-,+23.500000
LASER-,+24.50007,	GE-,+24.500000
LASER-,+25.50018,	GE-,+25.500000
LASER-,+26.50019,	GE-,+26.500000
LASER-,+27.50026,	GE-,+27.500000
LASER-,+28.50027,	GE-,+28.500000
LASER-,+29.50031,	GE-,+29.500000
LASER-,+30.50033,	GE-,+30.500000
LASER-,+31.50042,	GE-,+31.500000
LASER-,+32.50047,	GE-,+32.500000
LASER-,+33.50055,	GE-,+33.500000
LASER-,+34.50072,	GE-,+34.500000
LASER-,+35.50079,	GE-,+35.500000
LASER-,+36.50091,	GE-,+36.500000
LASER-,+37.50096,	GE-,+37.500000
LASER-,+38.50104,	GE-,+38.500000
LASER-,+39.50111,	GE-,+39.500000
LASER-,+38.50114,	GE-,+38.500000
LASER-,+37.50099,	GE-,+37.500000
LASER-,+36.50109,	GE-,+36.500000
LASER-,+35.50093,	GE-,+35.500000
LASER-,+34.50094,	GE-,+34.500000
LASER-,+33.50074,	GE-,+33.500000
LASER-,+32.50077,	GE-,+32.500000
LASER-,+31.50065,	GE-,+31.500000
LASER-,+30.50066,	GE-,+30.500000
LASER-,+29.50057,	GE-,+29.500000
LASER-,+28.50064,	GE-,+28.500000
LASER-,+27.50058,	GE-,+27.500000
LASER-,+26.50055,	GE-,+26.500000
LASER-,+25.50036,	GE-,+25.500000
LASER-,+24.50027,	GE-,+24.500000
LASER-,+23.50022,	GE-,+23.500000
LASER-,+22.50033,	GE-,+22.500000
LASER-,+21.50025,	GE-,+21.500000
LASER-,+20.50025,	GE-,+20.500000
LASER-,+19.50028,	GE-,+19.500000
LASER-,+18.50023,	GE-,+18.500000
LASER-,+17.50024,	GE-,+17.500000

```
LASER-,+16.50009,    GE-,+16.500000
LASER-,+15.50013,    GE-,+15.500000
LASER-,+14.50002,    GE-,+14.500000
LASER-,+13.50006,    GE-,+13.500000
LASER-,+12.50000,    GE-,+12.500000
LASER-,+11.50011,    GE-,+11.500000
LASER-,+10.49989,    GE-,+10.500000
LASER-,+09.49993,    GE-,+09.500000
LASER-,+08.49985,    GE-,+08.500000
LASER-,+07.49982,    GE-,+07.500000
LASER-,+06.49974,    GE-,+06.500000
LASER-,+05.49977,    GE-,+05.500000
LASER-,+04.49973,    GE-,+04.500000
LASER-,+03.49975,    GE-,+03.500000
LASER-,+02.49966,    GE-,+02.500000
LASER-,+01.49971,    GE-,+01.500000
LASER-,+00.49955,    GE-,+00.500000
LASER-,-00.00041,    GE-,+00.000000
 0              09:11:13:28:01              24.42
 1              09:11:13:28:01              24.64
 2              09:11:13:28:01              24.32
 3              09:11:13:28:01              24.62
 4              09:11:13:28:01              23.34
 5              09:11:13:28:01              23.44
 6              09:11:13:28:01              23.41
 7              09:11:13:28:01              24.57
 8              09:11:13:28:01              24.62
 9              09:11:13:28:01              24.82
 10             09:11:13:28:01              25.67
 11             09:11:13:28:01              24.34
 12             09:11:13:28:01              23.89
 13             09:11:13:28:01              23.49
 14             09:11:13:28:01              23.74
 15             09:11:13:28:01              23.44
 16             09:11:13:28:01              23.69
 17             09:11:13:28:01              24.59
 18             09:11:13:28:01              25.54
 19             09:11:13:28:01              24.47
 20             09:11:13:28:01              24.54
 21             09:11:13:28:01              24.29
 22             09:11:13:28:01              25.39
 23             09:11:13:28:01              24.69
 24             09:11:13:28:01              26.19
 25             09:11:13:28:01              25.52
 26             09:11:13:28:01              24.69
 27             09:11:13:28:01              25.12
 28             09:11:13:28:01              25.42
 29             09:11:13:28:01              25.69
 30             09:11:13:28:01              26.07
 31             09:11:13:28:01              25.77
 32             09:11:13:28:01              24.32
 33             09:11:13:28:01              24.57
 34             09:11:13:28:01              24.79
 35             09:11:13:28:01              25.09
 36             09:11:13:28:01              25.59
 37             09:11:13:28:01              25.52
 38             09:11:13:28:01              23.69
 39             09:11:13:28:01              25.19
```

4. CHARACTERIZATION OF CNC TURNING CENTER

A. Donmez

4.1 OVERVIEW

We have started the geometric and thermal characterization of the Monarch Metalist CNC turning center. The characterization procedure is similar to the previously explained procedure for the vertical machining center. The purpose of this characterization is to identify the geometric errors of the machine tool and the variation of these errors during the thermal transient period. In order to establish the error relationships with respect to the machine thermal state, we have carried out the geometric error measurements, repeatedly, for a period of at least 24 hours, in which we induced machine warm-up and cool-down intentionally to simulate normal cutting conditions. In the following sections, the details of these measurements and the data obtained will be described.

4.2 DATA ACQUISITION

The data acquisition system for machine characterization was described in the last year's report. The system we used for the turning center is similar except for the communication link to the machine tool controller. The only function of the serial communication link between the data acquisition computer and the machine tool controller is to establish synchronization in data acquisition. The data acquisition computer should know when to read the laser interferometer during the geometric error measurement cycle. Since the machine is programmed to move in predetermined steps along its travel axis, the direct communication with the controller is not necessary. We established this synchronization by activating unused M-codes at the end of each motion step in the NC program. As a response to the activation of the specific M-code in the NC program, a relay switches the corresponding signal level from low to high. By monitoring this signal via a digital voltmeter (DVM), the data acquisition computer determines when to read the laser interferometer data. A sample NC program used for the data acquisition is shown in Fig. 4.1.

The NC program is written to work with different measurement cycles. The starting point, end point, and the measurement interval can be modified via the NC parameter table. Parameter P71 is the measurement interval and parameter P53 is the end point. The program shown in Fig. 4.1 moves the tool holder along the z-axis starting at z = -1 in. The cycle proceeds to z = 26 in. and returns to z = -1 in. The laser interferometer measurements are taken in one inch increments or "steps", along the measurement axis. At the end of each step there is a delay executed by "G04 × 3.5" statement to give the laser time to settle down. "M14 and M15" statements generate a "pulse" which is detected by the data acquisition computer indicating the time to read the laser. The statement "G04 × 5.5" causes another delay to complete the laser reading.

Geometric errors are measured along the machine axes of motion at predetermined steps. The determination of step sizes should take the periodic behavior of the error into consideration. Figures 4.2 and 4.3 show the periodic linear displacement errors along the x and z axes of the machine, respectively. These data were obtained by measuring displacement error at every 0.001 inch along each axis. The linear displacement error has a period of 0.25 inch with a peak-to-peak amplitude of around 100 microinches. The measurement step should be set to correspond to integer multiples of the periodicity of this error. Otherwise, the periodic component will be buried in the measurement, and the data will seem less uniform than it actually is. Based on these preliminary measurements, the measurements along the x axis were taken at every 0.5 inch for a total of 9 inches of travel. The measurements along the z axis were taken at every inch for a total of 27 inches of travel. To determine a particular error component at any point along an axis of motion, a non-linear interpolation is applied based on the periodic characteristic of that error component.

During the past year we have completed the linear displacement and yaw error measurements along both the x and z axes of the turning center. Figures 4.4 through 4.10 show some of the characteristic data obtained from these measurements. In order to simulate realistic operational conditions, these measurements were taken during the thermal transient

period, in which the machine was warmed up and cooled down repeatedly. A typical measurement schedule starts with five sets of bidirectional error measurements upon start up of the machine when it is cold. This measurement consists of recording all the temperatures at the beginning and the end of each bidirectional pass, as well as the laser readings at each step along the travel axis during each pass. Figure 4.4 shows a set of data obtained from such a measurement cycle. The zero shift seen in the data is caused by the thermal growth of machine structural and position sensing components. The plot also shows an effective reversal error of about 200 microinches when the machine changes direction at $z = 27$ inches. This is contrary to the expectation of zero backlash due to the use of linear glass scales as the positional feedback elements. The reason for this reversal error is the combination of possible angular errors and the large Abbe offset between the linear scales and the axis of motion of the cutting tool, at which the error measurements were taken.

After the first set of measurements, the machine is warmed up for a period of one hour by moving the slide along the axis for which the measurement is being taken, back and forth along the full travel range. At the beginning of each forward travel, the temperatures and the laser reading are recorded to monitor the zero shift continuously during this warm-up cycle. Figure 4.5 shows the zero shift as a function of time during the initial warm up period. Figures 4.6 through 4.10 show the temperature rise at various locations around the machine structure during the same warm-up period.

Upon completion of this warm-up period, the geometric errors are measured along the axis of travel similar to the initial set of measurements. As shown in Fig. 4.11, the amount of zero shift is reduced significantly, but the slopes of the error curves increase as a result of thermal growth of the linear scales. Figure 4.12 shows the amount of zero shift during the next two hours of the warm-up period, in which the trend of the shift is reversed due to the changing thermal gradients along the machine structure.

The zero shift during a one-hour long cool-down period is shown in Fig. 4.13. This set of data was taken at predetermined time intervals while the machine axis was stationary at the starting point of its travel, thus cooling slowly. Note that the starting point for the time scale in these plots is the beginning of the measurements when the machine was cold. Data over to a period of approximately 28 hours was collected for each error component. Between each warm-up and cool-down period, the bidirectional geometric errors were measured along the travel axis to determine the effect of the thermal profile of the machine on its geometric errors. Figure 4.14 shows the total change in the z-displacement error as the machine goes through thermal cycles. Figures 4.15 through 4.19 show yaw error behavior along the x and z axes of the turning center, Fig. 4-20 shows periodic pitch error of z motion.

4.3 FUTURE WORK

This year, we will continue measurements of the remaining geometric error components such as the straightness errors, parallelism, and orthogonality errors as well as thermally induced spindle error motions. The analysis of the data obtained from these measurements is already underway. We will continue analyzing the data and establish correlations between the measured errors and the temperatures to complete the geometric and thermal model of the machine tool. This model will be used to predict and compensate for the systematic errors in the real-time control loop.

Monarch Metalist
Machine Tool Characterization
Laser Cycle Program Listing

```
N0010 (ID,PROG,007,GE-300XX)
N0020 G70
N0021 P23=1
N0022 (IF P32>0 GOTO N0024)
N0023 (GOTO N0030)
N0024 M14
N0025 M15
N0026 G94 T0
N0027 G04 X5.5
N0028 (GOTO N0061)
N0030 G94 T0
N0032 P23=1
N0033 P25=0
N0035 G01 Z(-01.0000) F100.0
N0038 (IF P25>0 GOTO N0065)
N0040 M14
N0050 M15
N0060 G04 X21.0
N0061 M14
N0062 M15
N0063 G04 X21.0
N0065 P71=1
N0066 M14
N0067 M15
N0068 G04 X6.0
N0070 P54=0
N0072 (IF P32>0 GOTO N0070)
N0074 M14
N0076 M15
N0077 G04 X4.0
N0080 P55=0
N0085 P70=0.0000
N0090 P53=P56/P58
N0100 G01 Z(P70) F125.0
N0105 P70=P70+P71
N0110 G04 X3.5
N0120 M14
N0130 M15
N0140 G04 X5.5
N0150 P54=P54+1
N0160 (IF P54<P53 GOTO N0100)
N0170 (IF P55>0 GOTO N0213)
N0180 P71=-P71
N0190 P54=0
N0200 P55=1
N0210 (GOTO N0100)
N0213 G01 Z(0.0000) F125.0
N0214 G04 X3.0
N0215 M14
N0216 M15
N0217 G04 X5.0
N0220 Z(P59)
N0222 G04 X5.0
N0225 M15
N0228 M15
N0230 P71=-P71
N0232 P23=P23+1
N0233 (IF P23>P24 GOTO N0240)
N0235 P25=P25+1
N0237 G04 X32.0
N0238 (GOTO N0038)
N0240 M30
N9999 (END.PROG)
```

Fig. 4.1

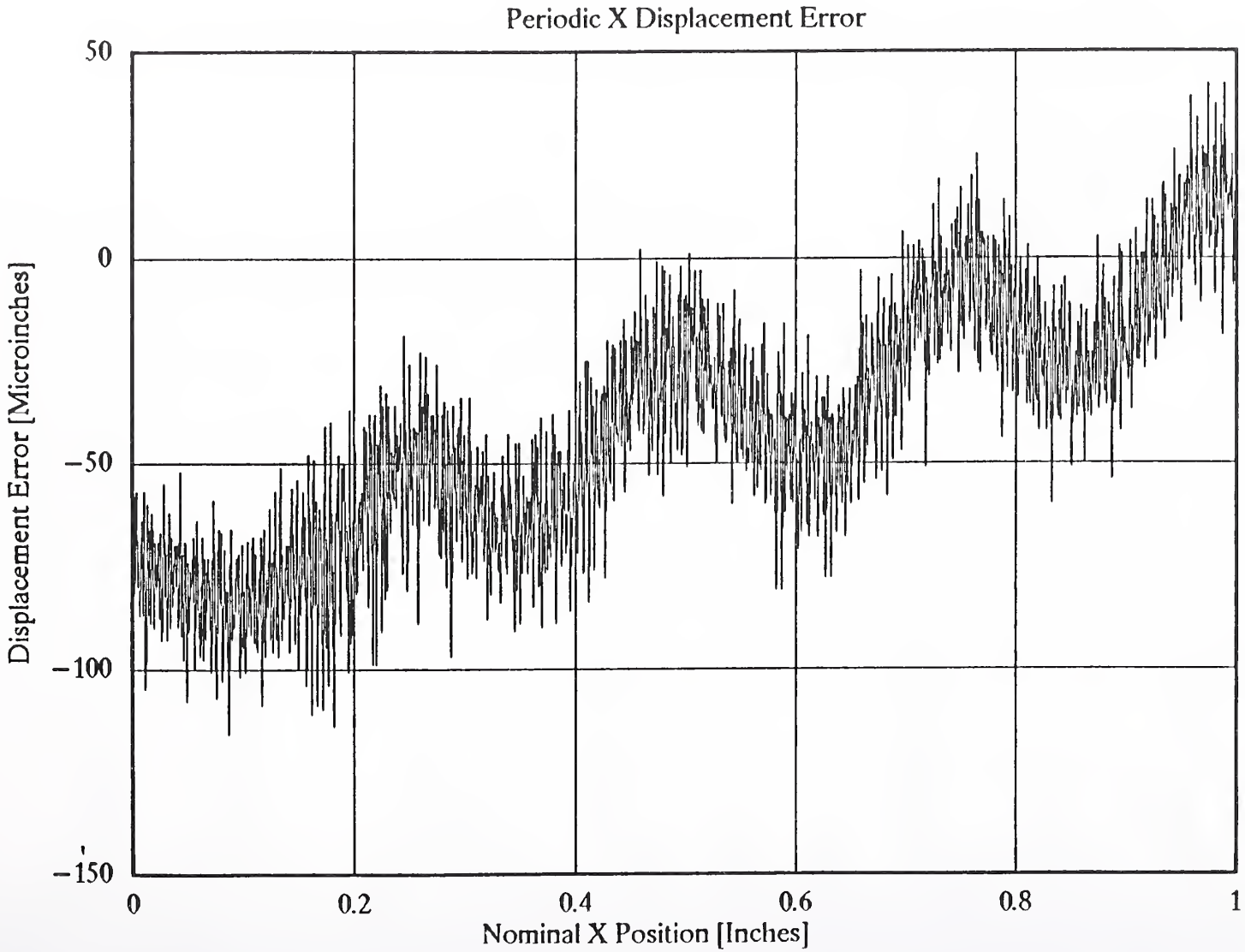
Periodic X Displacement Error
Displacement Error [Microinches]
50
0
−50
−100
−150
0
0.2
0.4
0.6
0.8
1
Nominal X Position [Inches]

Fig. 4.2

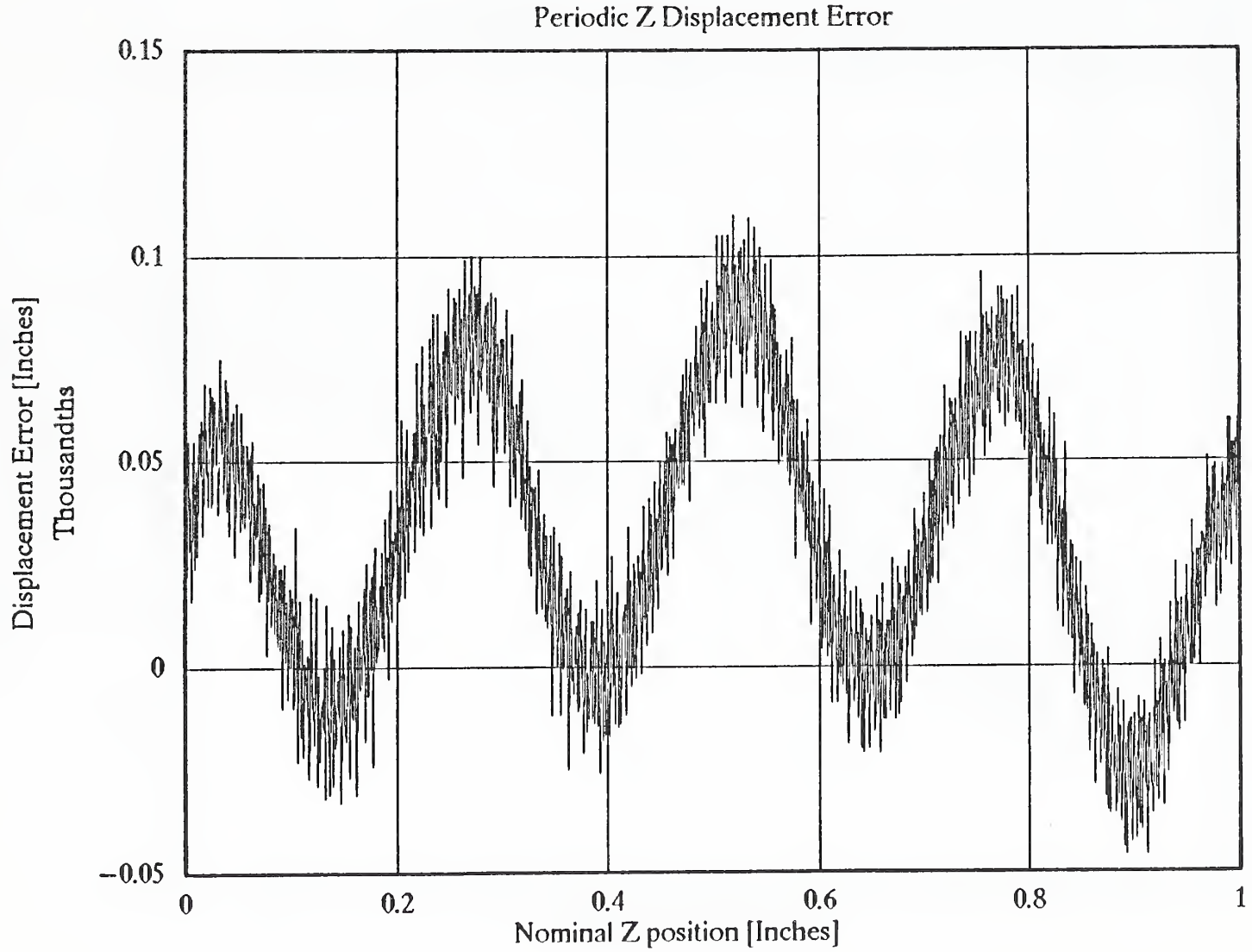
Periodic Z Displacement Error
Displacement Error [Inches]
Thousandths
0.15
0.1
0.05
0
−0.05
0
0.2
0.4
0.6
0.8
1
Nominal Z position [Inches]

Fig. 4.3

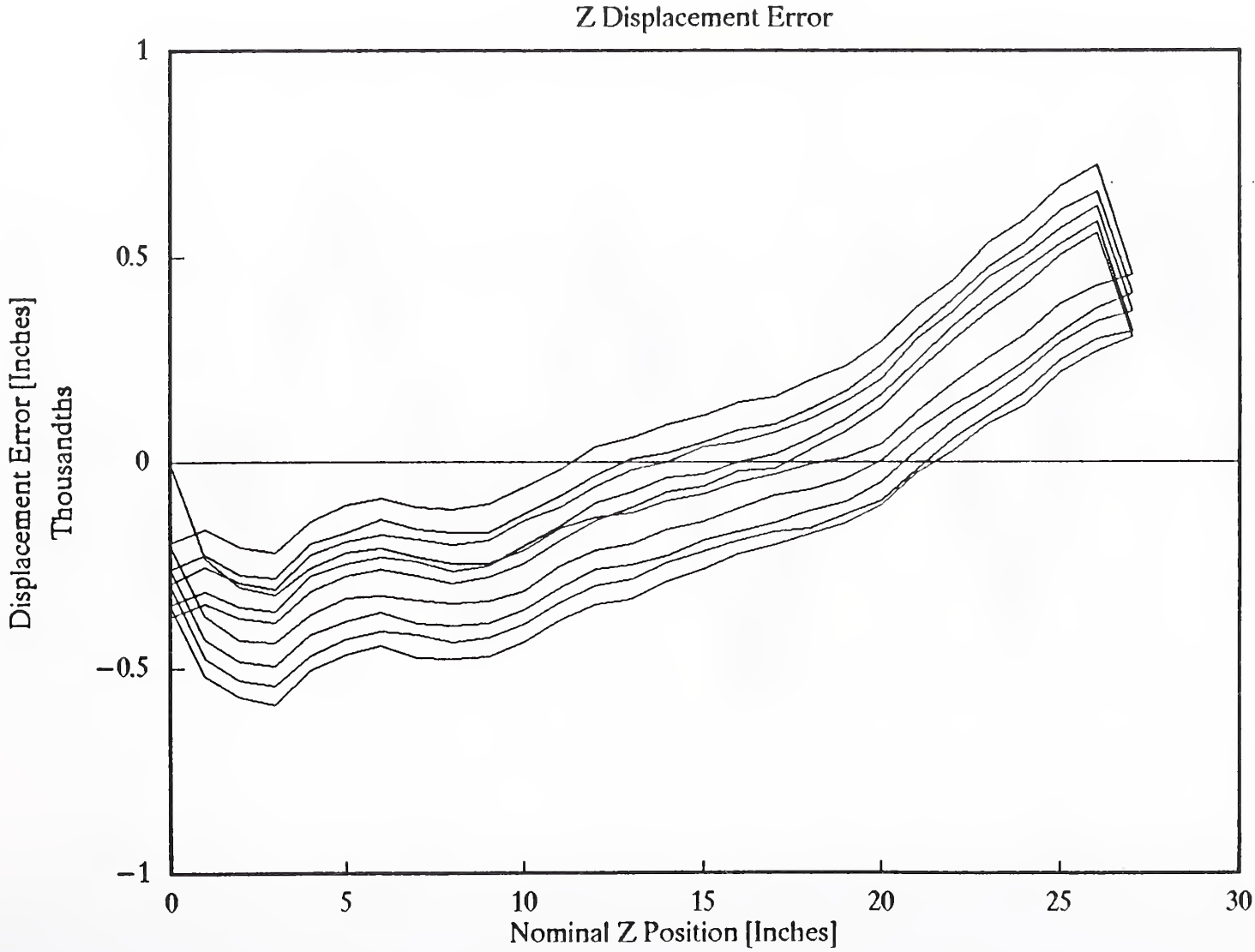
Z Displacement Error
Displacement Error [Inches]
Thousandths
1
0.5
0
−0.5
−1
0
5
10
15
20
25
30
Nominal Z Position [Inches]

Fig. 4.4

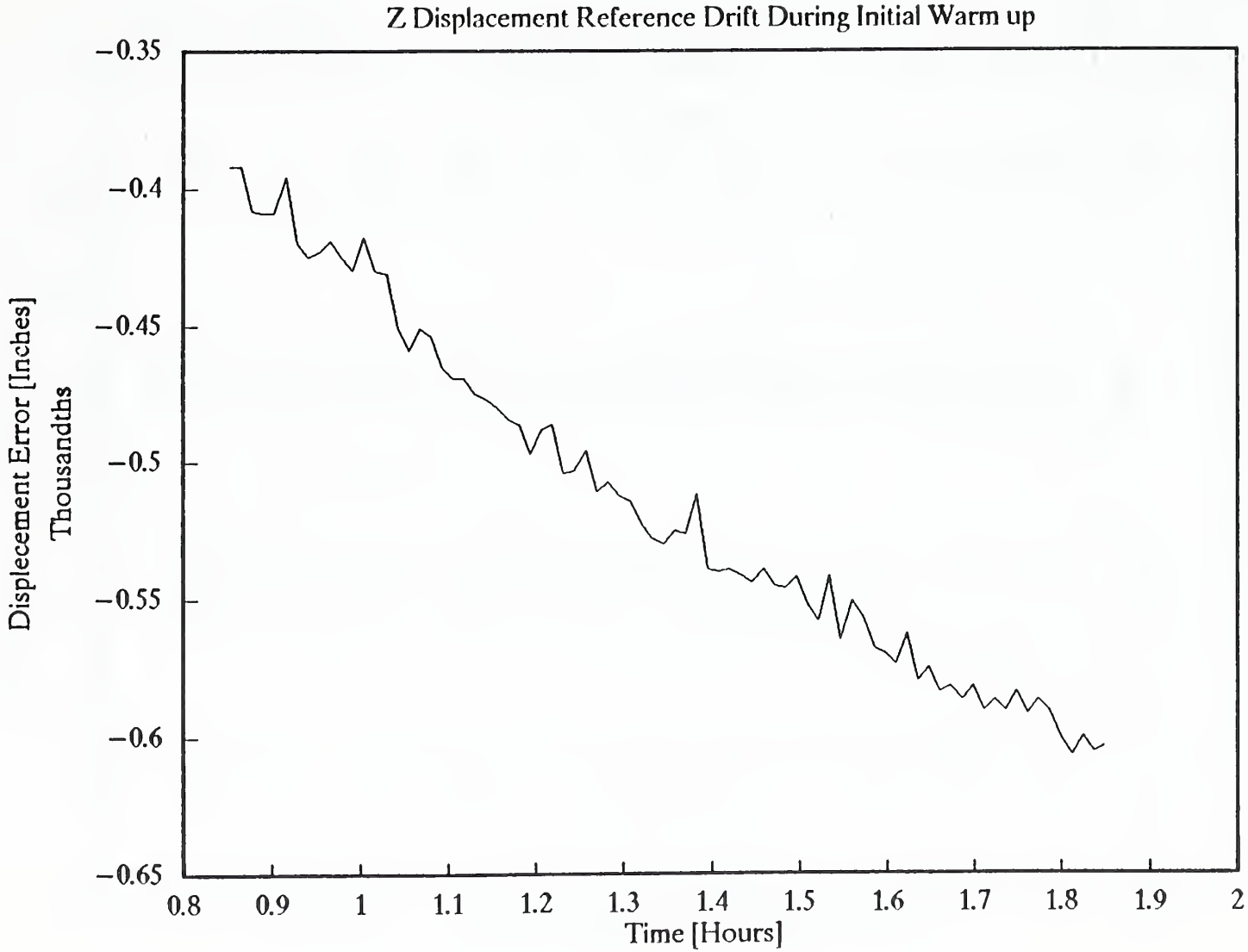
Z Displacement Reference Drift During Initial Warm up
Displecement Error [Inches]
Thousandths
−0.35
−0.4
−0.45
−0.5
−0.55
−0.6
−0.65
0.8
0.9
1
1.1
1.2
1.3
1.4
1.5
1.6
1.7
1.8
1.9
2
Time [Hours]

Fig. 4.5

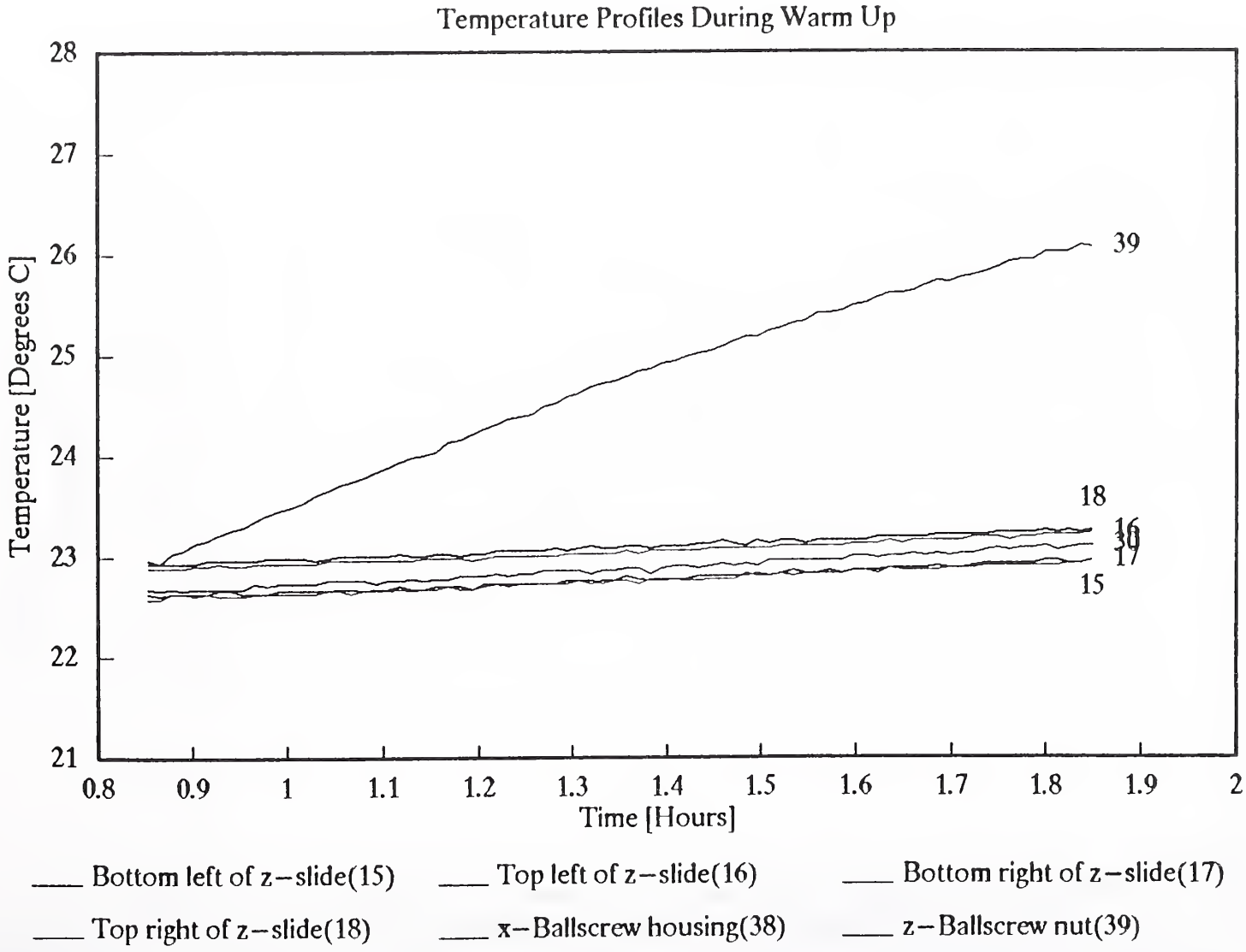
Temperature Profiles During Warm Up
Temperature [Degrees C]
28
27
26
25
24
23
22
21
0.8
0.9
1
1.1
1.2
1.3
1.4
1.5
1.6
1.7
1.8
1.9
2
Time [Hours]
39
18
16
30
17
15
Bottom left of z−slide(15)
Top left of z−slide(16)
Bottom right of z−slide(17)
Top right of z−slide(18)
x−Ballscrew housing(38)
z−Ballscrew nut(39)

Fig. 4.6

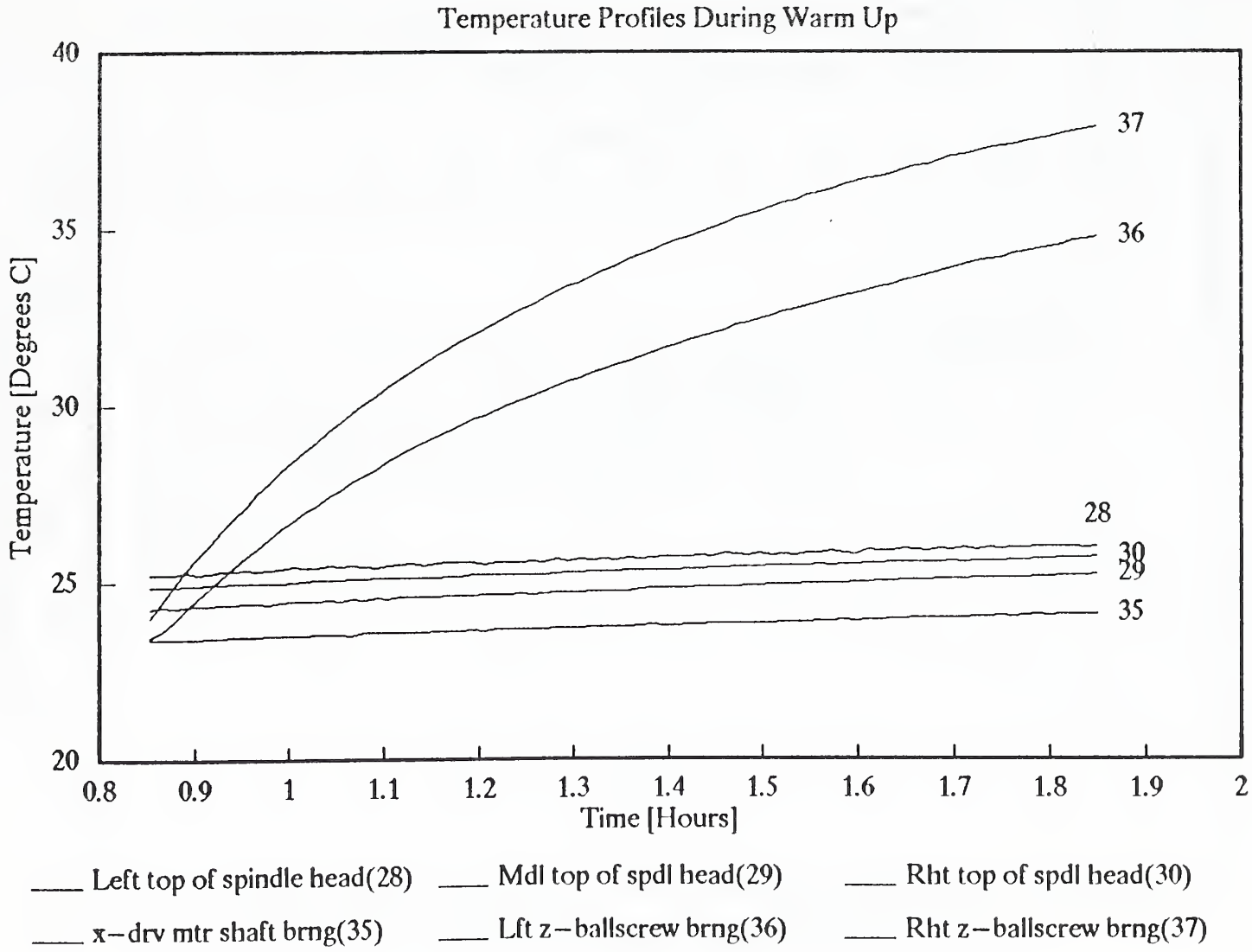
Temperature Profiles During Warm Up
Temperature [Degrees C]
40
35
30
25
20
0.8
0.9
1
1.1
1.2
1.3
1.4
1.5
1.6
1.7
1.8
1.9
2
Time [Hours]
37
36
28
30
29
35
Left top of spindle head(28)
Mdl top of spdl head(29)
Rht top of spdl head(30)
x-drv mtr shaft brng(35)
Lft z-ballscrew brng(36)
Rht z-ballscrew brng(37)

Fig. 4.7

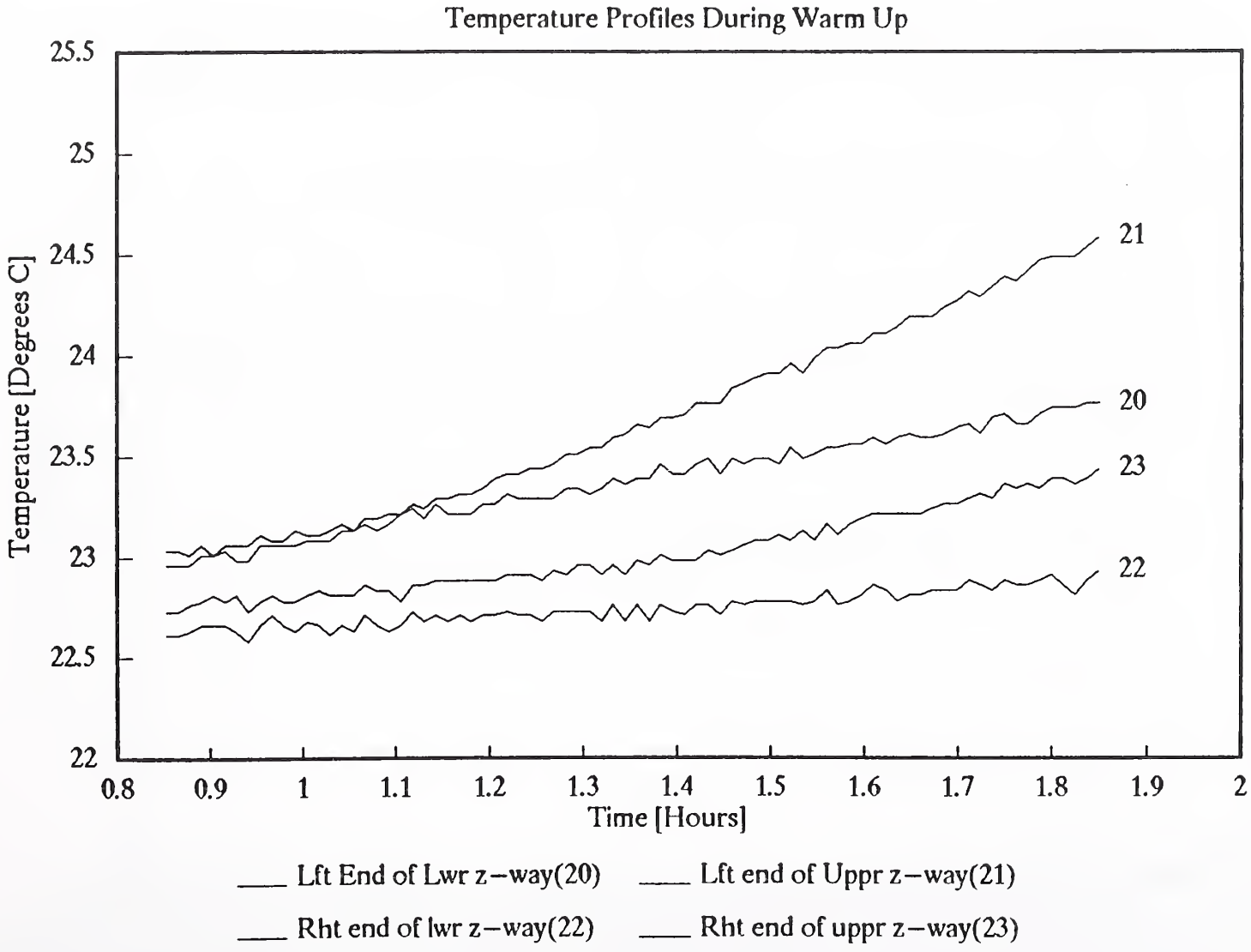
Temperature Profiles During Warm Up
Temperature [Degrees C]
25.5
25
24.5
24
23.5
23
22.5
22
0.8
0.9
1
1.1
1.2
1.3
1.4
1.5
1.6
1.7
1.8
1.9
2
Time [Hours]
21
20
23
22
Lft End of Lwr z−way(20)
Lft end of Uppr z−way(21)
Rht end of lwr z−way(22)
Rht end of uppr z−way(23)

Fig. 4.8

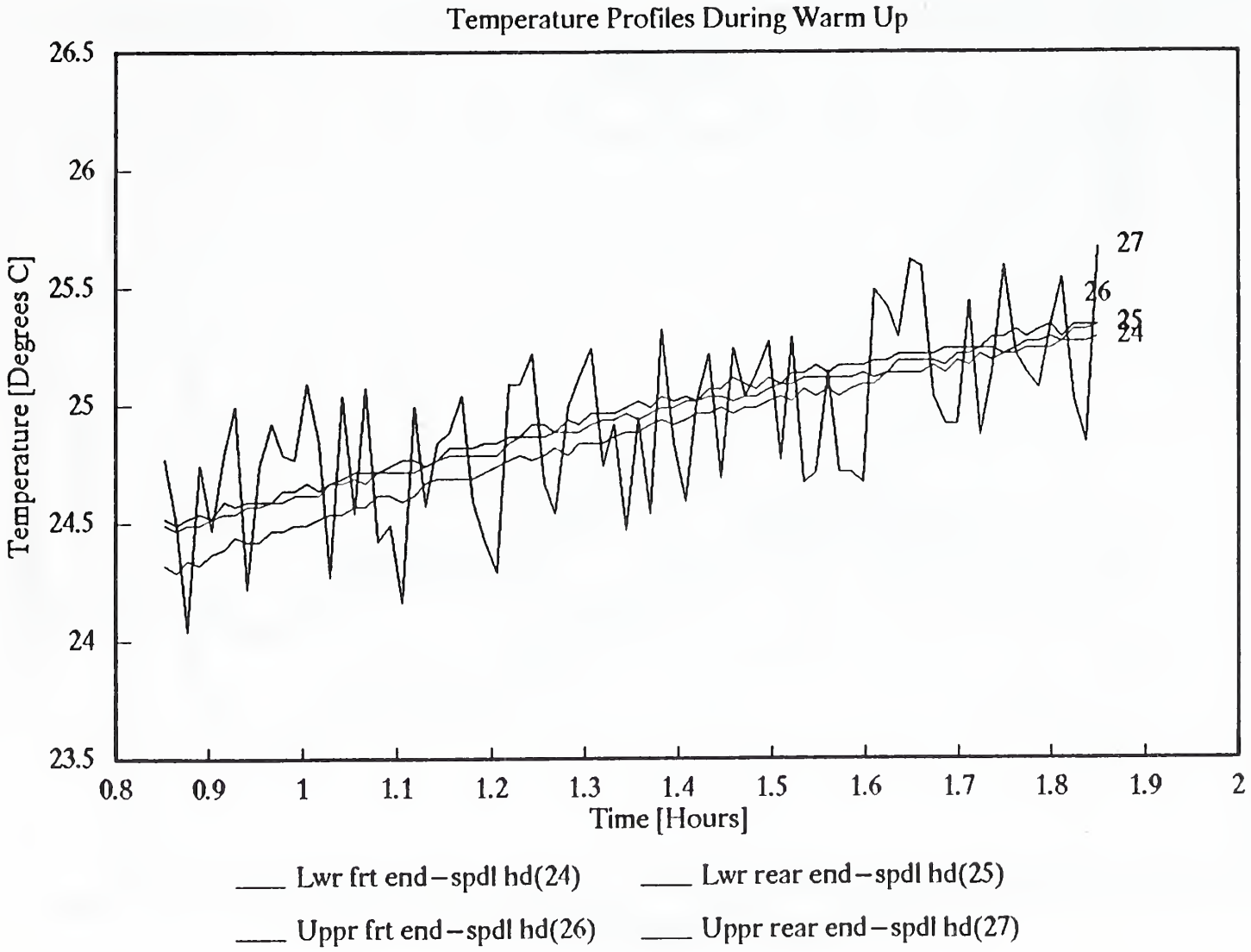
Temperature Profiles During Warm Up
26.5
26
25.5
25
24.5
24
23.5
Temperature [Degrees C]
0.8
0.9
1
1.1
1.2
1.3
1.4
1.5
1.6
1.7
1.8
1.9
2
Time [Hours]
27
26
25
24
Lwr frt end−spdl hd(24)
Lwr rear end−spdl hd(25)
Uppr frt end−spdl hd(26)
Uppr rear end−spdl hd(27)

Fig. 4.9

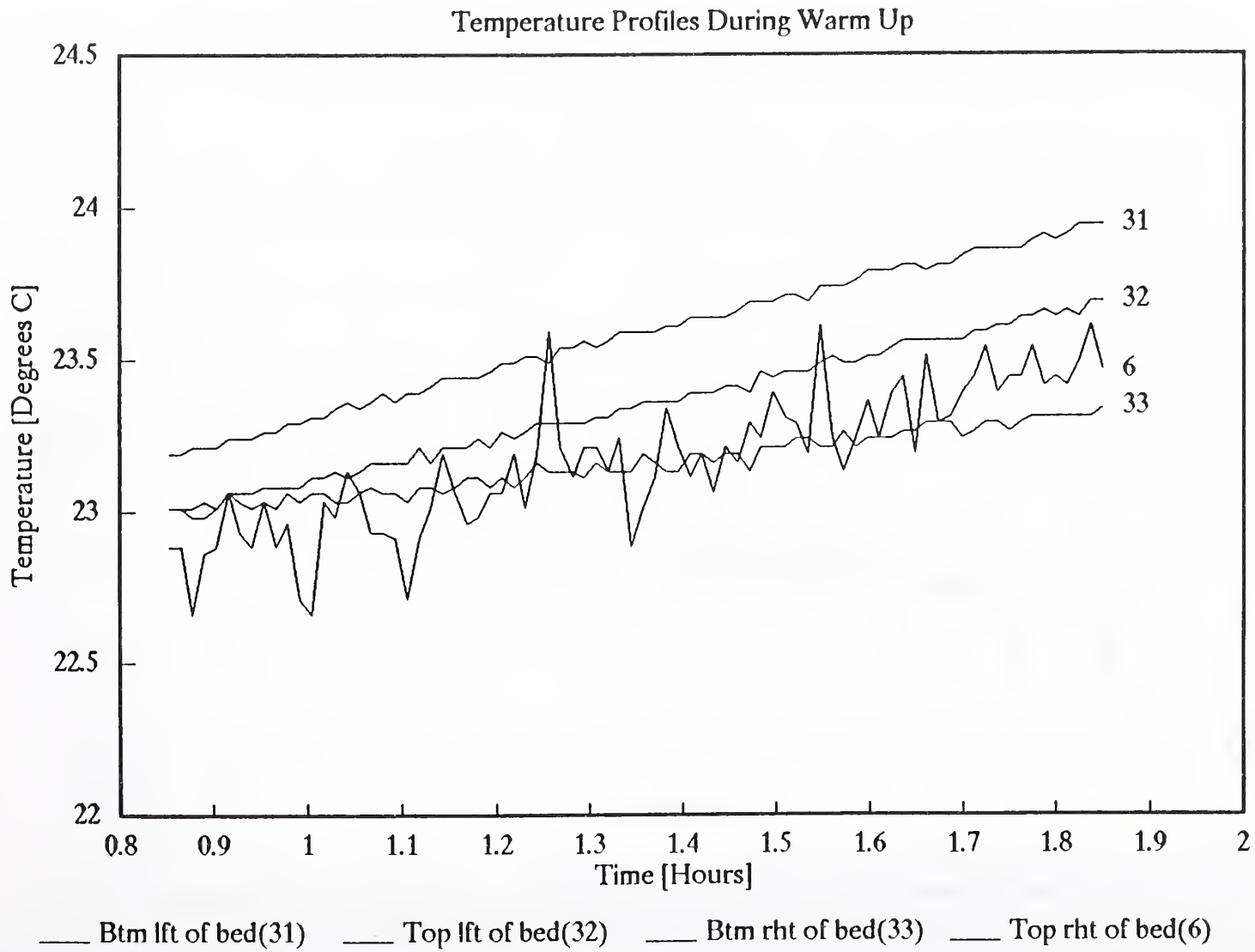
Temperature Profiles During Warm Up
24.5
24
23.5
23
22.5
22
Temperature [Degrees C]
0.8
0.9
1
1.1
1.2
1.3
1.4
1.5
1.6
1.7
1.8
1.9
2
Time [Hours]
31
32
6
33
Btm lft of bed(31)
Top lft of bed(32)
Btm rht of bed(33)
Top rht of bed(6)

Fig. 4.10

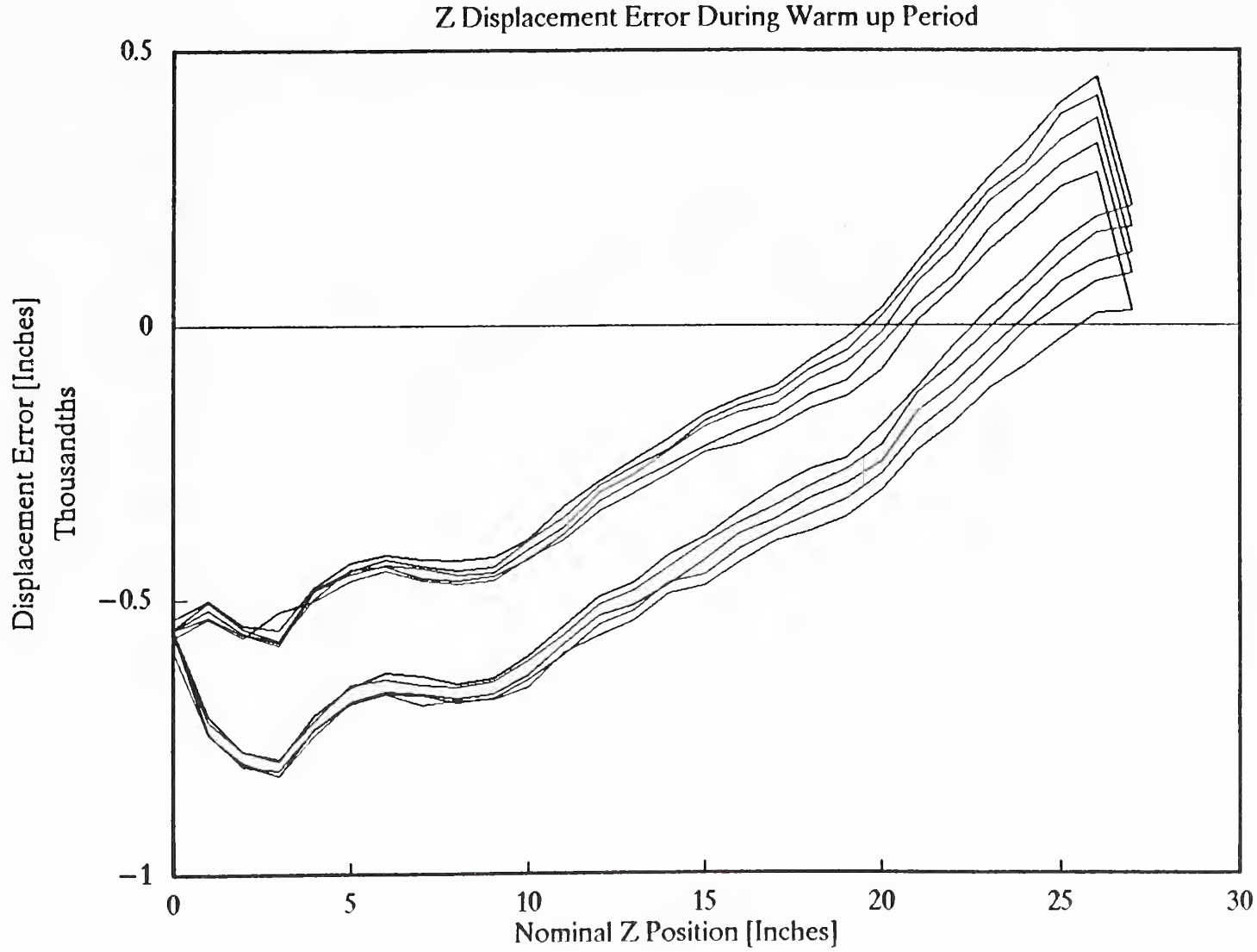
Z Displacement Error During Warm up Period
Displacement Error [Inches]
Thousandths
0.5
0
−0.5
−1
0
5
10
15
20
25
30
Nominal Z Position [Inches]

Fig. 4.11

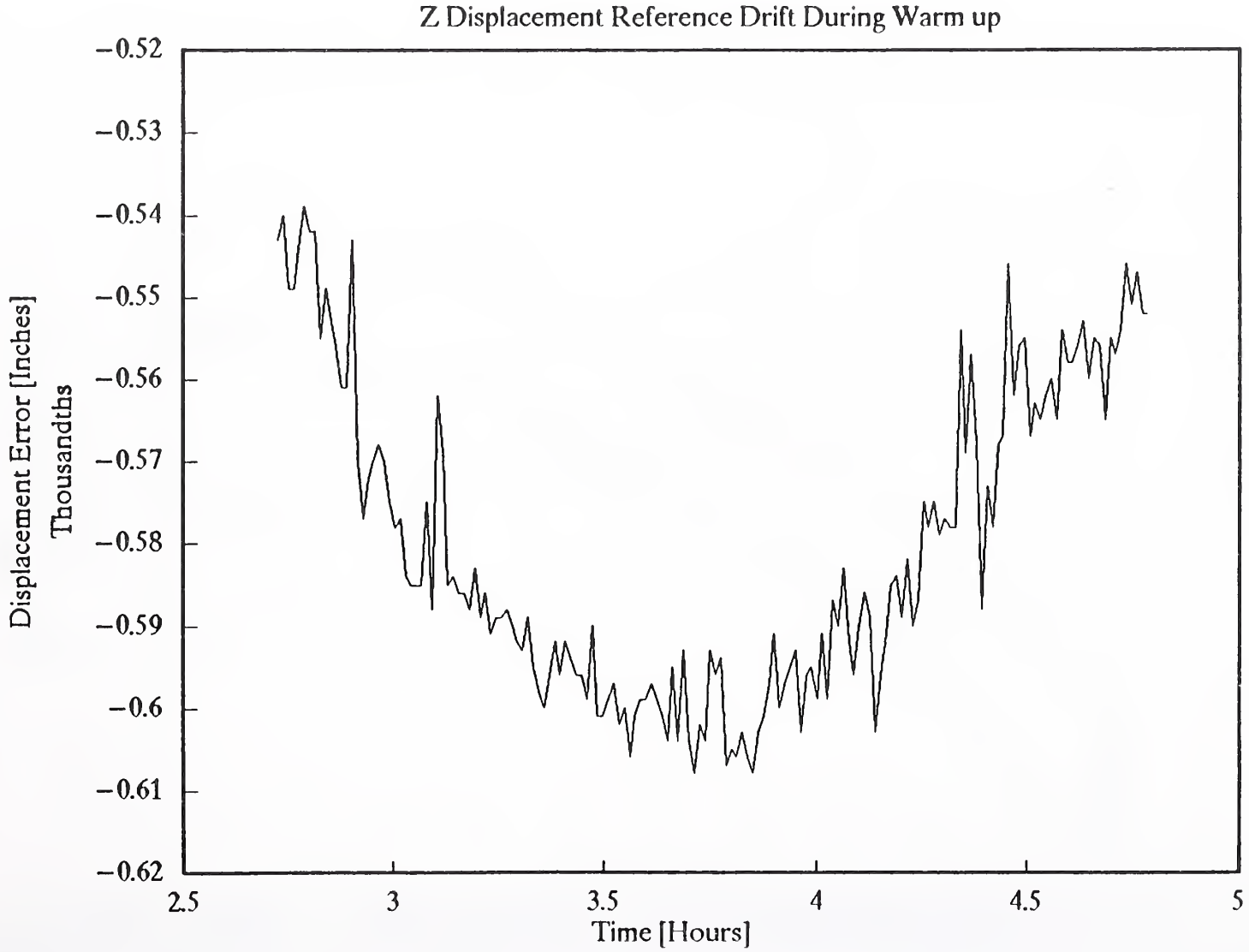
Z Displacement Reference Drift During Warm up
Displacement Error [Inches]
Thousandths
−0.52
−0.53
−0.54
−0.55
−0.56
−0.57
−0.58
−0.59
−0.6
−0.61
−0.62
2.5
3
3.5
4
4.5
5
Time [Hours]

Fig. 4.12

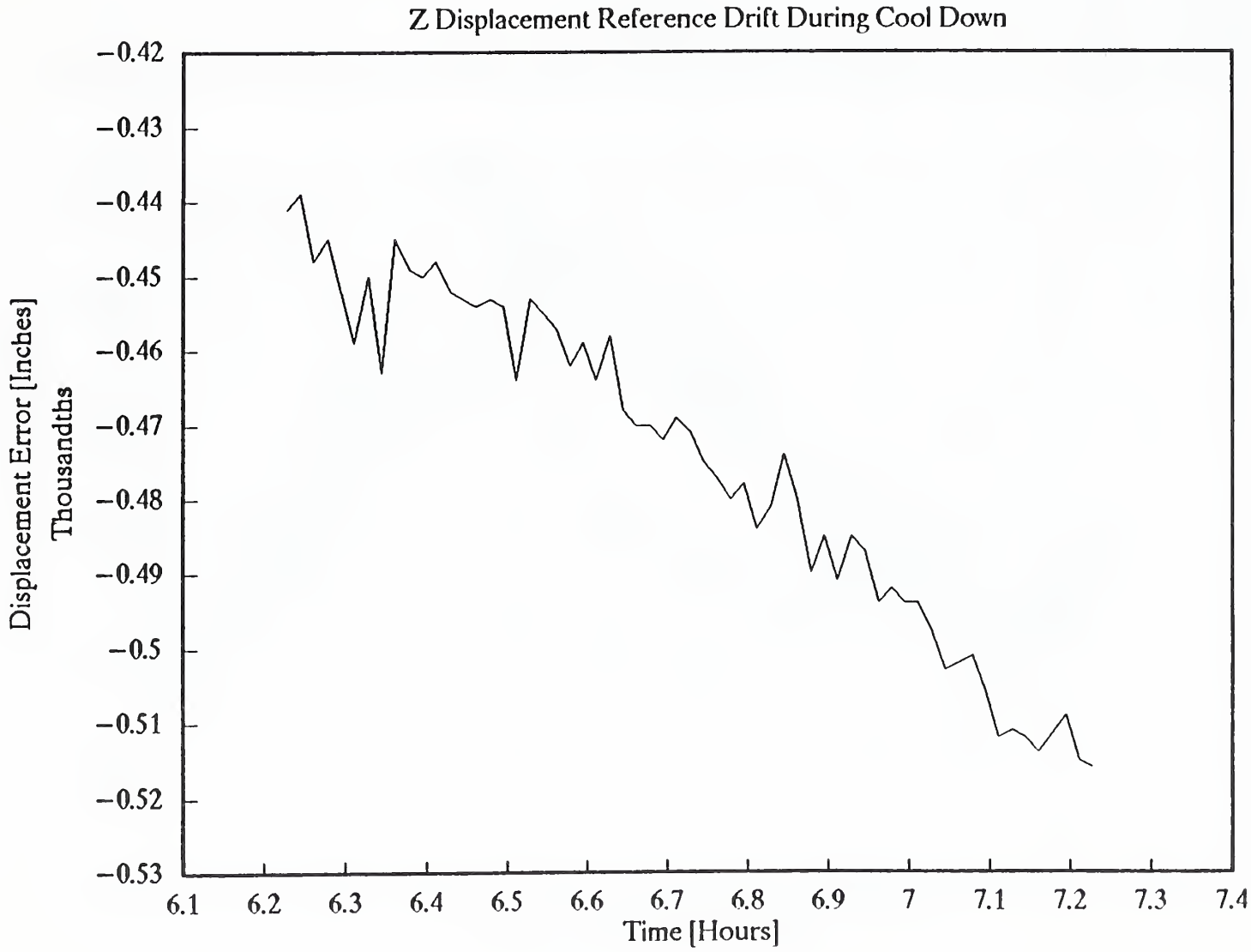
Z Displacement Reference Drift During Cool Down
Displacement Error [Inches]
Thousandths
−0.42
−0.43
−0.44
−0.45
−0.46
−0.47
−0.48
−0.49
−0.5
−0.51
−0.52
−0.53
6.1
6.2
6.3
6.4
6.5
6.6
6.7
6.8
6.9
7
7.1
7.2
7.3
7.4
Time [Hours]

Fig. 4.13

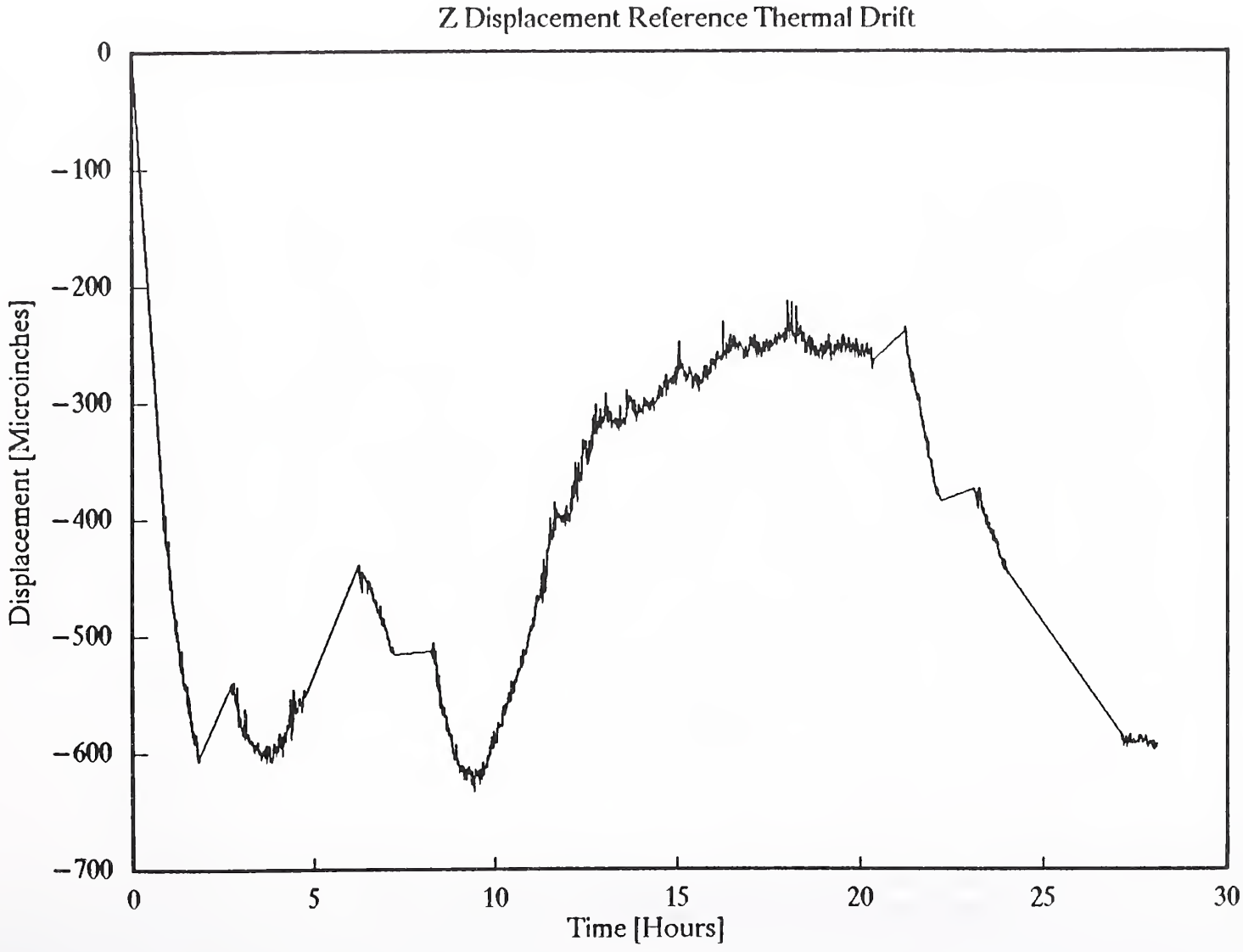
Z Displacement Reference Thermal Drift
Displacement [Microinches]
0
-100
-200
-300
-400
-500
-600
-700
0
5
10
15
20
25
30
Time [Hours]

Fig. 4.14

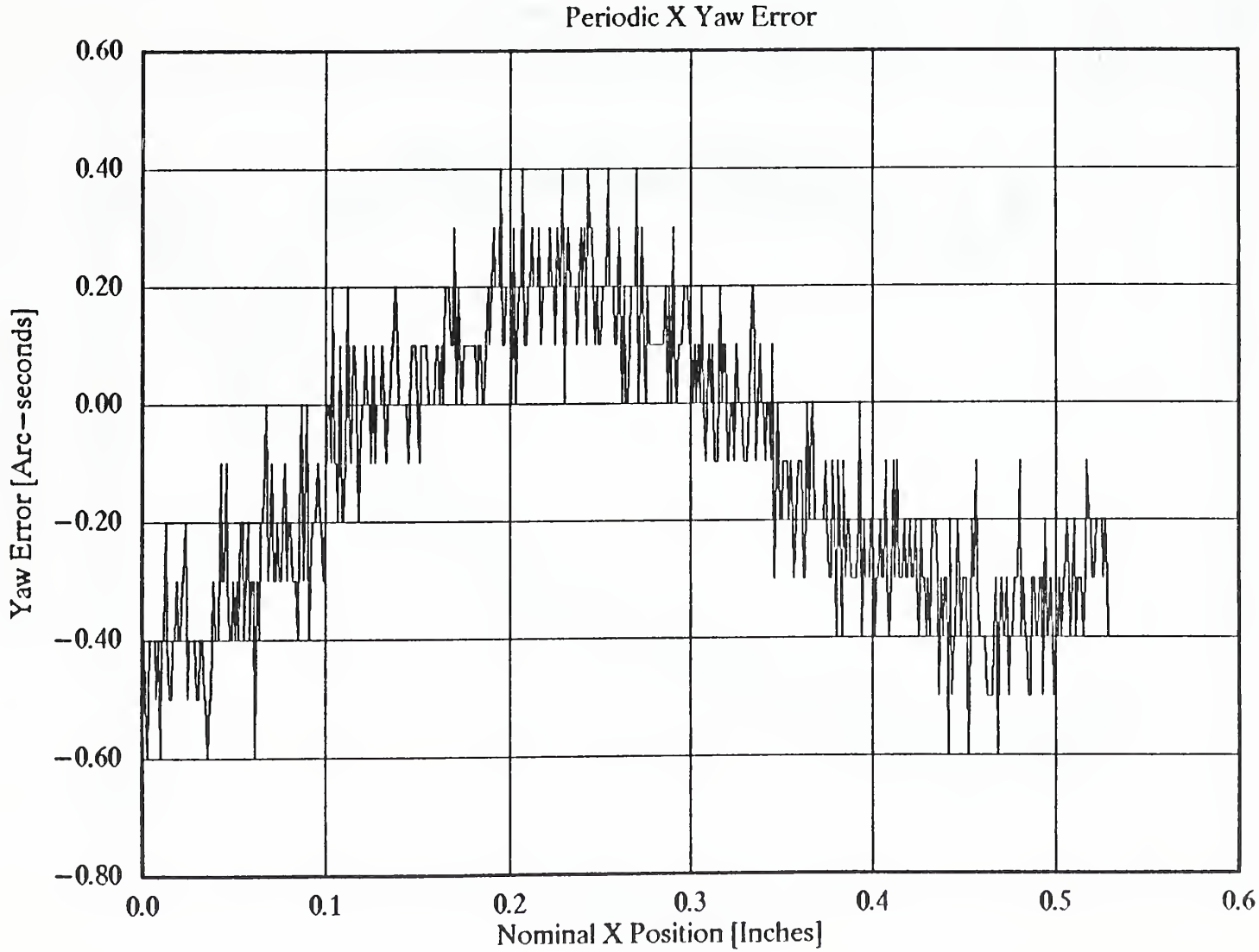
Periodic X Yaw Error
0.60
0.40
0.20
0.00
−0.20
−0.40
−0.60
−0.80
Yaw Error [Arc−seconds]
0.0
0.1
0.2
0.3
0.4
0.5
0.6
Nominal X Position [Inches]

Fig. 4.15

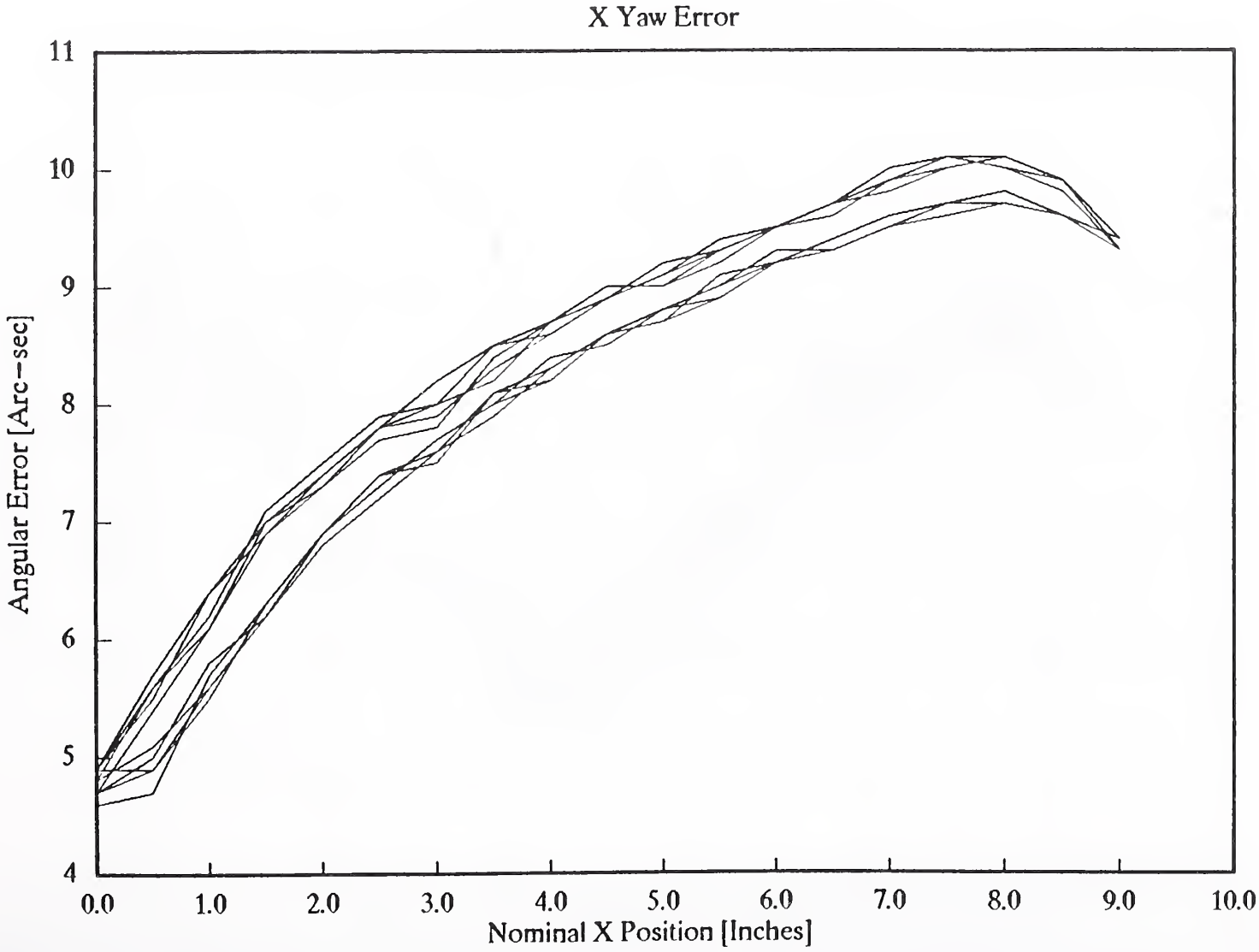
X Yaw Error
Angular Error [Arc-sec]
11
10
9
8
7
6
5
4
0.0
1.0
2.0
3.0
4.0
5.0
6.0
7.0
8.0
9.0
10.0
Nominal X Position [Inches]

Fig. 4.16

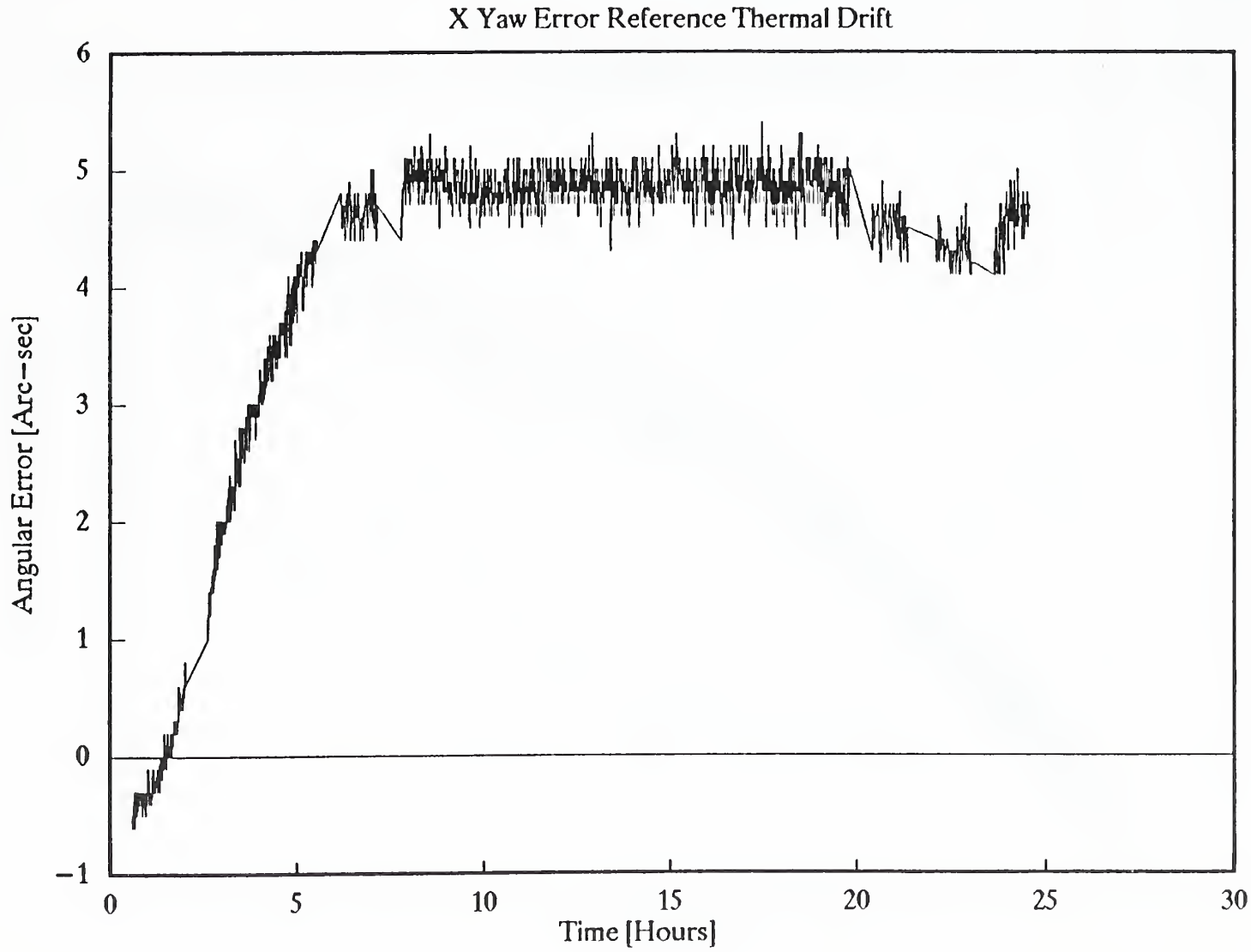
X Yaw Error Reference Thermal Drift
Angular Error [Arc-sec]
Time [Hours]
6
5
4
3
2
1
0
-1
0
5
10
15
20
25
30

Fig. 4.17

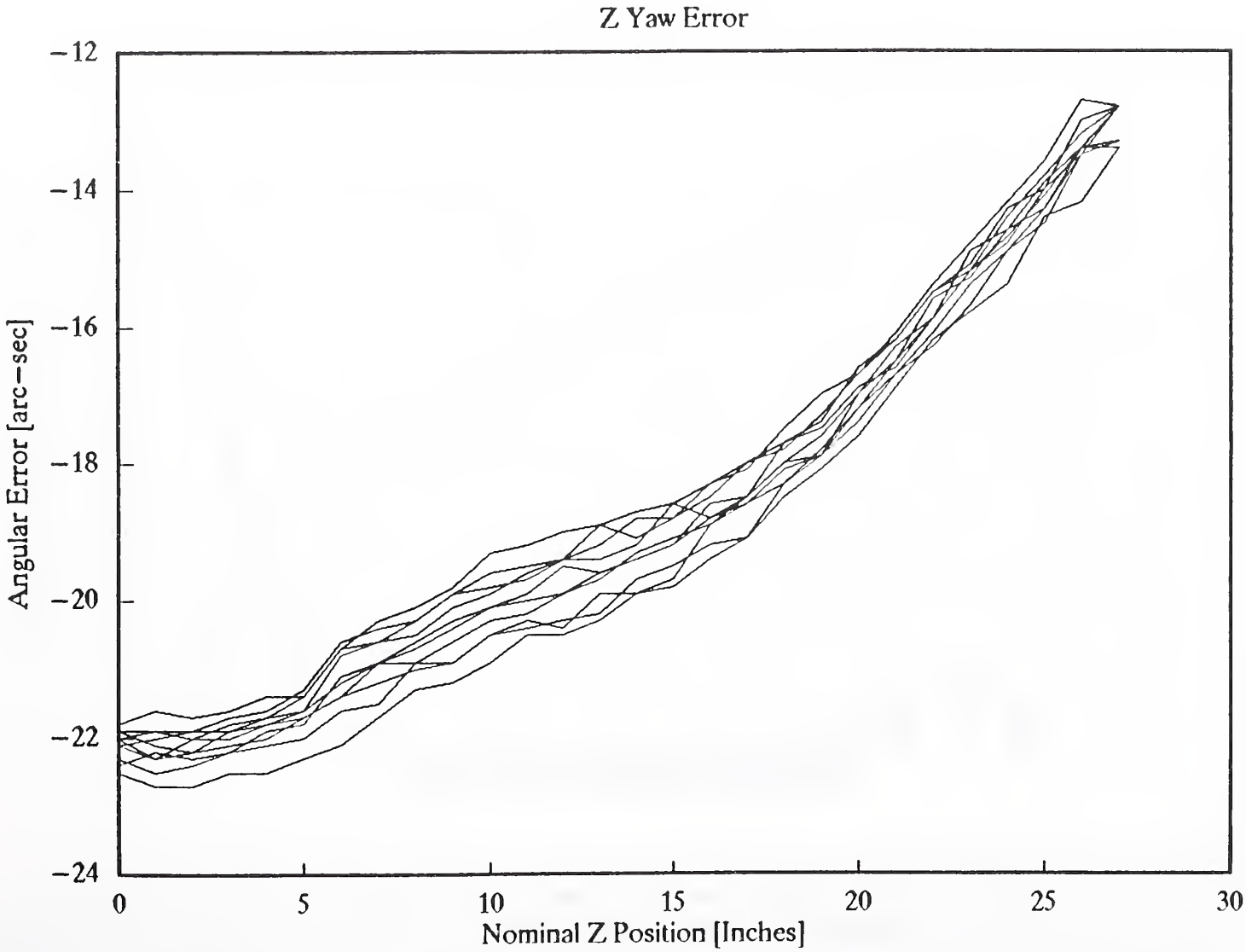
Z Yaw Error
−12
−14
−16
−18
−20
−22
−24
Angular Error [arc−sec]
0
5
10
15
20
25
30
Nominal Z Position [Inches]

Fig. 4.18

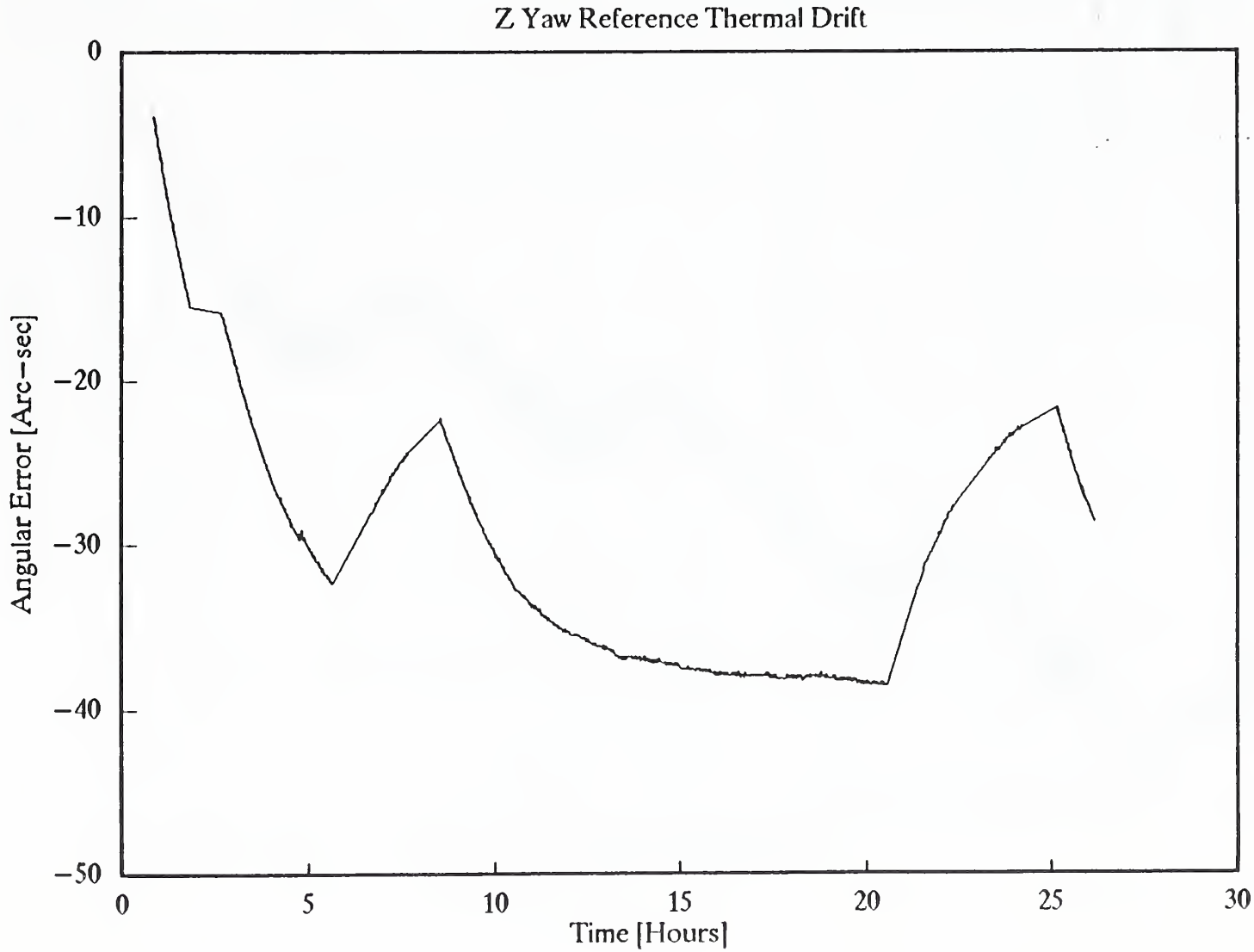
Z Yaw Reference Thermal Drift
0
−10
−20
−30
−40
−50
Angular Error [Arc−sec]
0
5
10
15
20
25
30
Time [Hours]

Fig. 4.19

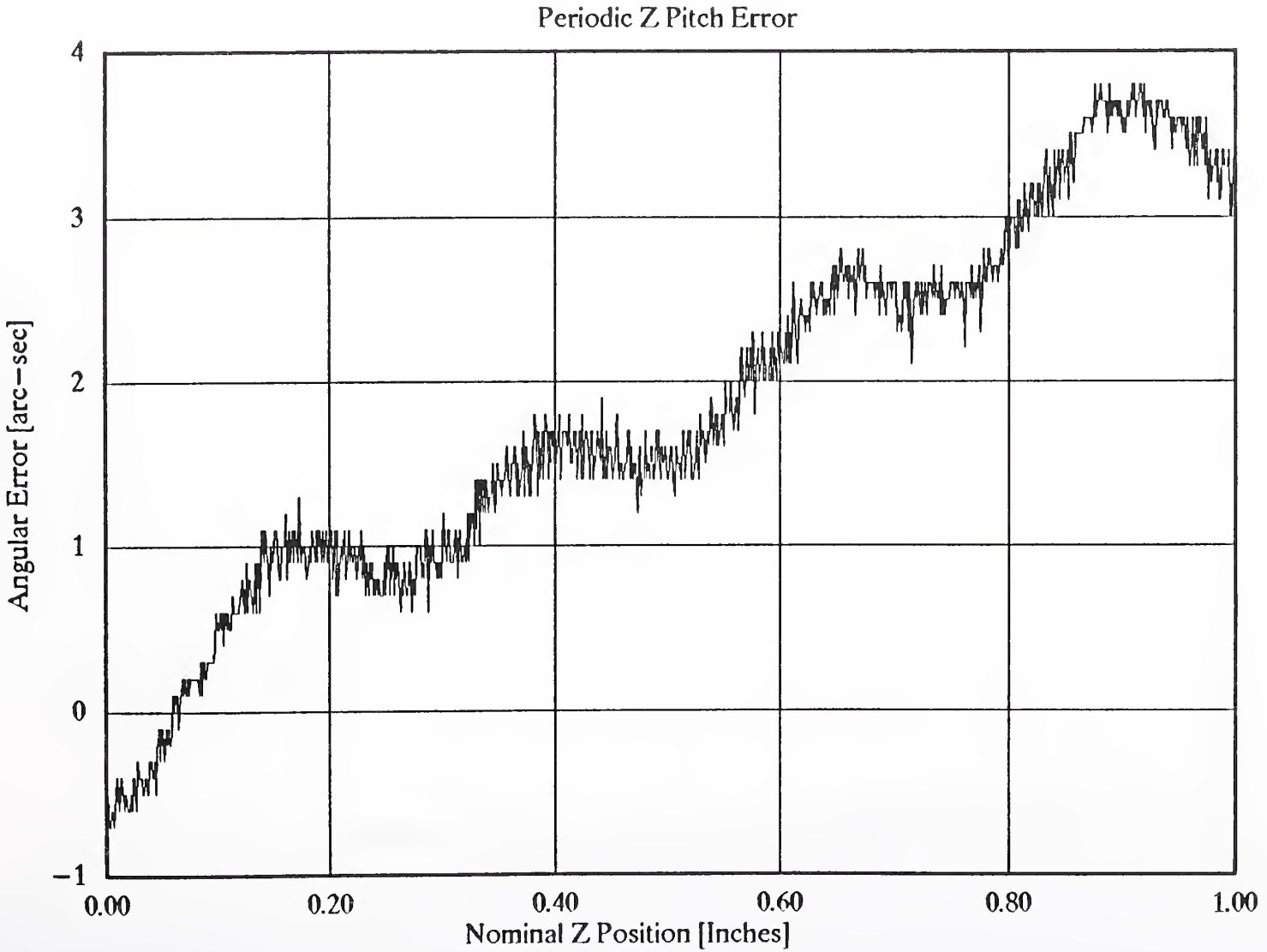
Periodic Z Pitch Error
Angular Error [arc-sec]
4
3
2
1
0
-1
0.00
0.20
0.40
0.60
0.80
1.00
Nominal Z Position [Inches]

Fig. 4.20

5. A PROTOTYPE PROGRAMMING LANGUAGE ENVIRONMENT FOR PROCESS-INTERMITTENT INSPECTION

J.C. Boudreaux

5.1 INTRODUCTION

The QIA project proposes to identify and reduce error throughout the manufacturing process. The QIA architecture supports (1) the real-time acquisition and processing of sensory data obtained from thermal, ultrasonic, vibration, and force sensors; and (2) adaptive machining algorithms which compensate for sensed environmental conditions by modifying the tool path as well as speed and feed rates. In order to provide these functional capabilities, the Automated Manufacturing Programming Language Environment (AMPLE) [5-1 through 5-7] is being enhanced and adapted for use on this project.

AMPLE has been designed to provide a uniform programming language environment for the construction of control interfaces to industrial manufacturing processes and to provide an integrated system of software tools for translating product design and process planning specifications into workstation- and equipment-level control programs. The central focus of the AMPLE project for QIA is to develop a logically coherent framework within which to define adaptive control mechanisms for workstations that are equipped with the ability to interpret commands and sensory feedback with respect to an internal world model.

5.2 THE AMPLE CORE INTERPRETER, VERSION 1.0

During FY89, Version 1.0 of the AMPLE Core Interpreter (**amcore**) and an associated **User's Guide** [5-6] were released for public review and comment. The **amcore** interpreter has been implemented in Microsoft C and runs on PC/AT compatibles with 80287 floating-point coprocessors. An EGA graphics adaptor is also recommended.

Amcore is a LISP dialect, specifically a small subset of Common Lisp which has been extended to include textport functions for interactive text windows, graphic viewport functions, and primitive object-oriented programming capabilities. A thorough overview of these capabilities is given in the **User's Guide** [5-6].

Amcore also contains an initial prototype of a collection of functions which are similar to those that will be needed for the definition of the real-time processor (rtp). These prototype functions have not yet been documented in the **User's Guide**, and will not be included until the technical basis of the rtp is more completely understood and a prototype version of it has been thoroughly tested.

The primary role of amcore is to define the primitive instruction set of an abstract machine. All higher level operations are to be defined in terms of that instruction set. Because of the inherent complexity of this application area, the set of base functions of amcore has been kept as small as practical. Some modules, such as those which provide disciplined access to Core Interpreter itself, are required by almost all application programs. Other modules are tailored to specific applications, such as those required to support the specific requirements of QIA.

5.3 REAL-TIME PROCESSING

In order to satisfy the programmatic objectives of the QIA project, AMPLE has to support both off-line and real-time modes of operation. A technically satisfactory definition of either of these terms is difficult to formulate, but some idea of their intended meaning can be grasped by considering some characteristic operations of both modes.

In off-line mode, the system may be used interactively to provide a wide variety of programming services, including software modules for analyzing and displaying data acquired during the manufacturing process, as well as software modules for modifying NC part program segments, which have been coded in conformity with EIA RS-274D. In general, off-line services are those for which timely termination, although desirable, is not an explicit

condition which needs to be taken into account in the verification procedure.

In real-time mode, AMPLE must support a digital interface with the Real-Time Error Corrector (RTEC), through which current status, axis position, and correction signals are transmitted. These transmissions are taking place while the machine tool is moving and are nearly instantaneous with respect to that movement, at least in the sense that the displacement of the tool during transmissions is very small. What makes these services real-time is the fact that the correctness of the algorithms which provide them depends not only on the mathematical correctness of the value that they return, e.g., the number of correction pulses to be inserted, but also on the timeliness of the returned values. It should be emphasized that timeliness greatly complicates the verification of real-time algorithms.

The real-time processor is a collection of primitive **amcore** functions. In order to guarantee that the **rtp** is programmable, this AMPLE component must include off-line services which allow it to be programmed for specific applications. Once the **rtp** has been programmed, the set of operations that it has been instructed to perform may be invoked by an **amcore** function call. After this call has been executed, the system returns to the off-line mode of operation.

The **rtp** must support two apparently conflicting goals: to complete its assigned tasks in a timely manner, it should run at nearly compiled C speeds; to be fully programmable, it should be able to use the entire range of entities which may be represented within **amcore**. This conflict can be resolved by paying close attention to the off-line services upon which initial configuration of **rtp** applications depend. Using those services, one must first build AMPLE objects which may then be accessed and updated using the special access functions within **amcore**. To prevent garbage collection during real-time processing, which would destroy the utility of the **rtp**, we shall also require that the access and update functions never actually cause the allocation of any free memory cells.

The clearest way to imagine the proposed model of the AMPLE real-time processing system is to see the **rtp** as a virtual machine with its own user interface provided by the off-line services, and its own instruction-set architecture provided by primitive functions within **amcore** itself. If this model is adopted, then the operation of **rtp** is determined by a script which creates an object in AMPLE core upon which the instructions operate. The general idea is that we pass in a pointer to the script, thereby defining the real-time environment. By selectively updating the script, rtp can keep track of its current state. When the system returns to off-line mode, the final state of the real-time environment is visible at the **amcore** level and is available for off-line analysis.

5.4 PROCESS-INTERMITTENT INSPECTION

In this section, a general overview will be given of an early prototype of the **rtp**, designed to support process-intermittent inspection on the Metalist Turning Center during the November 89 Automation Open House at NIST [5-8]. This overview will include descriptions of both the primitive **amcore** functions and the functions programmed directly in AMPLE for execution by **amcore** itself. Where appropriate, the behavior of these functions will be explained with pseudocode, a notation used to characterize the overall flow of control within an algorithm and main blocks into which it may be decomposed.

The first bit of business is to prepare a user-interface screen using the primitive **amcore textport** and **graphic viewport** functions. These functions have already been discussed in the **User's Guide**, and need not detain us here.

The second step establishes an interface between the AMPLE system and the RTEC. This interface is established by means of a digital I/O board. The board selected for this project contains seven Intel 8255A Programmable Peripheral Interface (PPI) chips, each containing three addressable I/O ports (A, B, and C) and an addressable register. The width of each port is one byte. The following table shows the manner in which the connection to the RTEC has been defined for the probing cycle:

Allocation of Ports in the Interface Board for the RTEC

PPI	Port	Data Logical Names	Direction(I/O)
8255A #1	A,B,C	**X.axis.status** : 4 bits; **X.axis.position** : 20 bits;	Input
8255A #2	A,B,C	**Y.axis.status** : 4 bits; **Y.axis.position** : 20 bits;	Input
8255A #3	A,B,C	**Z.axis.status** : 4 bits; **Z.axis.position**: 20 bits;	Input
8255A #4	A,B,C	**W.axis.status** : 4 bits; **W.axis.position** : 20 bits;	Input
8255A #5	A	**correction.C.x** : 1 byte;	Input
	B	**correction.C.y** : 1 byte;	Input
	C	**correction.C.z** : 1 byte;	Input
8255A #6	A	**correction.R.x** : 1 byte;	Output
	B	**correction.R.y** : 1 byte;	Output
	C	**correction.R.z** : 1 byte;	Output
8255A #7	A	**program.status** : 1 byte;	Input
	B		
	C	**correction.status** : 1 byte;	Output

Installation is accomplished by assigning a BASE address for the board by jumpering it, after which the low-level byte-oriented I/O operations **inp()** and **outp()** [5-6] may be done by adding a pre-defined offset to a BASE address.

Before being used the board must be initialized, which is accomplished by **outp**-ing a designated code to each register to define the I/O status of the port. That is, each port on the each of the seven PPI chips is initialized to accept either **inp or outp** operations. To accomplish this we use the function:

initialize_digital_io_board();

This primitive **amcore** function initializes the ports of each of the 8255A PPI chips for either Input or Output processing. These modes

do not change during the QIA probing cycle. This function should be run once during start-up.

After the board itself has been initialized, the next step is to create an entity in **amcore** which will allow common or shared access to the values of the variables obtained from this interface. The function for this step is:

initialize_diores ();

This primitive **amcore** function creates an AMPLE array object and associates it with the symbolic name DIORES. This object always retains its definitional status so that even if the real-time processor crashes, the debris will be visible from **amcore**. The components of this array object are initialized to zero.

After the QIA interface screen has been displayed and the start-up initialization sequence finished, the user must also supply information about the kind of operation to be undertaken. This selection process is handled by the programmed function **qia_real_time_process**, summarized in the following pseudocode:

```
qia_real_time_process is
   initialize_digital_io;
   get operation;
   begin
      if operation is probing then
        qia-probing-cycle;
      end-if;

      if operation is correcting then
        qia-correction-cycle;
     end_if;

     if operation is no_compensation then
       qia-no-compensation-cycle
     end_if;
  end;
```

The three modes of operation, **probing**, **correcting**, and **no_compensation** were discussed in Sec. 2.2.5.

During the period covered by this report, only the **qia-probing-cycle** has been prototyped. In order to understand the behavior of this cycle, a brief synopsis of the six functions added to **amcore** for the probing cycle are presented below.

1) **get_digital_io ();**

This primitive **amcore** function updates the array DIORES. It uses inp to read all of the input ports of the digital I/O board, which was diagrammed above. In the present configuration of the Metalist, only the **X.axis** (status and position), the **Z.axis** (status and position), the **correction.C** data, and **program.status** are assigned any significance. The Y and W data of Table 6.1 are not needed for a two-axis machine, and the **correction** output data are not needed for the process intermittent gauging operation. For the input data, **correction.C** and **program.status**, the current values can be used to update the internal representation without any further processing. Therefore **get_digital_io()** includes the following assignment statements, written in C:

```
/* get correction.C */
   (DIORES->n_vdata[21])->n_int = inp(0x290);
   (DIORES->n_vdata[22])->n_int = inp(0x291);
   (DIORES->n_vdata[23])->n_int = inp(0x292);

/* get program.status */
   (DIORES->n_vdata[31])->n_int = inp(0x298).
```

It should be noted that this use of pointers is required by the underlying data structure used to represent AMPLE arrays. Each of these assignment statements simply updates the array DIORES:

```
DIORES[21] = inp(0x290);
```

Note also that the arguments of the **inp** functions are the memory addresses of the ports. The processing of axis information requires an additional step in which the hi-order nibble (4 bits) of port A is taken as **axis.status**, and the lo-order nibble of port A together with

the values of ports B and C are combined into a single 20 bit integer; X(or Y) axis.position:

```
/* read X axis ports A,B,C */
   a = inp (0x280);
   b = inp (0x281);
   c = inp (0x282);
   axis_position = c + (256 * b) + (65536 * (0x0f & a));
   status = (0xf0 & a) >> 4;
```

After DIORES has been updated, the function **get_digital_io** returns the Boolean value **true** to the calling processes.

2) **put_digital_io ();**

This primitive **amcore** function gets the **correction.R** and **correction.status** values from the internal AMPLE representation DIORES, and writes them to the appropriate port:

```
/* get correction.R */
corr_r_x = getfixnum(getelement(DIORES, 26));
corr_r_y = getfixnum(getelement(DIORES, 27));
corr_r_z = getfixnum(getelement(DIORES, 28));

/* get correction.status */
 status = getfixnum(getelement(DIORES, 33));

/* output values to digital_io board */
 outp(0x294, corr_r_x);
 outp(0x295, corr_r_y);
 outp(0x296, corr_r_z);
 outp(0x29a, status);
```

The intended effect of the assignment statements is very simple. For example,

corr_r_x = DIORES[26].

In normal situations the references to the components of DIORES would be completely invisible to the programmer. The relative complexity here is caused by the techniques used in AMPLE to construct internal representations of array entities.

From the perspective of the QIA programmer, DIORES is a shared resource which is accessed by several functions: some retrieve information, some post new information, and some do both.

3) **display_digital_io ();**

This primitive **amcore** function is used to display the current values of the shared resource DIORES in the QIA textport.

4) **alarm ();**

This primitive **amcore** function gets an initial value of **X.axis.position** and **Z.axis.position** and then returns either **true** or **nil**. **Alarm** is sensitive to three events: (1) the NC part program, which moves the machine tool through the probing cycle, has concluded. This is signaled when the variable **program.status** becomes less than 255. (2) the operator wants attention and has depressed any key. When this happens, **kbhit()** is not 0. (3) the current value of either the **X.axis.position** or **Z.axis.position** is not equal to their initial values. If either (1) or (2) occurs, then **alarm** returns **nil**. If (3) occurs, then **alarm** returns **true**. Until at least one of these events occurs, **alarm** loops.

5) **program_active;**

This function is programmed in **amcore** and is not a primitive function. It starts an infinite loop that waits for **program.status** to be set, thus indicating that the machine is executing an NC program. Its operation is described by the following pseudocode.

```
program_active is
  loop
   if program.status >= 255 then
      return(t);
   end_if;
  end_loop;
end;
```

6) qia_probing_cycle;

This programmed amcore function is the main processor of process-intermittent inspection. The file archive, shown below, is a cumulative store of all of the latched values of the digital I/O board, which are recorded one after the other in the AMPLE array DIORES. Its operation is described by the following pseudocode:

```
qia-probing-cycle is

  open archive;
  set status #x9f;
  put_digital_io;
  print_digital_io;
  index := 1;

  until program_active
   loop
   end_loop;

  top
    if alarm then
      get_digital_io;
      print_digital_io;

        if x.axis.position > -3.000 then
          go top;
        end_if;

        if index = 1 then
          z.axis.0.reference := z.axis.position;
        end_if;

        print DIORES to archive;
        print_digital_io;
        increment index;
        go top;

    else
     close archive;
     return nil;
    end_if;
end;
```

Note that program_active is used to synchronize the activation of both the NC part program, which is used to define the sample of points to be inspected, and the data aquisition loop itself. As soon as this loop is started, alarm is activated. As explained above,

this causes an initial sample to be taken of **X.axis.position** and **Z.axis.position**. This function then loops until an unequal condition is detected. This event will be regarded as authentic and not a false signal only if it occurs within a defined interval of the part surface. If a false signal has been received, then control passes to the top of the loop and **alarm** is re-activated. Otherwise, the probe signal is accepted as authentic and the current value of DIORES is posted to **archive** for later processing. This loop will repeat until **alarm** returns the value **nil**, which can occur only if **program.status** is reset.

The final step in the QIA probing cycle is to compare the actual values of the inspected points with their predicted values. The difference between these two values is then pictured on a scale drawing of the part using the primitive graphic functions of **amcore**.

6. POST-PROCESS INSPECTION AND TEST PART MEASUREMENT RESULTS

S.D. Phillips, B. Borchardt, D. Stieren

6.1 POST-PROCESS INSPECTION

6.1.1 Introduction

The QIA program aims to provide quality assurance in an automated manufacturing environment. To this end, post-process inspection serves as a metrological anchor to the entire manufacturing process. It ultimately determines whether the finished parts meet dimensional specifications. Perhaps equally important, post-process inspection can monitor and provide the data to improve other quality assurance schemes, such as process-intermittent (PI) part probing and the geometrical-thermal (G-T) compensation algorithm of the machining center. Thus, post-process inspection can serve as a feedback element in those control loops, leading to a refinement of the machine tool parameters used in the quality control system. This is particularly important since geometry errors in the machining center which are not accounted for in the G-T model will not be detected by the PI probing.

An example of this condition might be a gradual change in squareness of the XY axis of the machine tool. Since the PI probing uses the same XY axis system for inspection as was used to machine the part, the PI probing will not detect the out-of-squareness condition. Post-process inspection, however, uses an entirely different machine structure, namely that of the coordinate measuring machine (CMM), to inspect the finished parts, and will readily detect this error.

In the post-process scenario, the results of each part inspection are forwarded to the quality monitor where they are evaluated. The quality monitor examines individual geometrical part features, e.g., the squareness of a machined corner, as measured by the post-process inspection results. These features are scrutinized for systematic

machining errors which are not being accounted for by the quality controller of the machining center which created the feature. Using this scheme, machining trends which prove to be statistically significant can be detected by the quality monitor before an out-of-tolerance condition occurs. The quality monitor then issues an appropriate corrective action, e.g., a change in the NC part program or in the geometrical-thermal model, based on the statistical analysis of the inspection results.

6.1.2 Automated Inspection

The objective of consistently machining quality parts is increasingly tied to automated inspection. Traditional methods of hard gauging are labor intensive, and a complete part inspection may require considerably longer than the unit production time. In an era of small batch production, manually gathering sufficient data to deduce machining trends may take longer than the entire production run. Hence, as the speed of production has been increased through the use of CAD/CAM and CNC machine tools, so must the rate of part inspection. The use of CMMs has met this need and greatly reduced inspection times while increasing the reliability and accuracy of the measurements. CMMs are available having different levels of sophistication; they include manual machines, joy stick controlled machines, and CMMs under direct computer control (DCC). DCC CMMs achieve high levels of accuracy by quantifying or eliminating operator-dependent parameters, such as probe approach distance. In this section we will concentrate on the DCC class of machines as they provide the highest levels of accuracy, throughput, and automation.

Until recently, DCC CMMs received their inspection instructions from either a part program, written by the operator in the particular language of the CMM, or through a teach mode which requires an operator to manipulate the CMM through a complete part inspection via the joy stick while the CMM remembers each step the operator has performed. Obviously this last technique requires at least one complete part to be produced before the inspection programming can begin. Each brand of CMM must be programmed in its own machine specific language. Some firms which have

many CMMs may have equally as many operating languages, thus requiring their operators to be CMM multilingual.

A consortium of companies known as Computer Aided Manufacturing International (CAM-I) has established an ANSI standard called the Dimensional Measurement Interface Specification (DMIS). This standard prescribes a format for communication between all dimensional measurement equipment (DME), including CMMs [6-1]. A single DMIS inspection program can be used with several different brands of CMMs. Some CMMs can utilize DMIS as their native language while others translate the DMIS input file, through a processor, into their own machine specific language. Similarly, the inspection results are produced directly into the DMIS format or are translated from the CMM language into a DMIS output file. Hence, part programs need only be written in the DMIS format, and are then accessible to a wide assortment of CMMs. This will also increase the exchange of inspection programs between users and aid in inspection round-robin programs for CMM performance testing.

The power of a standard format for inspection procedures is fully realized by its ability to be coupled to a CAD/CAM system. In the QIA program, we are developing a PC (80386) based system to control all aspects of the post-process inspection loop. The three-dimensional part geometry is created on this system using a CAD package produced by Cadkey, Inc. In this graphical environment, an inspection path may be defined in much the same way as the tool path is for a CNC machine. That is, the operator would use a mouse to specify inspection points and paths directly on the CAD/CAM graphic model. Some more sophisticated systems allow the user to view, through animation, a simulated inspection procedure showing both the part geometry and the CMM probe inspection path. This allows the inspection routine to be debugged without taking the CMM out of productive service. For the PC computer system utilized for post-process inspection, the inspection points and path, inspection simulation, and DMIS output file are created using PC DMIS, a product of Automation Software. This type of technology may eliminate the manual creation of part programs, i.e., writing inspection code programs, in much the same manner that CAM software has been developed for NC. Furthermore, the ease and speed with

which an inspection program can be constructed from a CAM design, e.g., importing the design through an IGES interface, allows "batch of one" parts to be effectively and economically inspected. The integration of DMIS as a standard format allows multiple and different CAD/CAM systems to be used together with a variety of different CMMs and other dimensional measuring equipment, see Fig. 6.1.

Although the QIA program is currently using only one inspection CMM (under direct computer control), the DMIS strategy has been adopted as a means of creating rapid and flexible inspection programs. DMIS will also serve as a communication standard between the CMM and other computer systems receiving or sending inspection data. The inspection results in DMIS format, in addition to being forwarded to the quality monitor, will also be available to view graphically and numerically at the CMM quality monitor. The QIA program is currently incorporating Qualstar, a metrology based analysis product of ICAMP. Inc., as a means of viewing the inspection results.

6.1.3 Inspection System

One goal of the QIA project is to maintain a tolerance of 0.001 inch or less for all dimensions of parts fabricated under the quality assurance system. Consequently, the inspection system must then be capable of much higher accuracy, i.e., 0.0001 inch. To be useful in a production environment where a high throughput of parts is necessary, high speed CMM motion is desirable. Finally the probing system must be sufficiently flexible to handle a wide range of part geometries which may be encountered in the flexible manufacturing environment. The instrument currently employed in the QIA project is a Cordax Apollo series CMM manufactured by Sheffield Measurement. The CMM is equipped with CMX Systems Incorporated laser interferometers for the axis scales, having a resolution of 0.1 μm (0.000004 inch). The accuracy of the machine (at standard 20° C temperature) is specified by the manufacturer as 1.7 μm (0.000068 inch) - 2.3 μm (0.000092 inch) over the range of travel dependent upon the axis length. Measurements carried out in our laboratory on a 12 inch gauge block measured along X,Y and XY diagonal are

shown in Table 6.1. The differences between the average measured values and the certified length of the block (12.000003 inches) are well within the sought after accuracy of .0001 inch.

The CMM has, within its measurement processor unit, an error compensation algrorithm for the twenty-one geometrical errors present in the machine structure [6-2]. This error map is created and installed by the manufacturer. The use of error-mapping techniques is well known as a means for correcting for small imperfections in the geometry of a machine structure. This general technique, which was substantially developed at NIST, exploits the property of machines that repeatability of motion is much more cost effective to achieve than exact geometrical accuracy in the machine hardware. By measuring the exact location of the probe end of the CMM ram with an external laser interferometer, and simultaneously recording the nominal position as measured by the CMM, a correction algorithm for repeatable errors can be created. This correction file or error map can then be implemented in real time to correct the machine motion, providing a level of geometrical accuracy up to ten times higher than the uncorrected machine [6-3].

As a means of characterizing the long term stability of the CMM, and to validate the error map supplied by the manufacturer, a parametric calibration of the CMM was performed [6-4]. An important technique for measuring the error map is with the use of a high resolution (0.000001 inch) external interferometer. For our tests we used a Hewlett Packard stabilized laser system. The pitch, roll, yaw, straightness, and scale errors of each axis were measured using the method outlined in Table 6.2. A comparison of the linear (straightness and scale) errors, measured with the CMM error compensation algorithm both activated and deactivated, demonstrated that the supplied error map provided a substantial improvement in CMM accuracy.

The CMM probe system consists of a Renishaw PH-9 motorized head and an autochange probe rack. The motorized head allows the probe two additional degrees of (rotational) freedom, in addition to the three translation motions provided by the CMM. The probe rack stores up to

eight probes, each of which can be automatically attached to the PH-9 by executing a command statement. Once the various probes have been calibrated, they can be automatically interchanged throughout the inspection procedure without the need for any further probe calibrations. For the results presented in this chapter, all measurements were performed with a TP12 piezoelectric touch-trigger probe. This probe is very accurate (Table 6.1) in the laboratory, but it is sensitive to oily or dirty surfaces, and so it may not be suitable for use in some industrial environments. In addition to the TP12 probe, a TP2 and TP6 are also mounted in the probe changer rack and provide reliable performance independent of part condition.

6.2 TEST PART MEASUREMENTS

6.2.1 Test Part Description

The test parts used to evaluate the performance characteristics of the machining centers are the National Aerospace Standard (NAS 979) composite cutting test for milling machines (Fig. 6.2) and the modified BAS test for the turning center [1-2, 1-3]. The test parts are designed to measure the accuracy and repeatability of numerically controlled machine tools under loaded conditions. These parts which were machined without the use of the QIA control scheme were previously inspected using a joy stick controlled CMM and the results were reported in the QIA report for FY88 [1-1]. We have remeasured the NAS parts produced by the horizontal workstation (HWS-1) and by the vertical workstation (VWS-1) using a part program to control the DCC CMM. The results are displayed in Table 6.3 (HWS-1) and Table 6.4 (VWS-1).

6.2.2 Measurement Procedure

In order to provide a thorough inspection of the performance characteristics of machining centers, an extensive inspection was performed on the NAS test parts. The specifications of the inspection procedure for the NAS 979 part are described in terms of the total indicator runout (TIR) of a dial gauge indicator. For purposes of

comparison, we have reported our results in this manner by recording the appropriate incremental range of the CMM measurements for a given feature. A complete inspection run (described below) was performed sequentially ten times. For each of the ten runs, a different set of points was probed on the part, providing information on the general applicability of the inspection procedure. It should be noted that the variation, i.e., the standard deviation, of the ten inspection runs reflects both the repeatability of the CMM and the uniformity, i.e., surface features, of the test part. Even using an ideal (perfect) measurement system, a nonzero standard deviation is expected. This reflects the fact that each inspection run contains a set of points which sampled slightly different positions on the machined part surface, and thus provides a slightly different set of data from which to determine the part dimensions. Similarly, for a part with perfect geometry and no surface variations, a nonzero standard deviation would be expected, reflecting the repeatability of the measurement system (the CMM and probe) used to measure the part. Since the CMM is highly repeatable (1.5 μm B89 manufacturer specification), the variations reported are dominated by the roughness of the machined surface.

6.2.3 Measurement Details

Ramps: The angle is measured between a best fit line through twenty data points per ramp, and the base plane of the part. The TIR is reported as the range of deviations from the best fit line in the plane perpendicular to the ramp surface.

Squares: Squareness and parallelism are measured between the respective best fit lines (20 points per line) relative to side 1 and reported as inches per inch deviation, multiplied by the length of the square side.

Circles: Diameter is found from the best fit circle using 20 points, roundness is the maximum to minimum range of radial deviations from the best fit circle center, concentricity is twice the distance between the best fit circle center and the center of the best fit circle (20 points) of the pre-bored center hole of the part (Fig. 6.2).

6.3 SUMMARY

A DCC CMM has been incorporated into the QIA program providing greater accuracy and automation than the previous joy-stick driven machine. Inspection programs for the NAS test parts have been written and an extensive inspection of the parts carried out. The DMIS standard has been selected as the preferred means of communication between the CMM and various computer systems. Integration of various CAD/CAM, inspection, and analysis software, supporting the DMIS standard, is currently underway.

THE INTEGRATED DMIS ENVIRONMENT

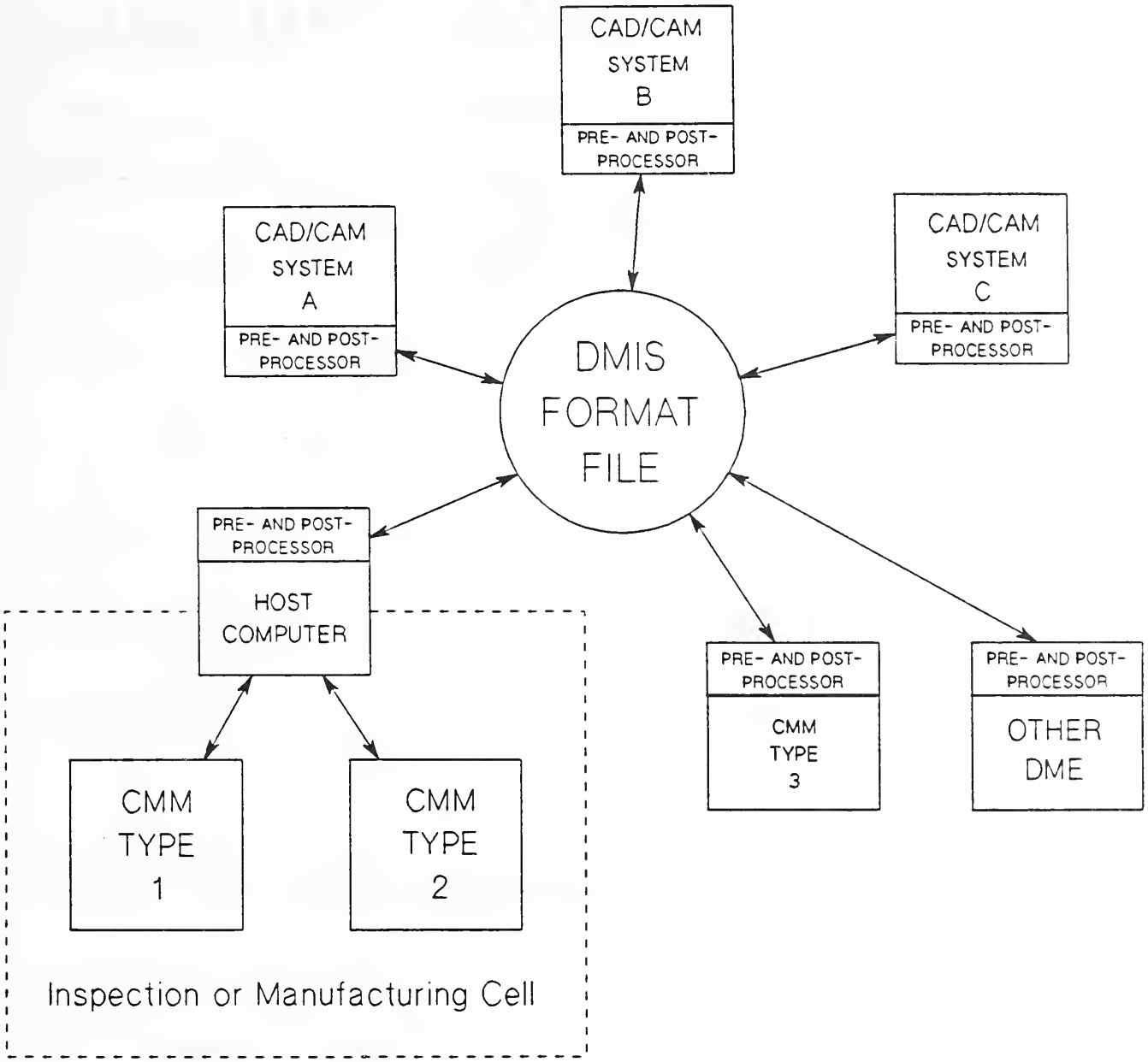

Fig. 6.1

NAS 979
Composite Cutting Test Part

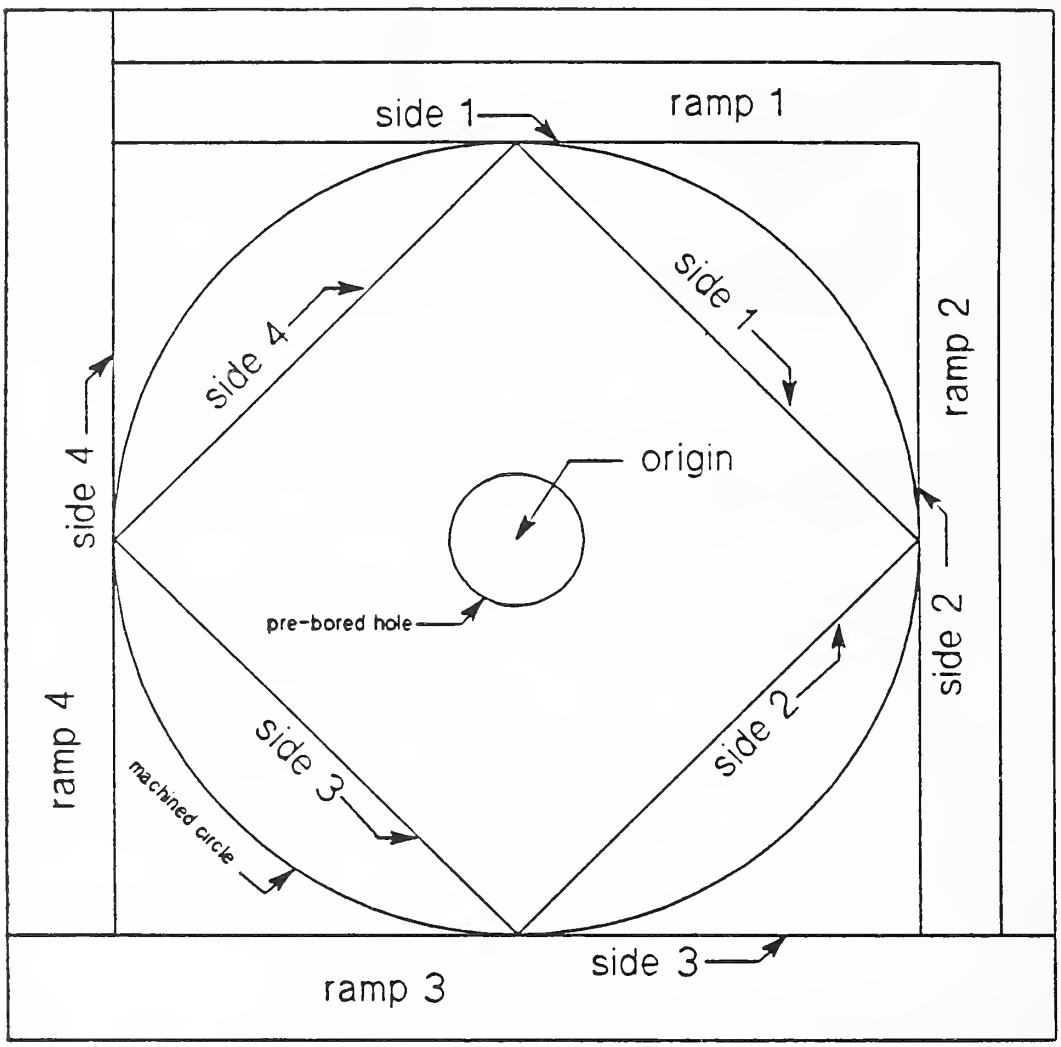

Fig. 6.2

TABLE 6.1

CMM ACCURACY TEST
(All Dimensions in Inches)

Orientation Direction	Measured Size	Standard Deviation
Y axis	12.000016	0.000016
X axis	11.999996	0.000025
XY diagonal	12.000036	0.000009
YX diagonal	11.999982	0.000013

Test Conditions

Gage Block Length: 12.000003, uncertainty of 0.000005 (3σ + systematic)

Location: Center of table

Temperature: 20 ± 0.1 C

Probe Type: TP12 (piezoelectric probe)

Probe Calibration: Performed using 0.750036 inch master sphere (nine touches), repeat ten times, use the average probe diameter, standard deviation = 0.000019.

Probe Approach Speed: 0.3 in/s

Probe Approach (Clearance) Distance: 0.5 in

Length Determination: Touch each end of the block at six different locations. Construct a best fit line at each end of the block, and find the minimum distance from the gage point location (on one best fit line) to the best fit line at the opposite end. Repeat the procedure ten times, report the average distance and the standard deviation of the ten measurements.

TABLE 6.2

MEASUREMENTS FOR ERROR COMPENSATION

Measurement	Axis	Method
Displacement	All Axes	Laser Interferometer
Straightness	All Axes	Laser Interferometer
Squareness	All Planes	Laser Interferometer
Pitch	All Axes	Laser Interferometer
Yaw	All Axes	Laser Interferometer
Roll	X and Y	Differential Levels
Roll	Z	Probe Offset and Straight Edge

TABLE 6.3

INSPECTION RESULTS FOR HWS - 1

(All Dimensions in Inches)

parameter	value	std. dev.	spec	Pass/Fail
RAMP 1	0.000379 TIR	0.000118	0.0020 TIR	P
RAMP 2	0.000359 TIR	0.000067	0.0020 TIR	P
RAMP 3	0.001470 TIR	0.000311	0.0025 TIR	P
RAMP 3	4.990230 DEG	0.001245		
RAMP 4	0.000810 TIR	0.000077	0.0025 TIR	P
RAMP 4	4.988019 DEG	0.000274		
LG SQ SIDE 1	0.000193 TIR	0.000041		
LG SQ SIDE 2	0.000148 TIR	0.000016		
LG SQ SIDE 3	0.000182 TIR	0.000021		
LG SQ SIDE 4	0.000577 TIR	0.000081		
LG SQ SIDE 1-3 SIZE	11.997929	0.000013	12 ± 0.0025	P
LG SQ SIDE 2-4 SIZE	11.998051	0.000008	12 ± 0.0025	P
LG SQ SIDE 1-2 SQ	0.001140 TIR	0.000036	0.0020 TIR	P
LG SQ SIDE 1-3 PAR	0.000600 TIR	0.000024	0.0020 TIR	P
LG SQ SIDE 1-4 SQ	0.000924 TIR	0.000024	0.0020 TIR	P
CIRCLE DIA	11.997241	0.000052	12 ± 0.0025	F
CIRCLE ROUNDNESS	0.001210	0.000110	0.0020	P
CIRCLE CONCEN	0.002150	0.000020	0.0020	F
SM SQ SIDE 1	0.000290 TIR	0.000021		
SM SQ SIDE 2	0.000309 TIR	0.000014		
SM SQ SIDE 3	0.000370 TIR	0.000031		
SM SQ SIDE 4	0.000337 TIR	0.000038		
SM SQ SIDE 1-3 SIZE	8.484177	0.000019	8.4853 ± 0.0025	P
SM SQ SIDE 2-4 SIZE	8.483687	0.000011	8.4853 ± 0.0025	P
SM SQ SIDE 1-2 SQ	0.000441 TIR	0.000034	0.0015 TIR	P
SM SQ SIDE 1-3 PAR	0.000289 TIR	0.000042	0.0015 TIR	P
SM SQ SIDE 1-4 SQ	0.000373 TIR	0.000017	0.00015 TIR	P

INSPECTION RESULTS FOR VWS - 1

(All Dimensions in Inches)

parameter	value	std. dev.	spec	Pass/Fail
RAMP 1	0.000367 TIR	0.000035	0.0020 TIR	P
RAMP 2	0.000898 TIR	0.000049	0.0020 TIR	P
RAMP 3	0.000893 TIR	0.000208	0.0025 TIR	P
RAMP 3	4.992177 DEG	0.000305		
RAMP 4	0.001501 TIR	0.000246	0.0025 TIR	P
RAMP 4	5.010651 DEG	0.000502		
LG SQ SIDE 1	0.000302 TIR	0.000055		
LG SQ SIDE 2	0.000349 TIR	0.000049		
LG SQ SIDE 3	0.000217 TIR	0.000025		
LG SQ SIDE 4	0.000196 TIR	0.000021		
LG SQ SIDE 1-3 SIZE	11.997109	0.000011	12 ± 0.0025	F
LG SQ SIDE 2-4 SIZE	11.997431	0.000009	12 ± 0.0025	F
LG SQ SIDE 1-2 SQ	0.000468 TIR	0.000072	0.0020 TIR	P
LG SQ SIDE 1-3 PAR	0.000048 TIR	0.000072	0.0020 TIR	P
LG SQ SIDE 1-4 SQ	0.000144 TIR	0.000072	0.0020 TIR	P
CIRCLE DIA	11.997346	0.000033	12 ± 0.0025	F
CIRCLE ROUNDNESS	0.001234	0.000092	0.0020	P
CIRCLE CONCEN	0.002334	0.000022	0.0020	F
SM SQ SIDE 1	0.000220 TIR	0.000028		
SM SQ SIDE 2	0.000244 TIR	0.000021		
SM SQ SIDE 3	0.000146 TIR	0.000018		
SM SQ SIDE 4	0.000219 TIR	0.000022		
SM SQ SIDE 1-3 SIZE	8.482657	0.000008	8.4853 ± 0.0025	F
SM SQ SIDE 2-4 SIZE	8.483489	0.000024	8.4853 ± 0.0025	P
SM SQ SIDE 1-2 SQ	0.000441 TIR	0.000051	0.0015 TIR	P
SM SQ SIDE 1-3 PAR	0.000475 TIR	0.000034	0.0015 TIR	P
SM SQ SIDE 1-4 SQ	0.000636 TIR	0.000025	0.00015 TIR	P

7. OPTICAL SCATTERING FOR ROUGHNESS INSPECTION

T.V. Vorburger, E. Marx, and A. Kiely

7.1 SUMMARY

Although the principal effort in the QIA project is directed towards the control of dimensional accuracy, we have also established a goal of measuring and controlling surface finish. During the past year we have learned a great deal about the usefulness and limitations of optical scattering as an area technique for measuring surface roughness. Some of these results should help as well in assessing the complementary technique of ultrasonic surface inspection [7-1]. The ultrasonic technique is useful for monitoring rougher surfaces and longer surface spatial wavelengths than the optical approach.

Briefly, optical scattering with incident radiation wavelength λ can assess rms surface roughness [7-2] up to an amplitude of $\sim\lambda/3$ [7-3,7-4]. This is a generalization of our results taken on a particular set of hand-lapped specimens but one that seems reasonable for a variety of machined reflecting surfaces. In addition to surface roughness amplitude, optical scattering also can assess the rms surface slope of metal surfaces for slopes up to ~0.16 [7-5].

7.2 BACKGROUND

When a laser beam or other type of electromagnetic or ultrasonic radiation illuminates a rough surface, the reflected radiation is scattered according to the laws of physical optics. The pattern of scattered radiation is very sensitive to the surface roughness.

For very smooth surfaces or, more precisely, when the heights of the surface asperities are much smaller than the illuminating wavelength, the surface behaves like a mirror. The vast majority of the scattered light flux is scattered in the specular direction. As for the diffuse radiation, its angular distribution is closely related to the Fourier

decomposition of surface spatial wavelengths [7-6]. Short spatial wavelengths on the surface tend to scatter the radiation into wide angles from the specular direction. Long spatial wavelengths scatter the radiation close to the specular beam.

As the surface roughness increases, the intensity of the specular beam decreases rapidly [7-7], and the width of the diffusely scattered radiation tends to increase.

In principle, the measurement of various properties of the scattered light can be used to detect average properties of the surface roughness over the area illuminated by the radiation. Hence, the scattering technique is one of a class of so-called area techniques [7-8] for assessing roughness. Area techniques have the advantage that a single measurement, or a small number of them, can yield knowledge about the surface roughness without the need for detailed profiling of the surface. Thus, optical or ultrasonic scattering has unique potential as an on-line technique for monitoring roughness in manufacturing provided that environmental problems such as surface contamination and the presence of metal chips can be minimized.

One disadvantage of this technique is that the area-averaged parameters cannot be related simply to conventional surface parameters obtained by profiling techniques. Consequently, area-averaged parameters can serve as predictors of profiling parameters only under carefully controlled measurement and manufacturing conditions.

Scattering from smooth surfaces has been studied extensively, both experimentally [7-9] and theoretically [7-6, 7-9, 7-10], and is well understood. As a result, optical scattering with visible light ($0.4\ \mu m < \lambda < 0.7\ \mu m$) has been applied in a practical way to the study of optical surfaces. Standard procedures have been developed and written for an angle integrated scattering technique known as total integrated scatter (TIS) [7-11, 7-12]. Similar procedures are being investigated for angle resolved scattering techniques [7-13].

For machined surfaces, where the asperity heights are a sizable fraction of the illuminating wavelength, the scattered light distribution is a complicated function of the surface topography. The complication occurs because a certain series approximation [7-6, 7-9] can no longer be made to first order in the mathematical description of the process. Nevertheless, certain surface texture information should still be predictable from the scattered light.

7.3 THE NIST PROGRAM IN LIGHT SCATTERING

For several years we have been engaged in an experimental and theoretical program to accomplish several things: 1) to understand how light scatters from moderately rough, machined surfaces, 2) to develop a surface model for rough surfaces to allow us to calculate surface parameters from light scattering measurements, and 3) to apply the above knowledge toward developing a practical on-line instrument to monitor surface roughness during manufacture.

Figure 7.1 shows a schematic diagram of a light scattering instrument. A laser illuminates the surface and the pattern of reflected radiation is measured by a set of detectors, one of which, detector 3, is in the specular direction. Our apparatus, called DALLAS [7-3, 7-4, 7-14] (detector array for laser light angular scattering), measures the distribution of scattered light intensity over most of the hemisphere above the specimen's surface and contains 87 detectors in the array. The source of light is a HeNe laser with a wavelength of 0.6328 μm.

The intensity distributions measured with DALLAS have been compared with theoretical calculations of the scattered light distribution, and the results agree very well. The theoretical calculations use a fairly rigorous description of the light scattering intensity distribution which itself requires as input the surface roughness topography map $z(x,y)$. For a machined surface with uniaxial machining marks, such as those produced by grinding, the surface is essentially smooth in one direction and surface profiles with only one dependent variable $z(x)$ are sufficient

input to the calculation. The surface profiles were measured by a stylus instrument with high resolution.

Excellent agreement between theory and experiment was obtained for all members of a set of nine hand-lapped stainless steel specimens with rms roughnesses ranging from 0.08 μm to 0.48 μm.

Results are shown in Fig. 7.2 for two surfaces with quite different light scattering signatures. In each figure we plot the intensity of the scattered light versus angle of scattering in the plane of incidence. The angle of incidence was +54°.

The lower graph in Fig. 7.2 was taken for the smoothest specimen in the set having a measured rms roughness of R_q = 0.08 μm. It is characterized by a strong narrow specular peak, which contains about 59% of the scattered light flux, and a diffuse scattering distribution. A surface yielding such a distribution looks visually like a clouded mirror with marks and imperfections.

The upper graph of Fig. 7.2 is for the roughest surface of the three with R_q = 0.48 μm. The specular peak is now unmeasurable and the distribution consists entirely of diffusely scattered light.

For both these cases and for the seven other surfaces in the set, the calculated distributions based on optical scattering integrals of measured surface profiles agree with the measured data. Both the diffuse scattering distributions and the relative contributions of the specular peak are reproduced by the calculated values. The only significant difference is that the calculations drop below the data for angles far from the specular direction. This is likely due to the lateral resolution limit of the stylus tip which was about 0.5 μm in width. Structures on the surface more closely spaced than 0.5 μm tend to scatter the light into wide angles but these are not well resolved by the stylus tip. Therefore, the scattering intensities into those angles are not well predicted.

7.4 RECENT RESULTS

The foregoing results show that the scattering theory can quantitatively describe the light scattering distribution from a knowledge of the surface topography. The next step is to learn how to use the light scattering distribution to measure roughness parameters. This requires that a statistical model of the surface with the appropriate geometrical parameters, such as R_q, be folded into the theoretical description of the light scattering. Hence, properties of the light scattering distribution, such as its effective width or the relative intensity of the specular beam, could be expressed in terms of the geometrical roughness parameters. Furthermore, those properties could serve as predictors of the geometrical parameters.

It had first seemed possible to fit the measured light scattering distribution to a theoretical one expressed in terms of two parameters, R_q and the surface autocorrelation length T [7-4], and hence derive both parameters. Unfortunately, although the degrees of fit were good, the determination of the parameters themselves proved ambiguous. That is, several sets of values of R_q and T gave equally good fits to the data.

Instead, two properties of the distribution seem to be useful indicators of surface roughness parameters: the relative intensity of the specular peak and the angular width of the scattered light distribution. We discuss the results below for each.

7.4.1 Specular Peak Intensity

It is well known that the intensity of the specular peak relative to the total amount of scattered light is related to the rms roughness [7-15,16]. For a Gaussian probability distribution of surface heights, a good approximation for many kinds of manufactured surfaces [7-17], the following relationship [7-15] may be derived:

$$I_s/I_o = \exp[-(4\pi\sigma\cos\theta_i/\lambda)^2] \quad ,$$

where I_s is the power in the specular peak, I_o is the total power in the scattered light distribution, θ_i is the angle of incidence with respect to the surface normal, and σ is the rms roughness as determined by the optical technique as opposed to R_q, the rms roughness as measured with a profiling technique.

Therefore, one can predict σ from a measurement of the ratio I_s/I_o. Although this relationship is known, it has not been widely used to estimate σ for optical measurement of moderately rough surfaces. This is probably due to uncertainties in the validity of the relationship if the surface height distribution is not quite Gaussian and experimental uncertainties associated with measuring the total diffuse scattering intensity.

In the present work, we attempted to determine the upper range of rms roughness over which that quantity could be estimated. The results are shown in Fig. 7.3 for five of the nine hand-lapped specimens in the study. In the figure we plot the rms roughness σ as determined by measuring the ratio I_s/I_o (and using the above specular beam equation) versus R_q as measured with a stylus instrument. The value for R_q was computed from nine or ten stylus profiles distributed over the surface. Each profile had a length of 800 μm and was otherwise undistorted by any long wavelength attenuation procedure. The correlation between the two quantities is excellent, and the correlation coefficient [7-18] is 0.986.

The data points do not lie along the 1:1 line, most likely because the bandwidths of surface wavelengths measured by the stylus and optical techniques are different [7-4]. The optical bandwidth is limited by the angular range and resolution of DALLAS and spans an approximate range of 0.35 μm - 0.50 μm. The bandwidth of the stylus instrument is limited by the stylus width and the traverse length of the data and spans a much larger range of 0.5 μm - 800 μm.

Although the correlation between the two types of measurements is very good, it is risky to use the optically measured σ as a predictor of R_q as conventionally measured by the stylus approach. The difference in

the measured surface bandwidths which depend on the instrumental parameters could lead to considerable divergence of the results from the two methods. However, the optical technique can certainly be used as a comparator method for monitoring roughness variations under controlled manufacturing and measurement conditions. The technique can also be used on its own terms as a direct measurement of a quantity we might call optical rms roughness over a fairly narrow spatial bandwidth.

The range of measurement of rms roughness is limited by the ability of the instrument to measure the true specular peak intensity on top of the diffusely scattered background in the specular direction. This is limited by the angular resolution and the random error in the intensity measurement and varies from one instrumental design to the next. However, the specular beam intensity decreases exponentially with the square of σ. Therefore, a significant improvement in instrument capabilities may lead to only a modest improvement in the range of measurable σ.

For example, in our instrument the upper limit is approximately 0.18 μm, corresponding (by the specular beam equation) to a lower limit of 0.012 for the measurement of I_s/I_o. If we could improve the instrument by an order of magnitude so that it could measure I_s/I_o down to 0.0012, the range of measurable σ would only increase to 0.22 μm.

Therefore, we conclude that the specular peak technique serves as a direct indicator of optical rms roughness up to about $\lambda/3$. At the other end of the scale, the lower limit of resolution for measuring σ depends on the capability of the instrument to measure a small amount of diffusely scattered light in the presence of a strong specular beam. That capability in turn depends on two things: the dynamic range of the detectors and the instrument signature [7-19], the amount of light scattered into the detection system by the surfaces and apertures of the instrument itself, independent of the measured surface.

The dynamic range of one of our detectors is $\sim 10^6$. That means that the approximate detector noise is about 10^{-6} times the maximum signal that the detector can measure before reaching saturation. If we attempt to

measure the total scattered light by summing the measured intensities in 81 of our detectors, then use of Poisson statistics suggests that the noise in such a measurement would be

$$\sqrt{81} \times 10^{-6} I_s \approx 9 \times 10^{-6} I_s \quad .$$

Thus we estimate that the resolution limit for our instrument occurs when the total intensity in the diffusely scattered light is at the resolution $10^{-5} I_s$. By using the specular beam equation, we therefore estimate that the lower limit for measurement of σ with DALLAS would be approximately $\sigma = 0.0004\lambda$, provided one could determine the instrument signature to the required accuracy.

This is probably not the case for DALLAS. Considering the uncertainty in the instrument signature, a more realistic estimate of the lower limit of sensitivity for DALLAS is approximately 0.002 μm or about 0.003λ. Therefore, we estimate that for HeNe light with $\lambda = 0.6328$ μm, the range of measurable σ is $0.002\ \mu m < \sigma < 0.20\ \mu m$, a range of finish attainable by polishing, lapping, fine grinding, or single point diamond turning, but below the range normally attainable by milling and conventional turning.

This range can be increased significantly by using an infrared source such as a CO_2 laser with $\lambda = 10.6$ μm or an ultrasonic source with a comparable wavelength. Ultrasonic systems to monitor roughness have been developed over the frequency range from 5 to 30 MHz, corresponding to a radiation wavelength range of 300 to 50 μm, respectively, in the water medium. In principle, practical ultrasonic transducers may be available with frequencies as high as 100 MHz and a corresponding wavelength of 15 μm.

All other things being equal, increasing the radiation wavelength results in a proportional increase in the lower limit of sensitivity of the measurement. Therefore, we estimate that, independent of the wavelength, the dynamic range in roughness measurement is approximately

100:1 for a sensitive technique where the detectors have a dynamic range of 100:1 or more. The roughness measurement range would be nearer 20:1 for a simpler technique where the detectors themselves have a small dynamic range of 1000:1, for example. Coincidentally, Blessing's measurements [7-1] of ultrasonic back scattering from rough surfaces with a single detection transducer spanned a range of rms roughness of 0.8 to 37.6 μm. The ultrasonic frequency was 6 MHz and the corresponding wavelength was 250 μm. Therefore, the range of measured roughness values was 0.003λ - 0.15λ.

As the radiation wavelength increases, the lower limit of measurable surface spatial wavelength also increases. The minimum detectable wavelength is the one that scatters the radiation into the largest angle at the horizon. This is expressible in terms of the first order diffraction condition

$$\sin\theta_s - \sin\theta_i = \lambda/D \ ,$$

where θ_i is the angle of incidence and θ_s is the scattering angle for a surface spatial wavelength D. Assuming for simplicity that $\theta_i = 0$, then the maximum possible value of θ_s (= 90°) corresponds to a minimum detectable surface wavelength equal to λ itself. The maximum detectable wavelength is related to the angular resolution of the instrument.

From all this information, we suggest in Fig. 7.4 a range of rms roughnesses and spatial wavelengths measurable by various wave scattering techniques. Four systems are compared: the DALLAS research apparatus, a commercial on-line optical device with $\lambda = 0.8$ μm, the ultrasonic device with $\nu = 6$ MHz, $\lambda = 250$ μm developed by Blessing and Eitzen, and a projected device with $\lambda \approx 10$ μm that could be based either on infrared or ultrasonic radiation. The range of rms roughnesses typical of various machining processes is also shown.

The use of such a roughness height vs. surface wavelength graph was first proposed by Church [7-20] for assessing the measurable range of

surface profiling instruments. Other surface assessment graphs were proposed by Stedman [7-21] and Teague et al. [7-22].

It appears then that scattering with optical or near infrared wavelengths can be used to monitor fine grinding, diamond turning, or lapping processes. Ultrasonic wavelengths are suitable for monitoring the rms roughness of milling and turning processes. Grinding processes might be monitored best by a proposed infrared or ultrasonic gauge with $\lambda \approx 10$ μm. The surface wavelengths produced by the machining processes (not shown in Fig. 7.4) are also expected to overlap in the same way with the instrument wavelength ranges shown in the figure.

7.4.2 Width of Scattering Distribution

It has been shown empirically that the width of the angular scattering distribution may be correlated with the rms surface slope [7-23,24]. Recently, Rakels [7-25] and Takacs et al. [7-26] have shown theoretically, with fairly reasonable assumptions, that the rms width of the light scattering distribution about its mean is proportional to the rms slope Δ_q of the surface. This relationship is easily obtainable for smooth surfaces, but Rakels shows that it holds for moderately rough surfaces as well. His result is expressed as

$$\Delta_q = w/2f \ ,$$

where the angular distribution is measured in the Fourier transform plane, w is its rms width, and f is the focal length of a Fourier transform lens [7-27] that would typically be used in a scattering instrument to image the angular distribution onto a detector array.

We have attempted to test this relationship for angular distributions measured by a particular optical surface gauge. We compare measured results of the gauge's response with predicted results based on stylus measurements and a model of the gauge.

The optical surface gauge, developed by Brodmann et al. [7-23], is shown in Fig. 7.5 and a schematic diagram of its optical system is shown in Fig. 7.6. A light emitting diode is the source of infrared light with $\lambda = 0.8$ μm. This is collimated and then redirected and focused on the specimen by the special measuring lens which serves as the Fourier transform lens. If the surface is smooth, the reflected light produces a small spot on the array detector, containing 20 photodiode elements. If the surface is rough, the reflected light is scattered into a broad pattern and this broadening is detected by the array.

The gauge software calculates the mean square width (variance) of the light scattering distribution. This quantity, termed S_N, was compared to the rms surface slope measured with a stylus instrument for several sets of roughness comparison specimens that were replicas of ground surfaces with average roughnesses R_a [7-2] ranging from 0.08 μm to 0.76 μm. There were 15 surfaces in all.

Figure 7.7 compares the measured and predicted results. The individual data points are the measured results for S_N plotted versus the results for rms slope Δ_q measured with a stylus instrument. The stylus results were average values of rms slope measured from 5 profiles. Each profile was 1-mm long and was undistorted by any long wavelength attenuation procedure.

The curved line shows the locus of S_N values predicted by a model developed by Kiely et al. [7-5] that uses Rakels' Equation (above), the measured rms slopes, and a model for the response of the gauge. This model takes into account both the angular width of the optical beam and the truncation of the measured scattered light distribution by the finite length of the diode array (equivalent to a range of scattering angles of $\pm 15°$).

The correlation of the measured S_N results with Δ_q and the agreement between the measured results and the model suggests that the rms surface slope may be measured optically up to rms slopes of ~0.16, or slope angles of 9°, a fairly large slope for a machined surface.

This is not to say that optical measurements may be used as predictors of stylus measurements of rms slope. There is appreciable methods divergence [7-28] between the two approaches which nominally measure the same quantity but actually can yield different results because they are sensitive to different systematic effects. This can lead to a large scatter in the measured results about the instrumental model. Indeed, the rms surface slope is not an intrinsic property of the surface roughness topography. Its value for a digitized profile, for example, is a sensitive function of the sampling interval of the profile itself [7-29].

Nevertheless, when taken on its own terms, the quantity S_N or some other estimate of the width of the optical scattering distribution can serve as an optical measure of surface slope over the range of rms slope angles up to 9°.

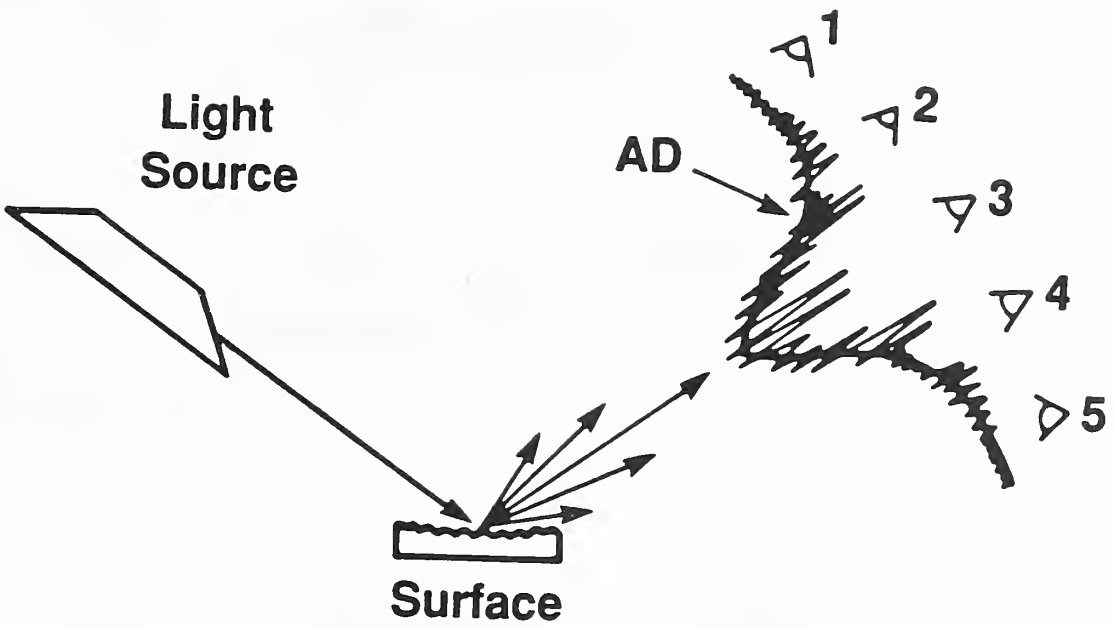

Fig. 7.1

Schematic Diagram of an Optical Scattering Instrument to Measure Surface Roughness

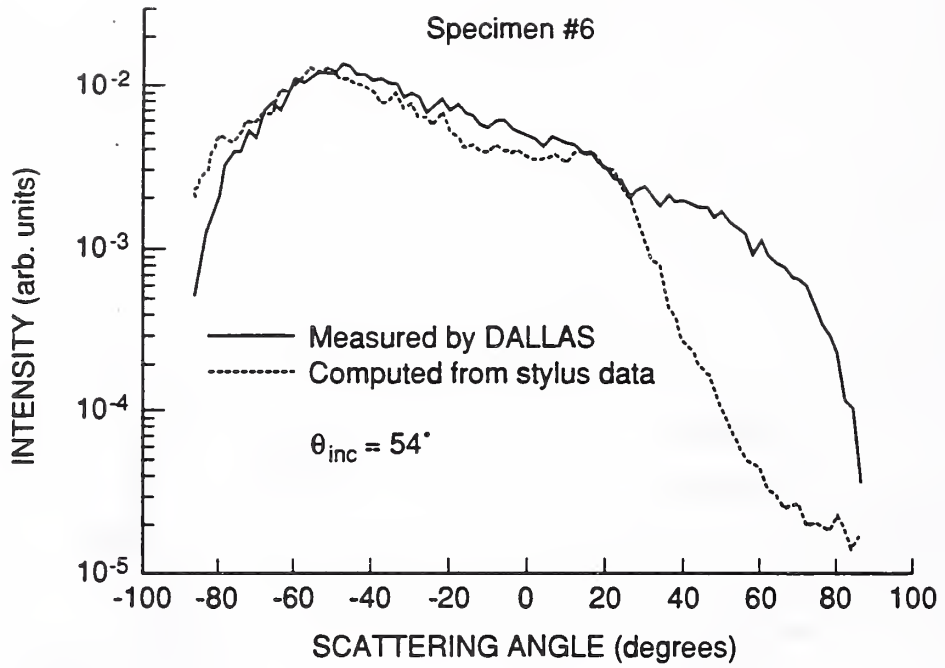

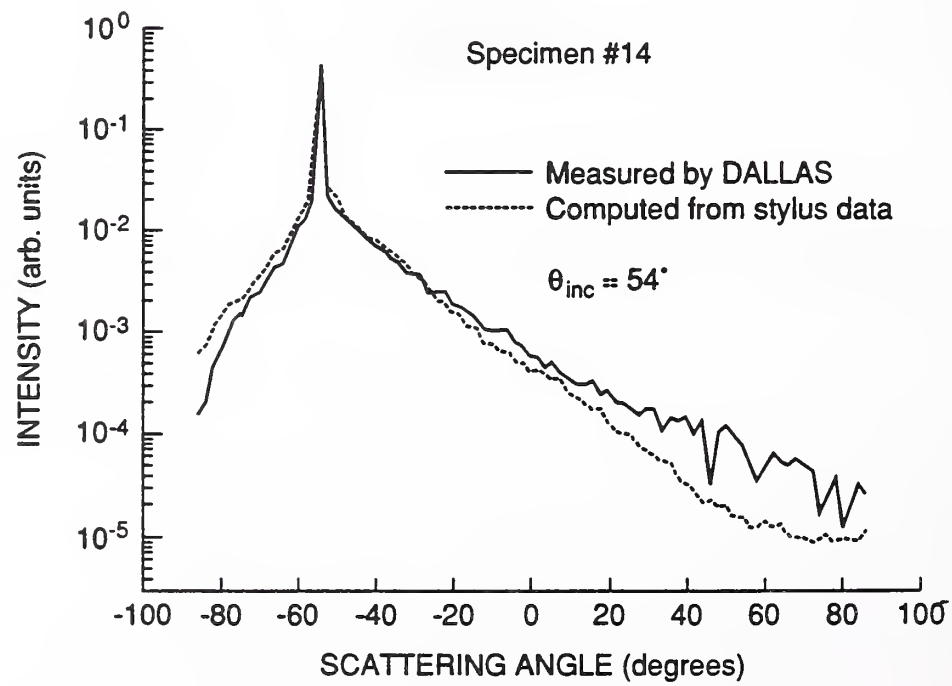

Fig. 7.2
Comparison of Theoretical and Experimental Angular Scattering Distributions for Two Stainless Steel Hand-lapped Surfaces

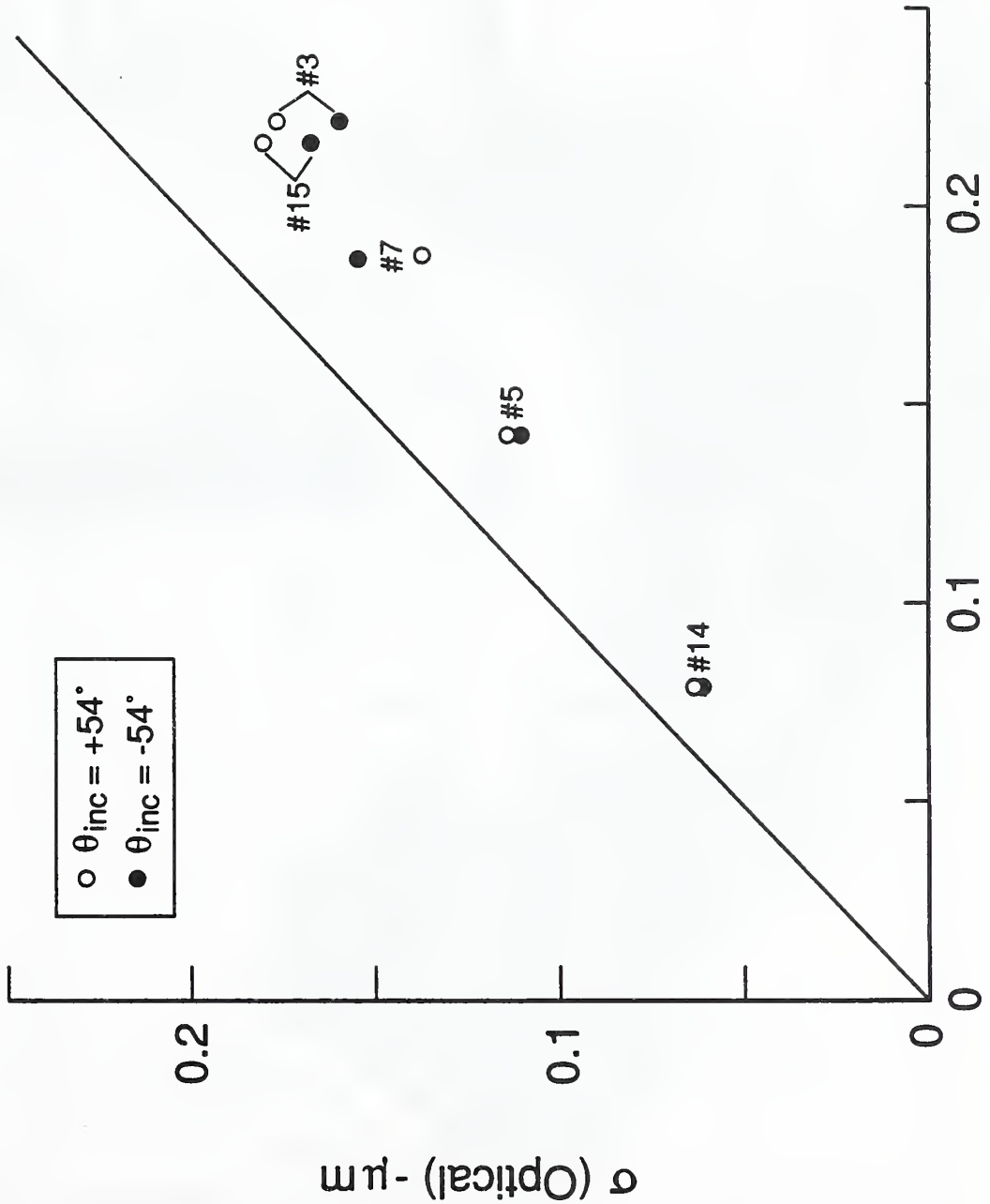

Fig. 7.3

rms Roughness (σ) Measured By Optical Scattering vs. Rq Measured By Stylus for Hand-lapped Stainless Steel Surfaces

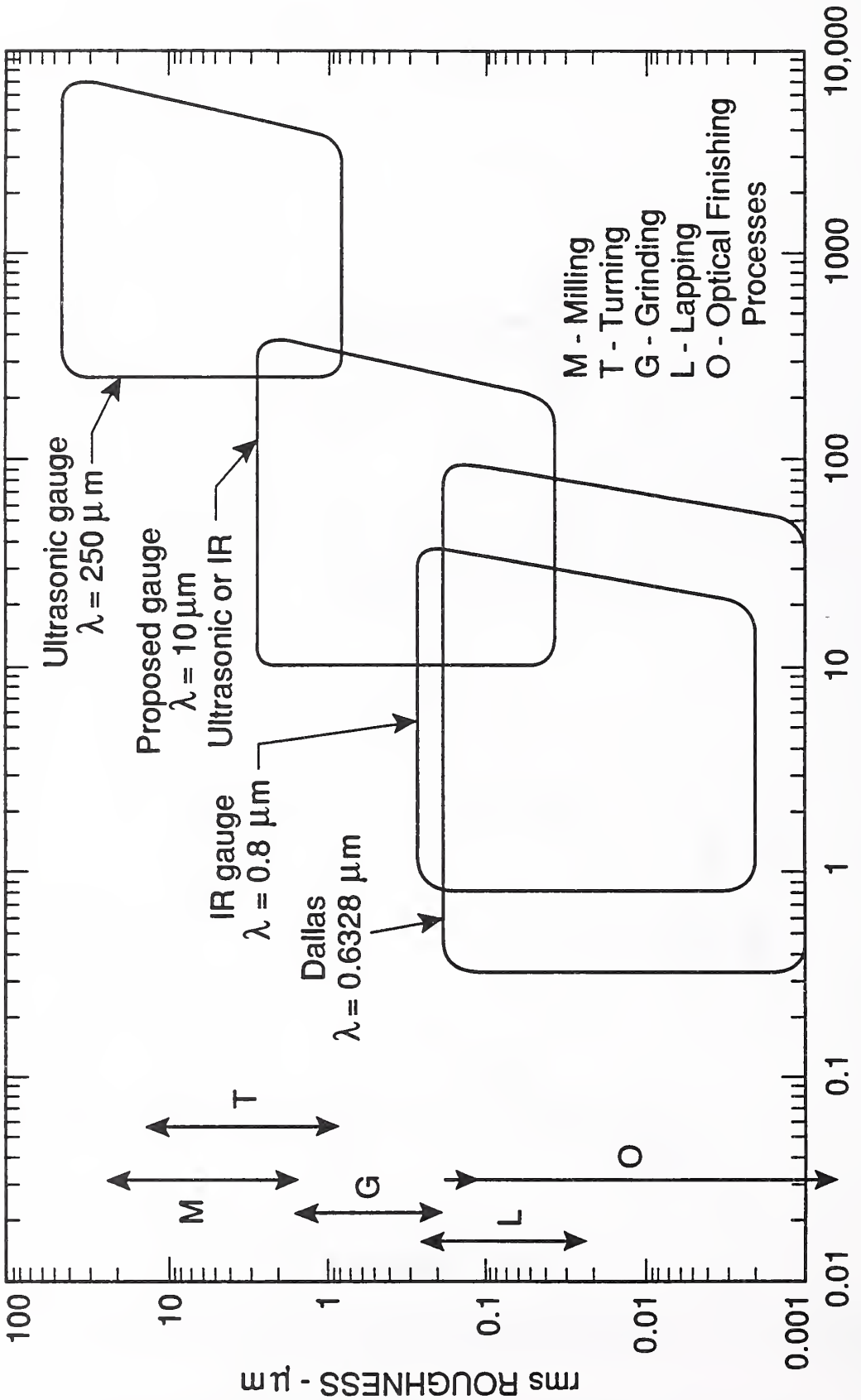

Fig. 7.4

Roughness Regimes Measured By Various Scattering Instruments

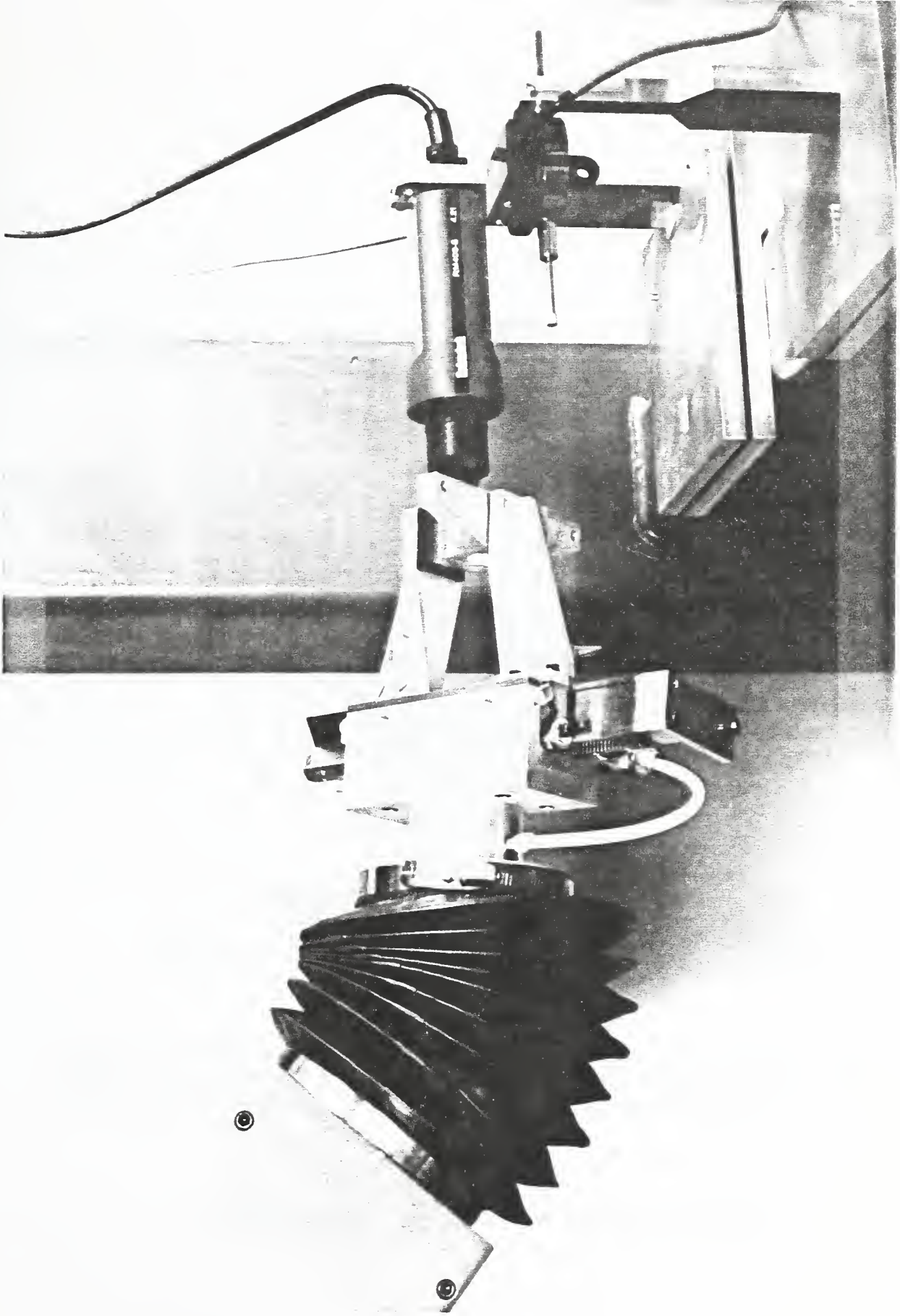

Fig. 7.5

Optical Roughness Gauge Inspecting Component Surface

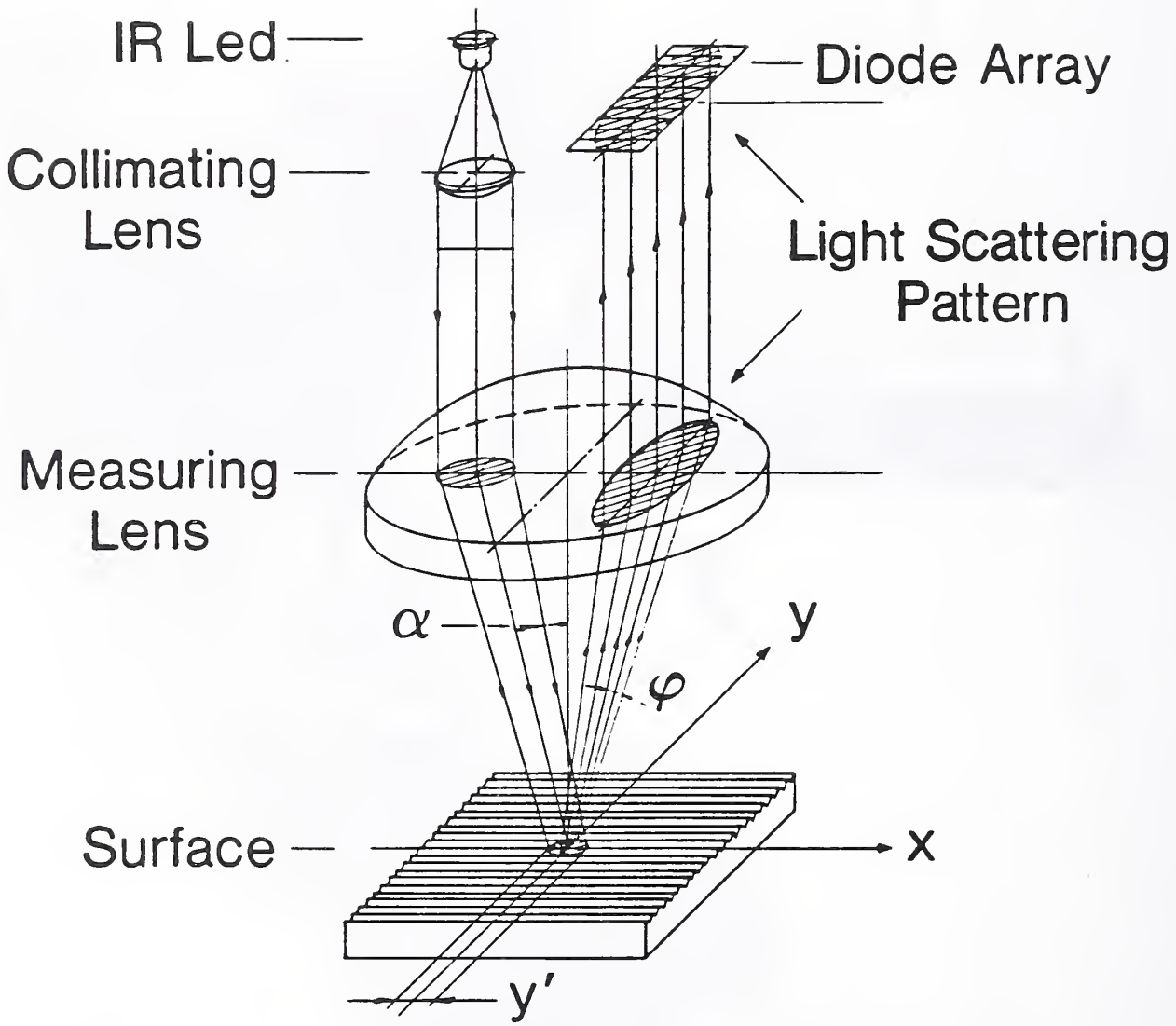

Fig. 7.6

Schematic Diagram of the Optical Roughness Gauge

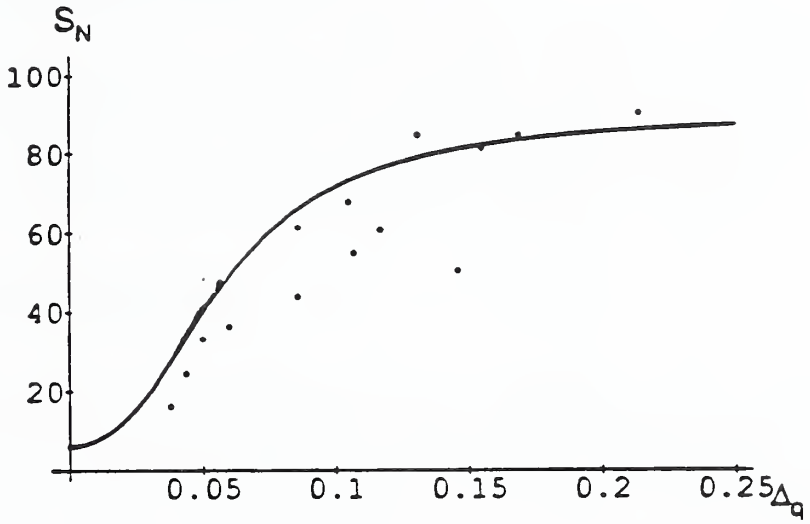

Comparison of predicted and measured values of S_N versus roughness rms slope Δ_q for 15 ground surfaces. S_N is the second moment of the angular scattering distribution. Δ_q is measured with a stylus instrument.

Fig. 7.7

8. CONCLUSION

T.V. Vorburger

In the preceding sections we have outlined the work completed so far in the QIA project. In this section, we discuss the plans for the current fiscal year (FY90) and for next year.

8.1 PLANS FOR CURRENT FISCAL YEAR

The project may be divided into four major tasks to implement the four loops discussed in the overall architecture shown in Fig. 1.1. An overview of subtasks in the project is given in Fig. 8.1 and the planned activities for FY90 are discussed below for each major task.

Pre-Process Characterization

The geometrical characterization of both machines as a function of temperature will be completed during FY90 as will the preliminary formulation of the geometrical/thermal model arising from the analysis of these data. This model will become part of the real-time control system described below.

Real-Time Sensing

Preliminary experiments on a prototype of the real-time error corrector (RTEC) were successful, and the hardware unit has been designed and constructed. During FY90 the software for real-time control will be installed and its full operation will be tested.

Process-Intermittent Gauging

The fast probing system was demonstrated during FY89 using the RTEC hardware discussed in Section 2. During FY90, the process-intermittent gauging system will be integrated under the real-time control software as

a single system and its operation will be demonstrated along with the real-time mode of operation.

Post-Process Gauging

During FY89 the coordinate measuring machine was installed, tested, and used. During FY90 a number of elements in the architecture of the quality monitor will be completed. One set of tasks involves the development of software for visualizing a machined and measured workpiece. This software will be installed on the post-process inspection system (the CMM workstation) and will be compatible with the Dimensional Measurement Interface Specification (DMIS) [6-1]. It will enable the operator to compare directly the designed part with the dimensional measurements obtained from the CMM.

In parallel with the part visualization effort the functional requirements of the quality monitor will be formulated and the prototype diagnostic system will be installed. This system will likely be the first generation in a software family whose knowledge and degree of automation will increase rapidly. Hence, an important attribute of the prototype will be its upward compatibility with future systems.

8.2 PLANS FOR FY91

By the beginning of FY91, the real-time control and process-intermittent gauging systems should be integrated together and operating on the turning center. A similar system will then be developed on the vertical machining center.

Based on the first round of cutting experiments, the geometrical/thermal models in the real-time control systems will be enhanced for both machines. The first-generation software for the quality monitor will also be completed and integrated with the post-process gauging system.

Finally, the software packages for force sensing, chatter detection, and ultrasonic roughness detection will be engineered and installed. The strategies for controlling chatter vibration will likely be modelled on the results and analysis of Smith, Tlusty, and Delio [8-1,8-2] for the milling process. As discussed in the FY88 report [1-1], the initial strategies based on ultrasonic roughness detection and force gauging will likely call for manual intervention when the sensed parameters exceed certain prescribed values to be determined.

The installation of the sensor packages should be the final step in the QIA system development. Once these are installed, the system will be fully operational over all three control loops. However, the quality monitor system for diagnosis of the machining processes is an open ended system. We anticipate considerable development of the QM beyond its initial stage as detailed knowledge of machines, machining processes, and the means to control them grows.

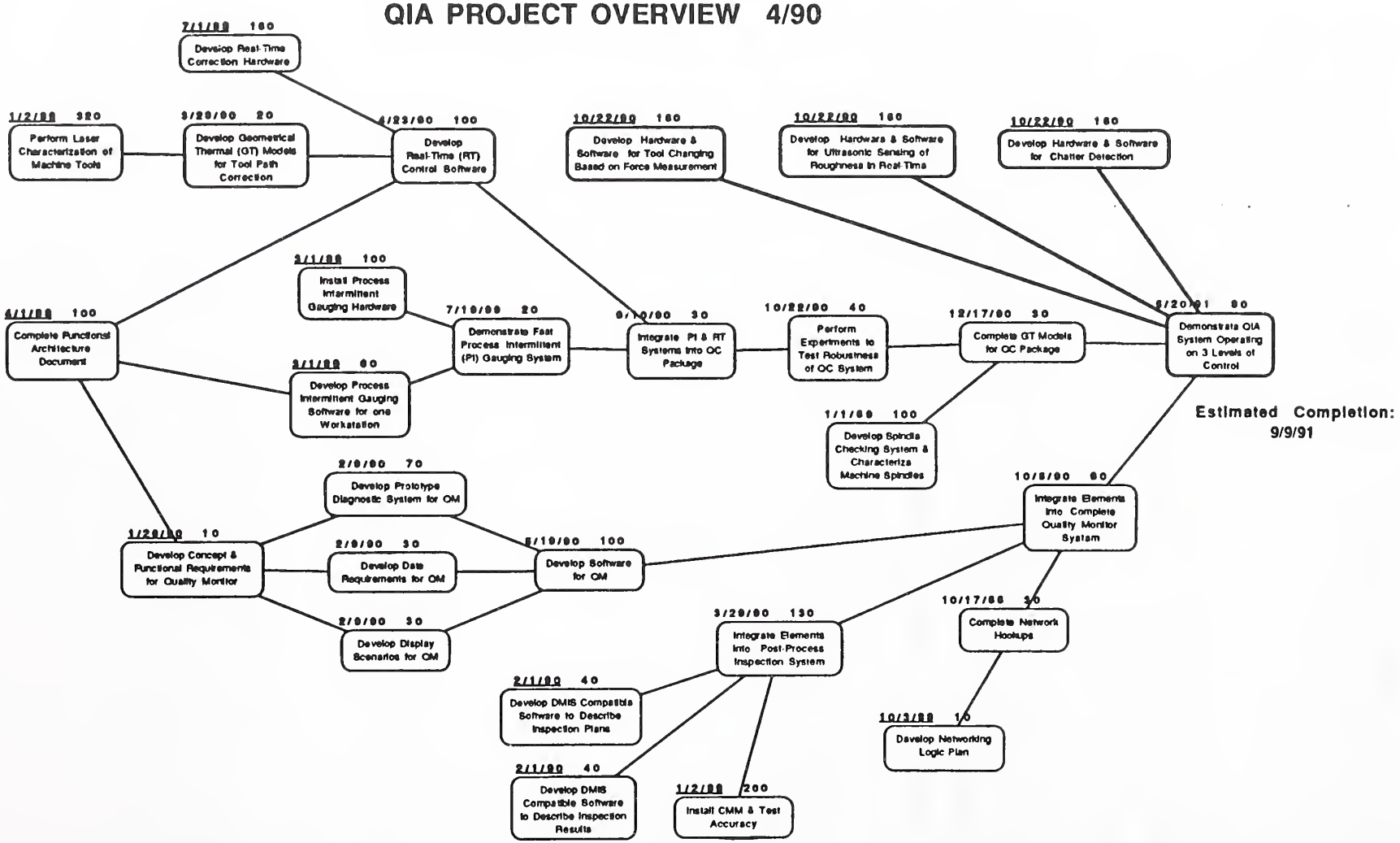
QIA PROJECT OVERVIEW 4/90
7/1/88 160
Develop Real-Time Correction Hardware
1/2/88 320
Perform Laser Characterization of Machine Tools
3/28/90 20
Develop Geometrical Thermal (GT) Models for Tool Path Correction
4/23/90 100
Develop Real-Time (RT) Control Software
10/22/90 160
Develop Hardware & Software for Tool Changing Based on Force Measurement
10/22/90 160
Develop Hardware & Software for Ultrasonic Sensing of Roughness in Real-Time
10/22/90 160
Develop Hardware & Software for Chatter Detection
3/1/88 100
Install Process Intermittent Gauging Hardware
4/1/88 100
Complete Functional Architecture Document
7/10/88 20
Demonstrate Fast Process Intermittent (PI) Gauging System
8/10/90 30
Integrate PI & RT Systems into QC Package
10/22/90 40
Perform Experiments to Test Robustness of QC System
12/17/90 30
Complete GT Models for QC Package
9/20/91 80
Demonstrate QIA System Operating on 3 Levels of Control
3/1/88 60
Develop Process Intermittent Gauging Software for one Workstation
1/1/89 100
Develop Spindle Checking System & Characteriza Machine Spindles
Estimated Completion: 9/9/91
2/8/90 70
Develop Prototype Diagnostic System for QM
10/8/90 60
Integrate Elements into Complete Quality Monitor System
1/29/90 10
Develop Concept & Functional Requirements for Quality Monitor
2/8/90 30
Develop Data Requirements for QM
8/10/90 100
Develop Software for QM
2/8/90 30
Develop Display Scenarios for QM
3/29/90 130
Integrate Elements into Post-Process Inspection System
10/17/88 30
Complete Network Hookups
2/1/90 40
Develop DMIS Compatible Software to Describe Inspection Plans
10/3/88 10
Develop Networking Logic Plan
2/1/90 40
Develop DMIS Compatible Software to Describe Inspection Results
1/2/88 200
Install CMM & Test Accuracy

Fig. 8.1

9. REFERENCES

1-1 Progress Report of the Quality in Automation Project for FY88, C.D. Lovett, ed., National Institute of Standards and Technology (US), NISTIR 89-4045, 1989.

1-2 BAS Machine Tests (Sveriges Mekanföbound, Box 5506, S11485, Stockholm, Sweden).

1-3 National Aerospace Standard NAS979, Uniform Cutting Tests - NAS Series Metal Cutting Equipment Specifications (National Standards Association, Washington, DC, 1969).

2-1 Technology of Machine Tools/Machine Tool Accuracy, Vol. 5, R.J. Hocken, ed. (Lawrence Livermore National Laboratory, Livermore, Calif., 1980).

2-2 Donmez, M.A.; Blomquist, D.S.; Hocken, R.J.; Liu, C.R.; Barash, M.M., "A General Methodology for Machine Tool Accuracy Enhancement by Error Compensation," Prec. Eng. 4, 187, 1986.

2-3 Donmez, M.A.; Liu, C.R.; Barash, M.M., "A Generalized Mathematical Model for Machine-Tool Errors," Modeling, Sensing, and Control of Manufacturing Processes, PED-Vol.23/DSC-Vol.4, Book No. H00370, K. Srinivasan, D.L.E. Hardt, and R. Komanduri, eds. (American Society of Mechanical Engineers, New York, 1987).

2-4 Donmez, M.A.; Lee, K.L.; Liu, C. R.; Barash, M.M., "A Real-Time Error Compensation System for a Computerized Numerical Control Turning Center," Proc. IEEE Int. Conf. on Robotics and Automation, (IEEE Computer Soc., Washington, D.C., 1986).

2-5 Boyes, G.S., Synchro and Resolver Conversion (Memory Devices Ltd., Surrey, UK, 1980).

2-6 "Programming and Operator's Manual Metalist, TC1 or TC1A, with GE2000T Control," (Monarch, Sidney, OH) p. 1-19F.

2-7 "Part Programming Manual 2000T CNC," GEK-25383 (General Electric Co., Charlottesville, VA) p. 11-17.

2-8 "User's Guide," Each for LP2, MP4, MP9 Probe Systems, (Renishaw plc., Gloucestershire, U.K.).

5-1 Bandy, H.T.; Carew, V.E. Jr.; Boudreaux, J.C., An AMPLE Version 0.1 Prototype: The HWS Implementation, National Bureau of Standards (US), NBSIR 88-3770, 1988.

5-2 Boudreaux, J.C., The Ample Project, National Bureau of Standards (US), NBSIR 86-3496, 1986.

5-3 Boudreaux, J.C., "AMPLE: A Programming Language Environment for Automated Manufacturing," in The Role of Language in Problem Solving - 2, J.C. Boudreaux, B. Hamill, and R. Jernigan, eds. (North Holland, Amsterdam, 1987).

5-4 Boudreaux, J.C., "Requirements for Global Programmed Languages," Proc. Symp. on Manufacturing Application Languages, MAPL, 107 (1988).

5-5 Boudreaux, J.C., "Representing and Querying Objects in AMPLE," in Engineering Database Management, Proc. ASME International Computers in Engineering Conference, 1989, p. 73-79.

5-6 Boudreaux, J.C., "AMPLE Core Interpreter: User's Guide," NISTIR, forthcoming.

5-7 Staley, S.M.; Boudreaux, J.C., "Programming Language Environments for CIM," Proc. PROCIM, 70 (1988).

5-8 Proceedings of the Nov. 1989 NIST Automation Open House, (to be published).

6-1 "DMIS 2.1, Specification CAM-I Standard 101 (CAMI, Inc., Arlington, TX, 1990).

6-2 Hocken, R.J., "Three Dimensional Metrology," Annals of the CIRP 26/2, 403 (1977).

6-3 Zhang, G., "Error Compensation of Coordinate Measuring Machines," Annals of the CIRP 34/1, 445 (1985).

6-4 ANSI B89 Reference Document "Parametric Calibration of Coordinate Measuring Machines," (to be published).

7-1 Blessing, G.V.; Eitzen, D.G., "Surface Roughness Sensed by Ultrasound," Surface Topography 1, 253 (1988).

7-2 ANSI/ASME B46.1-1985, "Surface Texture, Roughness, Waviness, and Lay" (ASME, New York, 1985).

7-3 Marx, E.; Vorburger, T.V., "Light Scattered by Random Surfaces and Roughness Determination," in Scatter from Optical Components, Proc. SPIE 1165, 72 (1989).

7-4 Marx, E.; Vorburger, T.V., "Direct and Inverse Problems for Light Scattered by Rough Surfaces," Appl. Opt. (in press).

7-5 Kiely, A.; Lettieri, T.R.; Vorburger, T.V. (to be published).

7-6 Church, E.L.; Jenkinson, H.A.; Zavada, J.M., "Relationship Between Surface Scattering and Microtopographic Features," Optical Engineering 18, 125 (1979).

7-7 Beckmann, P.; Spizzichino, A., The Scattering of Electromagnetic Waves from Rough Surfaces (Pergamon Press, London, 1963).

7-8 Vorburger, T.V.; Hembree, G.G., "Characterization of Surface Topography," in Navy Metrology - Research & Development Program Conference Report (Corona, CA, April 1989).

7-9 Elson, J.M.; Bennett, H.E.; Bennett, J.M., "Scattering from Optical Surfaces," in Applied Optics and Optical Engineering, Vol. VII (Academic Press, New York, 1979), Chapter 7.

7-10 Elson, J.M.; Bennett, J.M., "Relation Between the Angular Dependence of Scattering and the Statistical Properties of Optical Surfaces," J. Opt. Soc. Amer. 69, 31 (1979).

7-11 Detrio, J.A.; Miner, S.M., "Standardized Total Integrated Scatter Measurements of Optical Surfaces," Optical Engineering 24, 419 (1985).

7-12 ASTM F1048-87, "Standard Test Method for Measuring the Effective Surface Roughness of Optical Components by Total Integrated Scattering" (ASTM, Philadelphia, 1987).

7-13 Leonard, T.A.; Pantoliano, M., "BRDF Round Robin," in Stray Light and Contamination in Optical Systems, Proc. SPIE 967, 226 (1988).

7-14 Vorburger, T.V.; Teague, E.C.; Scire, F.E.; McLay, M.J.; Gilsinn, D.E., "Surface Roughness Studies with DALLAS - Detector Array for Laser Light Angular Scattering," J. Res. NBS 89, 3 (1984).

7-15 Bennett, H.E.; Porteus, J.O., "Relation Between Surface Roughness and Specular Reflectance at Normal Incidence," J. Opt. Soc. Amer. 51, 123 (1961).

7-16 Porteus, J.O., "Relation Between the Height Distribution of a Rough Surface and the Reflectance at Normal Incidence," J. Opt. Soc. Amer. 53, 1394 (1963).

7-17 Thomas, T.R. (ed), Rough Surfaces (Longman, London 1982).

7-18 Bevington, P.R., Data Reduction and Error Analysis for the Physical Sciences (McGraw-Hill, New York, 1969) p. 121.

7-19 Stover, J.C., "Optical Scatter," Laser & Optronics 7, No. 7 (1988).

7-20 Church, E.L., "The Measurement of Surface Texture and Topography by Differential Light Scattering," Wear 57, 93 (1979).

7-21 Stedman, M., "Basis for Comparing the Performance of Surface-Measuring Machines," Precision Engineering 9, 149 (1987).

7-22 Teague, E.C.; Vorburger, T.V.; Maystre, D., "Light Scattering from Manufactured Surfaces," CIRP Annals 30, 563 (1981).

7-23 Brodmann, R.; Allgauer, M., "Comparison of Light Scattering from Rough Surfaces with Optical and Mechanical Profilometry," in Surface Measurement and Characterization, Proc. SPIE 1009, 111 (1988).

7-24 Cao, L.X.; Vorburger, T.V.; Lieberman, A.G.; Lettieri, T.R. (to be published).

7-25 Rakels, J.H., "Recognised Surface Finish Parameters Obtained from Diffraction Patterns of Rough Surfaces," in Surface Measurement and Characterization, Proc. SPIE 1009, 119 (1988).

7-26 Takacs, P.Z.; Hewitt, R.C.; and Church, E.L., "Correlation Between the Performance and Metrology of Glancing-Incidence Synchrotron-Radiation Mirrors Containing Millimeter-Wavelength Shape Errors," in Proc. SPIE 749, 119 (1987).

7-27 Goodman, J.W., Introduction to Fourier Optics (McGraw-Hill, New York, 1968).

7-28 Teague, E.C., "Uncertainities in Calibrating a Stylus Type Surface Texture Measuring Instrument with an Interferometrically Measured Step," Metrologia 14, 39 (1978).

7-29 Chetwynd, D.G., "The Digitization of Surface Profiles," Wear 57, 137 (1978).

8-1 Smith, S; Delio, T., "Sensor Based Control for Chatter-free Milling by Spindle Speed Selection," (to be published).

8-2 Smith, S.; Tlusty, J., "Modelling and Simulation of the Milling Process," Proc. of the 1988 ASME Winter Annual Meeting, Publ. PED-32 (ASME, New York, 1988).

NIST-114A
(REV. 3-90)

U.S. DEPARTMENT OF COMMERCE
NATIONAL INSTITUTE OF STANDARDS AND TECHNOLOGY

BIBLIOGRAPHIC DATA SHEET

1. PUBLICATION OR REPORT NUMBER
NISTIR 4322

2. PERFORMING ORGANIZATION REPORT NUMBER

3. PUBLICATION DATE
JUNE 1990

4. TITLE AND SUBTITLE

Progress Report of the Quality in Automation Project for FY89

5. AUTHOR(S)
Edited by T. V. Vorburger and B. R. Scace

6. PERFORMING ORGANIZATION (IF JOINT OR OTHER THAN NIST, SEE INSTRUCTIONS)

U.S. DEPARTMENT OF COMMERCE
NATIONAL INSTITUTE OF STANDARDS AND TECHNOLOGY
GAITHERSBURG, MD 20899

7. CONTRACT/GRANT NUMBER

8. TYPE OF REPORT AND PERIOD COVERED

9. SPONSORING ORGANIZATION NAME AND COMPLETE ADDRESS (STREET, CITY, STATE, ZIP)

10. SUPPLEMENTARY NOTES

11. ABSTRACT (A 200-WORD OR LESS FACTUAL SUMMARY OF MOST SIGNIFICANT INFORMATION. IF DOCUMENT INCLUDES A SIGNIFICANT BIBLIOGRAPHY OR LITERATURE SURVEY, MENTION IT HERE.)

This document describes the progress of the Quality in Automation (QIA) Project at the National Institute of Standards and Technology during the fiscal year 1989. The project's purpose is to develop a quality assurance program that demonstrates "deterministic metrology" in an automated manufacturing environment using commercially available and affordable equipment. The document addresses several activities within the project in detail. A vertical machining center and a CNC turning center are both undergoing pre-process characterization. A prototype of the "real time error corrector" hardware is currently under test. High speed on-machine probing of test parts at speeds of up to 100 in/min has been demonstrated. A system architecture and programming language environment has been selected. A commercial coordinate measuring machine has been installed and is currently undergoing characterization. Several methods of real-time surface texture analysis are under consideration. One of these methods is the use of optical scattering analysis. Once the initial experiments have been completed and the system components have been procurred and tested, the entire system will undergo testing using standard test parts.

12. KEY WORDS (6 TO 12 ENTRIES; ALPHABETICAL ORDER; CAPITALIZE ONLY PROPER NAMES; AND SEPARATE KEY WORDS BY SEMICOLONS)
controller; inspection; machine tool; monitor; optical scattering; process certification; process intermittent gauging; quality; real time control; sensors; surface roughness; temperature

13. AVAILABILITY

[X] UNLIMITED

[ ] FOR OFFICIAL DISTRIBUTION. DO NOT RELEASE TO NATIONAL TECHNICAL INFORMATION SERVICE (NTIS).

[ ] ORDER FROM SUPERINTENDENT OF DOCUMENTS, U.S. GOVERNMENT PRINTING OFFICE, WASHINGTON, DC 20402.

[X] ORDER FROM NATIONAL TECHNICAL INFORMATION SERVICE (NTIS), SPRINGFIELD, VA 22161.

14. NUMBER OF PRINTED PAGES
158

15. PRICE
A08

ELECTRONIC FORM